

**Structural Studies of the Rab Prenylation
Mechanism and of RabGGTase in Complex
with Inhibitors**

Dissertation

Zur Erlangung des akademischen Grades

eines Doktor der Naturwissenschaften

der Fakultät für Chemie der Technischen Universität Dortmund

angefertigt am Max-Planck-Institut für molekulare Physiologie

in Dortmund

Eingereicht von Dipl. Chemiker Zhong Guo

aus Shenyang

Dortmund, Juni 2008

Die vorliegende Arbeit wurde in der Zeit von Februar 2006 bis Juni 2008 am Max-Planck-Institut für molekulare Physiologie in Dortmund unter der Anleitung von Prof. Dr. Roger S. Goody und Dr. Kirill Alexandrov durchgeführt.

1. Gutachter: Prof. Dr. Roger S. Goody
2. Gutachter: Prof. Dr. Henning Mootz

Hiermit versichere ich, dass ich die vorliegende Arbeit selbstständig angefertigt habe und keine anderen als die angegebenen Hilfsmittel verwendet habe.

Dortmund, Juni 2008

Zhong Guo

Contents

1	INTRODUCTION	1
1.1	GTP-binding proteins (GNBPs)	1
1.2	Rab proteins	2
1.3	Protein prenyltransferases	8
1.4	Structural features of protein prenyltransferases	11
1.4.1	Overall structures of protein prenyltransferase	11
1.4.2	Zinc binding site	13
1.5	Substrate specificity	13
1.5.1	Isoprenoid diphosphate substrate specificity	13
1.5.2	Protein substrate specificity	14
1.6	Mechanism of the prenylation reaction	15
1.6.1	Prenylation by CAAX-prenyltransferases	15
1.6.2	Geranylgeranylation by RabGGTase	17
1.7	Protein prenyltransferases inhibitors	20
2	AIMS OF THE PROJECT	24
3	MATERIALS AND METHODS	25
3.1	Materials	25
3.1.1	Bacterial strains	25
3.1.2	Media and antibiotics	25
3.1.3	Biochemicals and chemicals	26
3.1.4	Kits	28
3.1.5	Equipments	29
3.2	Molecular biological methods	31
3.2.1	Agarose gel electrophoresis	31
3.2.2	Preparation of plasmid DNA	31
3.2.3	Polymerase chain reaction (PCR)	32

3.2.4	DNA digestion	32
3.2.5	Ligation	32
3.2.6	Preparation of competent cells	32
3.2.7	Transformation	33
3.2.8	Bacteria storage	33
3.2.9	DNA sequencing	33
3.3	Expression and purification of proteins	34
3.3.1	Growth and harvest of bacteria expressing prenyltransferases	34
3.3.2	Nickel-NTA affinity chromatography	34
3.3.3	Removal of 6×His-tag and size exclusion chromatography	34
3.3.4	Concentrating proteins by ultra-filtration	35
3.3.5	SDS-PAGE	35
3.4	Biochemical and biophysical methods	36
3.4.1	Determination of protein concentration	36
3.4.2	Fluorescence spectroscopy	36
3.5	Crystallographic methods	37
3.5.1	Crystallisation	37
3.5.2	Crystallisation by vapour diffusion methods	37
3.5.3	Co-crystallisation and crystal soaking	37
3.5.4	Cryo-crystallography	38
3.5.5	Data collection	38
3.5.6	Matthews coefficient and solvent content analysis	39
3.5.7	Phase determination	39
3.5.8	Phase determination using molecular replacement (MR)	40
3.5.9	Refinement	40
3.5.10	Representation of structures	41
4	RESULTS AND DISCUSSIONS	42
4.1	Engineering of rat RabGGTase mutants	42
4.2	Purification of engineered RabGGTases from <i>E. coli</i>	44
4.3	Engineering of rat FTase mutants	45
4.4	Purification of wild-type and engineered FTases from <i>E. coli</i>	47
4.5	Crystallisation and structural determination of RabGGTase_αΔLRRΔIG mutant	49

4.6	Crystallisation and structural determination of FTase mutants	51
4.7	Structure of RabGGTase_ α LRR Δ IG in complex with its lipid substrate GGPP	55
4.8	The structures of RabGGTase_ α LRR Δ IG in complex with FPP, GGMP and GGTP	60
4.9	Phosphoisoprenoid specificity of protein prenytransferases	65
4.10	Design of FTase and GGTase-I mutants capable of utilising Biotin-GPP as a lipid substrate	68
4.11	Structures of the truncated RabGGTase in complex with mono- and di-prenylated Rab7 C-terminal peptides	71
4.12	Model of Rab prenylation process	78
4.13	Structures of RabGGTase_ α LRR Δ IG in complex with peptidomimetic inhibitors: MT650 and MT670	81
4.14	Structures of RabGGTase_ α LRR Δ IG in complex with the first selective peptidomimetic inhibitor: KT90102	86
4.15	Structure of RabGGTase_ α LRR Δ IG in complex with a specific inhibitor: psoromic acid	89
5	SUMMARY AND CONCLUSION	99
5.1	Summary and Conclusion (English)	99
5.2	Summary and Conclusion (Deutsch)	101
6	ACKNOWLEDGEMENTS	104

1 Introduction

1.1 GTP-binding proteins (GNBPs)

Guanine nucleotide binding proteins are involved in a wide range of intracellular processes including signal transduction¹, vesicular transport², cell growth and differentiation³, receptor mediated endocytosis⁴, protein synthesis⁵ and protein targeting⁶. Over 200 different small GTP-binding proteins, or small GTPases, have been identified in eukaryotic cells⁷. Most of these proteins cycle between a GDP-bound ‘OFF’ state and a GTP-bound ‘ON’ state by using a conserved switch mechanism (Figure 1.1)⁸. Only the GTP-bound form can interact with downstream effector molecules and carry out signal transduction.

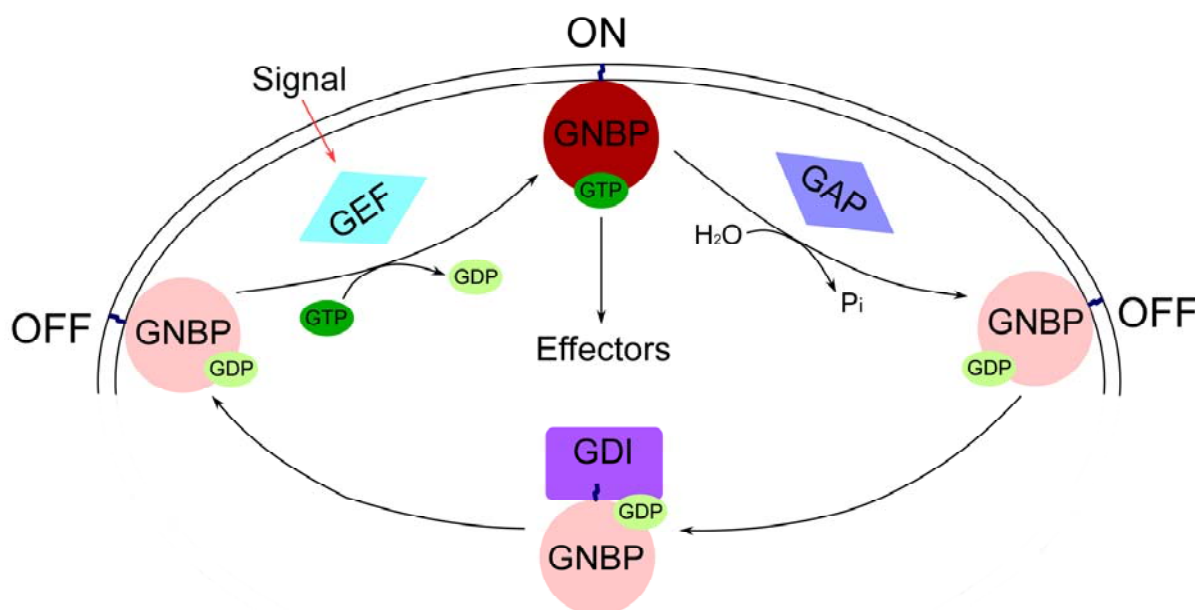


Figure 1.1: Schematic representation of the GTPase cycle. Cycling of switch GTPases occurs between an ‘Off’ state and an ‘On’ state. Intrinsic slow activation by GDP dissociation is accelerated by guanine nucleotide exchange factors (GEFs) and slow intrinsic GTP hydrolysis is accelerated by GTPase activating proteins (GAPs). GDP dissociation is inhibited by guanine nucleotide dissociation inhibitors (GDIs) in some cases.

The GTPases are activated by the exchange of GDP for GTP, in which an intrinsically slow nucleotide exchange process is accelerated by guanine nucleotide exchange factors (GEFs). The GTPases are deactivated by the hydrolysis of GTP to GDP, in which an intrinsically slow hydrolysis of GTP to GDP is accelerated by GTPase activating proteins (GAPs). GAP

catalysed rates of hydrolysis of up to 100,000-fold over the intrinsic rate have been observed⁹. In some cases (members of the Rho and Rab families), another set of regulators, guanine nucleotide dissociation inhibitors (GDIs) are involved in the cycle. These molecules stably bind to GTPases preventing GDP dissociation and mask the attached isoprenyl group, thereby increasing the solubility of GNBPs (see 1.2)^{10;11}.

The members of the Ras superfamily are central regulators of diverse important cellular processes. Over 170 small GTP-binding proteins have been identified in mammalian cells and subclassified on the basis of sequence into the Ras, Rho^{12;13}, Rab^{14;15}, Arf^{16;17}, and Ran families¹⁸⁻²⁰. Comparative analysis of primary sequences within the superfamily reveals a conserved primary structure with 30-55% sequence identity. Within the Ras family, each protein shares high sequence similarity with 50-55% amino acid identity, whereas the Rho and Rab family members share ~30% amino acid identity with the Ras family members²¹.

Similar to the other GTPases the members of the Ras superfamily have consensus amino acid sequences responsible for specific interaction with GDP and GTP and for GTP cleavage^{8;21}. In addition, the members of the Ras, Rho and Rab subfamily undergo post-translational lipid modifications such as farnesylation, geranylgeranylation or palmitoylation at their C-termini^{22;23}, whereas Arf proteins undergo myristoylation at the N-terminal glycine residue²⁴.

1.2 Rab proteins

Rab proteins form the largest family of monomeric small GTPases in the Ras superfamily. Eleven Rab (Ytp/Sec4p) proteins have been identified in the yeast *Saccharomyces cerevisiae* and at least 60 in humans²⁵. Following protein synthesis and lipid modification Rab proteins are localized to distinct intracellular compartments and regulate intracellular vesicular transport between organelles²⁶ (Figure 1.2).

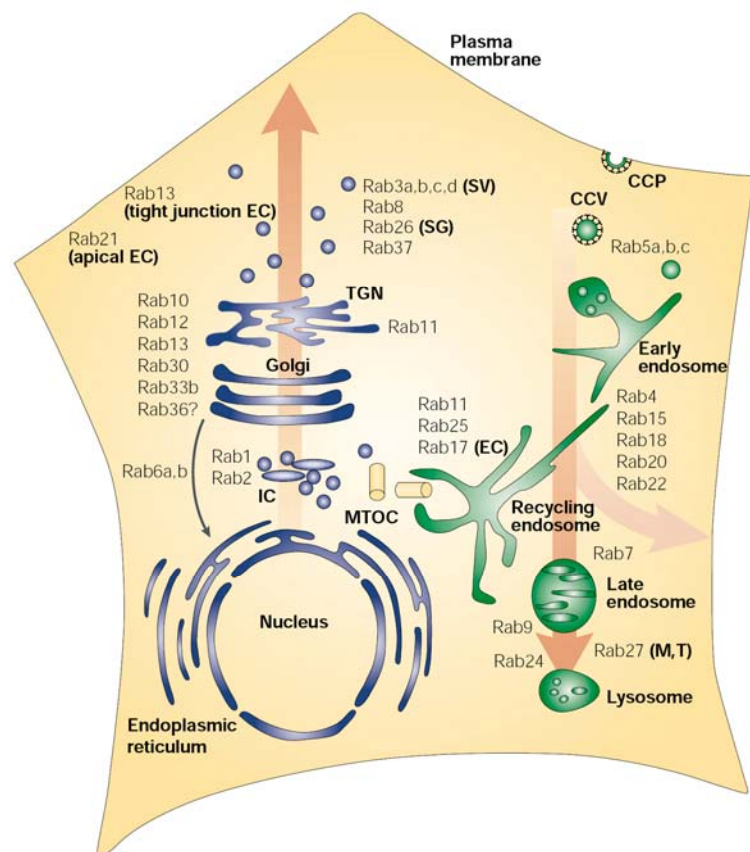


Figure 1.2: Intracellular localization of Rab proteins in mammalian cells adopted from²⁵. Some Rabs are cell specific (Rab3a in neurons), tissue specific (Rab17 in epithelia) or cell-type-specific localization (Rab13 in tight junctions).

Newly synthesized GDP-bound Rab proteins bind to Rab Escort Protein REP, which mediates their post-translational lipid modification and membrane association. One or two C-terminal cysteine residues of all Rab proteins are prenylated using GGPP as a lipid donor (see 1.6.2). The geranylgeranylated Rab proteins are escorted to be localized to specific intracellular membranes by REP, which sequesters the insoluble geranylgeranyl moiety to a hydrophobic tunnel and helps to stabilize Rab proteins in a soluble form. Once the geranylgeranylated Rab protein is presented to the specified target membrane, REP dissociates from Rab and recycles to the cytosol for additional rounds of Rab escorting (Figure 1.3, steps 1–4). REP proteins share sequence homology with another type of Rab regulatory protein, Rab GDP dissociation inhibitor (RabGDI). Similar to REP, RabGDI binds GDP-bound Rab proteins, solubilising the hydrophobic geranylgeranyl groups and producing soluble RabGDI:Rab:GDP complexes in the cytosol. However, in contrast to REP, the main function of GDI is extraction of Rab:GDP from intracellular membranes and its re-delivery to donor membranes (Figure 1.3, steps 11–

14). Major conformational changes in RabGDI are thought to occur upon binding to membrane associated Rab:GDP, resulting in the dissociation of the RabGDI:Rab:GDP complex from acceptor membranes²⁷. Recycling of Rab:GDP proteins to specific target membrane compartments is a process which is not yet understood in detail. Factors which are thought to play a role are RabGDI displacement factor (GDF), which may serve as RabGDI:Rab:GDP receptors^{28;29} and specific exchange factors³⁰ localized on individual membranes. Upon binding to donor membrane receptors, RabGDI dissociates from Rab:GDP and becomes available for additional rounds Rab:GDP extraction and transport.

In addition to cycling between distinct intracellular compartments, all Rab proteins also cycle between the inactive GDP-bound and the active GTP-bound state in a similar manner to other GTPases (Figure 1.3, steps 5–10). The rate of nucleotide exchange from GDP to GTP is greatly accelerated by specific guanine nucleotide exchange factors (GEFs). The GTP-bound Rab proteins interact with their specific effector molecules facilitating transport, tethering, and fusion of vesicles at their appropriate destination³¹⁻³³ (see below). GTP hydrolysis results in the return of Rab proteins to the inactive GDP-bound state. The intrinsic rate of GTP hydrolysis is greatly accelerated by GTPase activating proteins (GAPs).

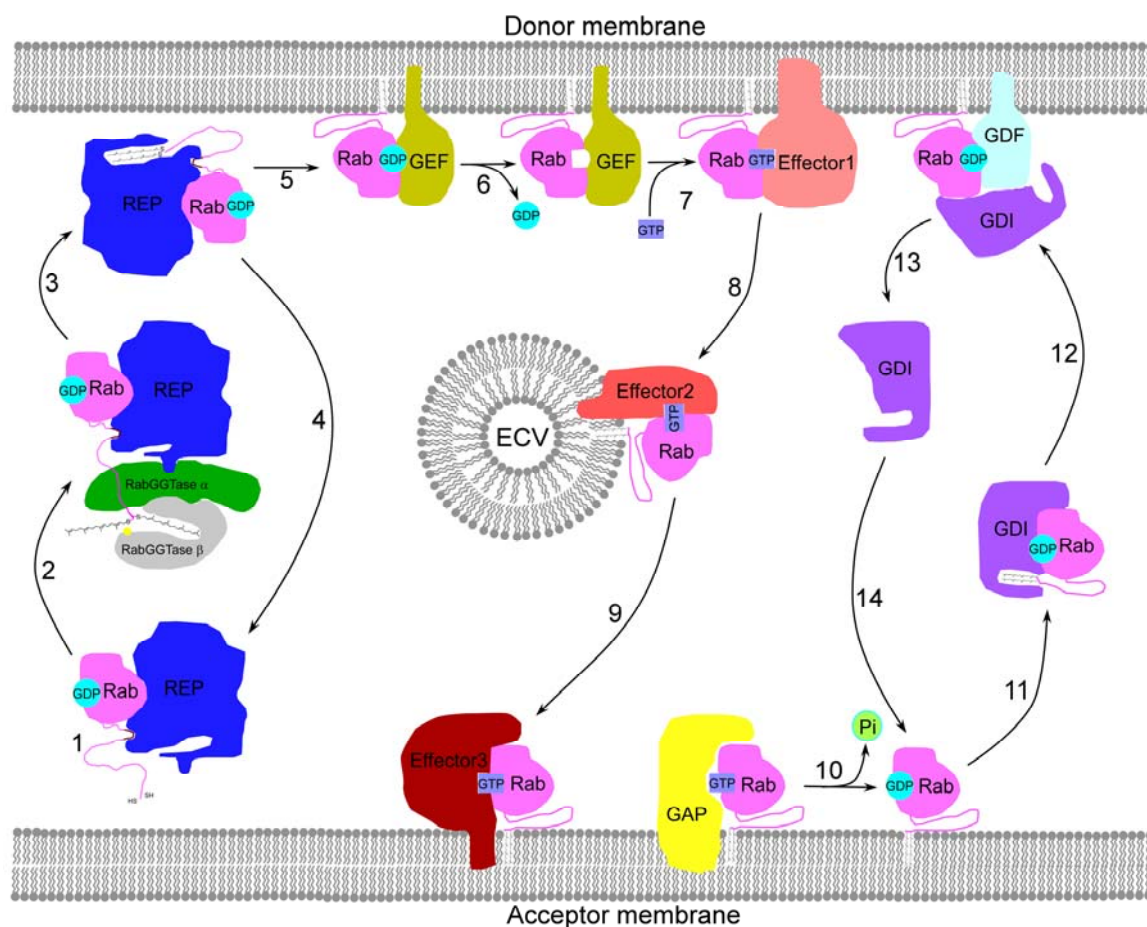


Figure 1.3: Rab prenylation, membrane localization and nucleotide cycling. First, REP recognizes newly synthesized GDP-bound Rab proteins (1) and presents them to RabGGTase (2). Following their geranylgeranylation, Rab proteins are escorted by REP and localized to their specific donor membrane by inserting of lipid residues (3). REP dissociates from Rab and is available for additional rounds of Rab escort (4). Subsequently, Rab proteins undergo nucleotide exchange from GDP to GTP mediated by GEFs (5–7). GTP-bound Rab proteins interact with effector molecules facilitating transport, tethering, and fusion of vesicles at their appropriate destination (8–9). The slow intrinsic GTP hydrolysis is accelerated by GAPs, resulting in dissociation of effector molecules from Rab proteins (10). The extraction of GDP-bound Rab proteins from acceptor membranes is mediated by GDI, which solubilizes Rabs and delivers them back to the donor membrane (11). GDI mediates the dissociation of GDI from Rab proteins and the reinserting of Rab proteins into the donor membrane (12), and GDI is available for additional rounds of Rab extraction (13,14).

Vesicular transport can be divided into four essential steps, consisting of vesicle budding, transport, tethering and fusion (Figure 1.4)^{34;35}. RabGTPases have been shown to be involved in the regulation of each of these steps³⁶.

During vesicle budding several Rabs are involved in vesicle formation³⁷⁻⁴⁰. Rab4 and its interactor rabaptin-5/rabex-5 complex regulate the receptor recycling from endosomes back to the plasma membrane, which is mediated by adaptor protein (AP)-1/clathrin-coated vesicles. Rab4 is required for the generation of the endosome-derived vesicles⁴⁰. Several studies suggest that Rabs also play a role in cargo selection. The affinity between a cargo selection protein TIP47 (tail-interacting protein of 47 kDa) and its cargo mannose 6-phosphate receptors (MPRs) is enhanced by the binding of TIP47 to a GTP-bound Rab9^{37;41}. This indicates that Rab9 stimulates cargo capture by the enhancement of the affinity of TIP47 for its cargo.

Following budding the vesicles are transported to their target membranes along the cytoskeleton (Figure 1.4), i.e. either along microtubules or actin^{42;43}. Molecular motors, including kinesin, dynein and myosin, and several RabGTPases have been implicated in this process. Both isoforms of Rab6, Rab6a and Rab6a', can stimulate microtubule-dependent Golgi-to-ER transport. These two isoforms of Rab6 regulate the association of their effector proteins (BicD) to the motor complex dynein-dynactin⁴⁴. A recent study revealed that two Rabs (Rab7 and Rab27a) regulate the transport of melanosome by controlling two different motor proteins⁴⁵. Rab7 recruits the motor complex dynein-dynactin through its effector Rab7-interacting lysosomal protein (RILP)⁴⁶ and regulates the microtubule-mediated transport of early melanosomes. Rab27a then regulates the subsequent actin-dependent transport of mature melanosomes by controlling myosin Va motor protein mediated by Rab27a effectors (melanophilin/Slac2-a)⁴⁷⁻⁴⁹. In addition, it is also proposed that Rab7 is involved in late endocytic transport through the binding of its effector RILP to the motor complex dynein-dynactin⁵⁰.

The next step, tethering, is a process that brings a carrier vesicle and its specific target membrane into close proximity. Several Rab proteins play a critical role in the initial recognition between a vesicle and its target membrane by the interaction of GTP-bound Rab on the vesicle with a tethering factor (also called tether) on the target membrane. Tethering factors are divided into two categories: large multisubunit complexes and long coiled-coil proteins^{34;36;51}. Seven of eight identified tethering factors of large multisubunit complexes serve as Rab effectors, including the Exocyst, COG, GARP/VFT, HOPS, CORVET, TRAPPI, and TRAPP II. One example of a Rab effector of the long coiled-coil protein class is the tethering factor p115. GTP-bound Rab1 binds to p115 to recruit p115 into carrier vesicles⁵².

Following tethering the carrier vesicle undergoes membrane fusion with the target organelle mediated by soluble N-ethylmaleimide-sensitive factor attachment protein receptors (SNAREs)⁵³. The crystal structure of SNAREs reveal that it is folded into a four-helical coiled-coil bundle^{54;55}. The interaction network formed by one arginine (R) and three glutamines (Q) from the four helices plays a central role for association of the helices to a bundle. Based on the presence of the arginine and glutamine the four helices fall into two groups: R- and Q-SNAREs⁵⁶. Before formation of trans-SNARE complexes (the helices of the bundle located on different membrane) by vesicular v-SNAREs and target t-SNAREs, the cis-SNARE complexes (the helices of the bundle located on same membrane) are disassembled mediated by the ATPase NSF (N-ethylmaleimide sensitive fusion protein) and its cochaperone α -SNAP (soluble NSF-attachment protein)⁵⁷. This process is called initial priming (Figure 1.4)⁵⁷. Subsequently, the disassembled cis-SNAREs complexes form the trans-SNAREs complexes. At last, a pore is formed by exerting of a mechanical force on the membranes through the tight association of trans-SNAREs complexes⁵⁸ and the cargos are delivered to target organelle. Although several lines of evidence suggest that RabGTPases are involved in the membrane fusion process^{25;59-61}, the exact functions of the RabGTPases at this point in the mechanism have not yet been determined.

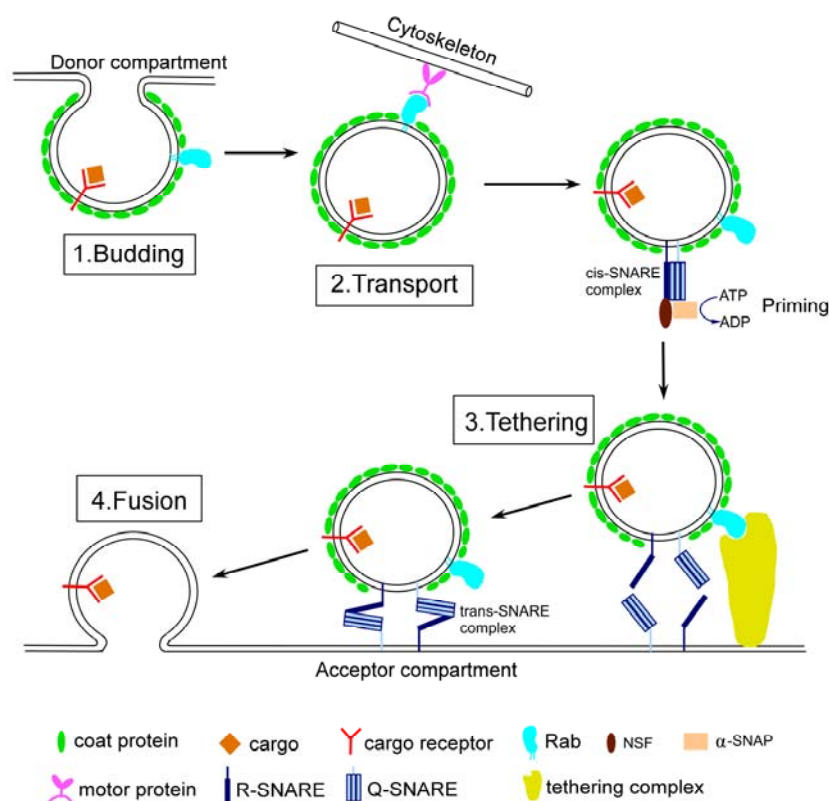
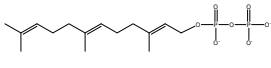
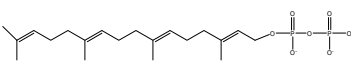
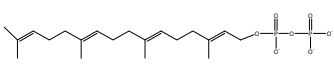
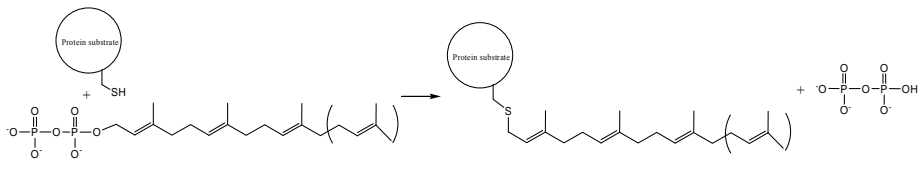


Figure 1.4: RabGTPases in regulation of vesicular trafficking. The four steps of vesicle trafficking are consisted of vesicle budding, transport along the cytoskeleton, membrane tethering and fusion of the two membranes.

1.3 Protein prenyltransferases

Protein prenylation is a type of lipid modification involving covalent addition of either farnesyl (15-carbon) or geranylgeranyl (20-carbon) isoprenoids via a thioether linkage to cysteine residues at or near the C-terminus of intracellular proteins. Farnesyl and geranylgeranyl groups are polyisoprenes, unsaturated hydrocarbons with a repeating unit of five carbons; the chain is 15 carbons long in the farnesyl moiety and 20 carbons long in the geranylgeranyl moiety (see Table 1.1)⁶². The importance of prenylation is due to the involvement of prenylated proteins (such Ras, Rho and Rab) in critical cellular pathways and diseases^{63;64}. Prenylation is necessary for the proper functions of prenylated protein.

Table 1.1: Comparison of the three protein prenyltransferases in mammalian cells.

	Farnesyltransferase (FTase)	Geranylgeranyltransferase I (GGTase-I)	Geranylgeranyltransferase II (GGTase-II or RabGGTase)
Subunit composition (mammalian)	48 kDa (α) 46 kDa (β)	48 kDa (α) 43 kDa (β)	65 kDa (α) 37 kDa (β)
Protein substrate motif	C-terminal -CA ₁ A ₂ X box	C-terminal -CA ₁ A ₂ X box	C-terminal such as -CC, -CXC, -CCX, -CCXX, -CCXXX, or -CXXX
Examples of protein substrates	Ras, nuclear lamins, Rhodopsin kinase, kinetochore proteins	Rho, Rac, Rap, heterotrimeric G protein γ subunit	Rab
Lipid donor substrate	Farnesyl diphosphate (FPP) 	Geranylgeranyl diphosphate (GGPP) 	Geranylgeranyl diphosphate (GGPP) 
Metal requirements	Zn ²⁺ , Mg ²⁺	Zn ²⁺	Zn ²⁺
Reaction			

Lipid anchors can mediate the subcellular localization of proteins. Other lipid modifications, such as myristoylation^{65;66} and palmitoylation^{67;68}, are mainly important for association of the protein to membranes. However, it appears that the prenylation mediated by protein prenyltransferases has a more complex role⁶⁹⁻⁷¹. On the one hand, the conjugated lipid residues (farnesyl or geranylgeranyl group) is required for membrane localization of the modified protein; on the other hand, the lipid group takes part in the specific protein-protein interactions based on either a direct interaction between lipid chains and proteins or conformational changes caused by prenylation⁷²⁻⁷⁶.

The protein prenyltransferases in mammals are divided into three types. Protein farnesyltransferase (FTase) and geranylgeranyltransferase I (GGTase-I) both recognize a

'CA₁A₂X' motif on their protein substrates, and are thus called CAAX prenyltransferases⁷⁷⁻⁷⁹. Many members of the Ras superfamily of small GTPases are farnesylated by FTase, such as H-Ras, K-Ras, N-Ras, Ras2, Rap2, RhoB (which is also maybe geranylgeranylated), RhoE, Rheb, TC10, and TC21. Other typical protein substrates for farnesylation mediated by FTase include the nuclear lamina proteins lamin A and B, the kinetochore proteins CENP-E and CENP-F, fungal mating factors, cGMP phosphodiesterase, the α and γ subunit of trimeric G proteins, DnaJ heat-shock protein homologs, rhodopsin kinase and the peroxisomal membrane proteins Pex19 and PxF⁶². Small GTPases, such as Rac1, Rac2, RalA, Rap1A, Rap1B, RhoA, and RhoB, RhoC, Cdc42, are geranylgeranylated by GGTase-I. Some γ -subunit variants of trimeric G proteins, cGMP phosphodiesterase β and the plant calmodulin CaM53, are also protein substrates for GGTase-I. Rab8, Rab11 and Rab13 can be geranylgeranylated by both GGTase-I and RabGGTase⁶².

Following prenylation mediated by CAAX protein prenyltransferases the prenylated proteins are delivered to their specific membrane, where the prenylated proteins usually undergo the cleavage of the C-terminal tripeptide (-A₁A₂X) catalysed by a prenyl-protein-specific protease. Subsequently, the C-terminal prenylcysteine is methylated under the catalyse of isoprenylcysteine carboxyl methyltransferase⁸⁰⁻⁸³. Palmitoylation is another lipid modification that is often combined with prenylation⁸⁴.

In the case of RabGGTase the recognition of the protein substrate is mediated by Rab escort protein (REP)^{85,86}. There is no pronounced sequence conservation in the C-termini of Rab proteins. The C-terminus contains a prenylation motif often arranged as -CC, -CXC, -CCX, -CCXX, -CCXXX or, in a few cases, with only a single cysteine as in -CXXX. Thus RabGGTase is sometimes referred to as a non-CAAX prenyltransferase²².

All protein prenyltransferases are heterodimers formed by two subunits, α and β . The α subunit of FTase and GGTase-I is encoded by the same gene (see Table 1.1). Each prenyltransferase is a zinc-metal enzyme. Zinc ions are essential for the catalytic activity of all protein prenyltransferases (see 1.6). In addition, Mg²⁺ ion is required for optimal enzymatic activity of FTase⁸⁷.

1.4 Structural features of protein prenyltransferases

During the last decade, crystal structures of FTase and GGTase-I in complex with lipid substrates, protein substrates, and prenylated products have been determined at high resolution^{88;89}. These structures help us to understand the prenylation process mediated by CAAX prenyltransferases. However, to date only the apo structure of RabGGTase and its structure as a complex with REP-1 are available due to technical difficulties associated with crystallisation of RabGGTase⁹⁰.

1.4.1 Overall structures of protein prenyltransferase

The overall structures of FTase and GGTase-I are very similar and largely composed of α helices^{89;91}. The structures of the α subunits in both enzymes are almost identical, with minor differences caused by the association with different β subunits. The α subunit consists of 14 α helices and is folded into seven successive pairs that form a series of righthanded antiparallel coiled coils. These coiled coils adopt a crescent-shaped superhelix and surround the β subunit (Figure 1.5). The α and β subunits associate through a large interface (burying $>3,000 \text{ \AA}^2$ surface area).

The α subunit of RabGGTase (567 amino acids) is much larger than that of FTase and GGTase-I (377 amino acids). The structure of RabGGTase reveals that the α subunit of RabGGTase is folded into three domains: a helical domain, an immunoglobulin-like (IG) domain and a leucine-rich repeat (LRR) domain⁹⁰. Despite the only 22% sequence identity between the α subunit of FTase and the respective helical domain in the α subunit of RabGGTase, they are structurally very similar. In comparison with FTase and GGTase-I, the most striking difference in RabGGTase is the presence of two additional domains of the α subunit: the IG domain and the LRR domain. These two domains are absent both in CAAX protein prenyltransferases and in lower eukaryote versions of RabGGTase. The functions of the additional domains in RabGGTase is unclear, however the structural studies reveal that they are not directly involved in the interaction with lipid donor, protein substrates or the Rab prenylation mediator REP^{90;92;93}. The IG domain is composed of 115 amino acids (238 α to 352 α) and LRR domain 126 (442 α to 567 α). Both domains are composed mainly of β sheets (Figure 1.5C). The IG domain is inserted into the helical domain and connects helices $\alpha 11$ and $\alpha 12$ by two loops, whereas the LRR domain is arranged at the C-terminus of the α subunit.

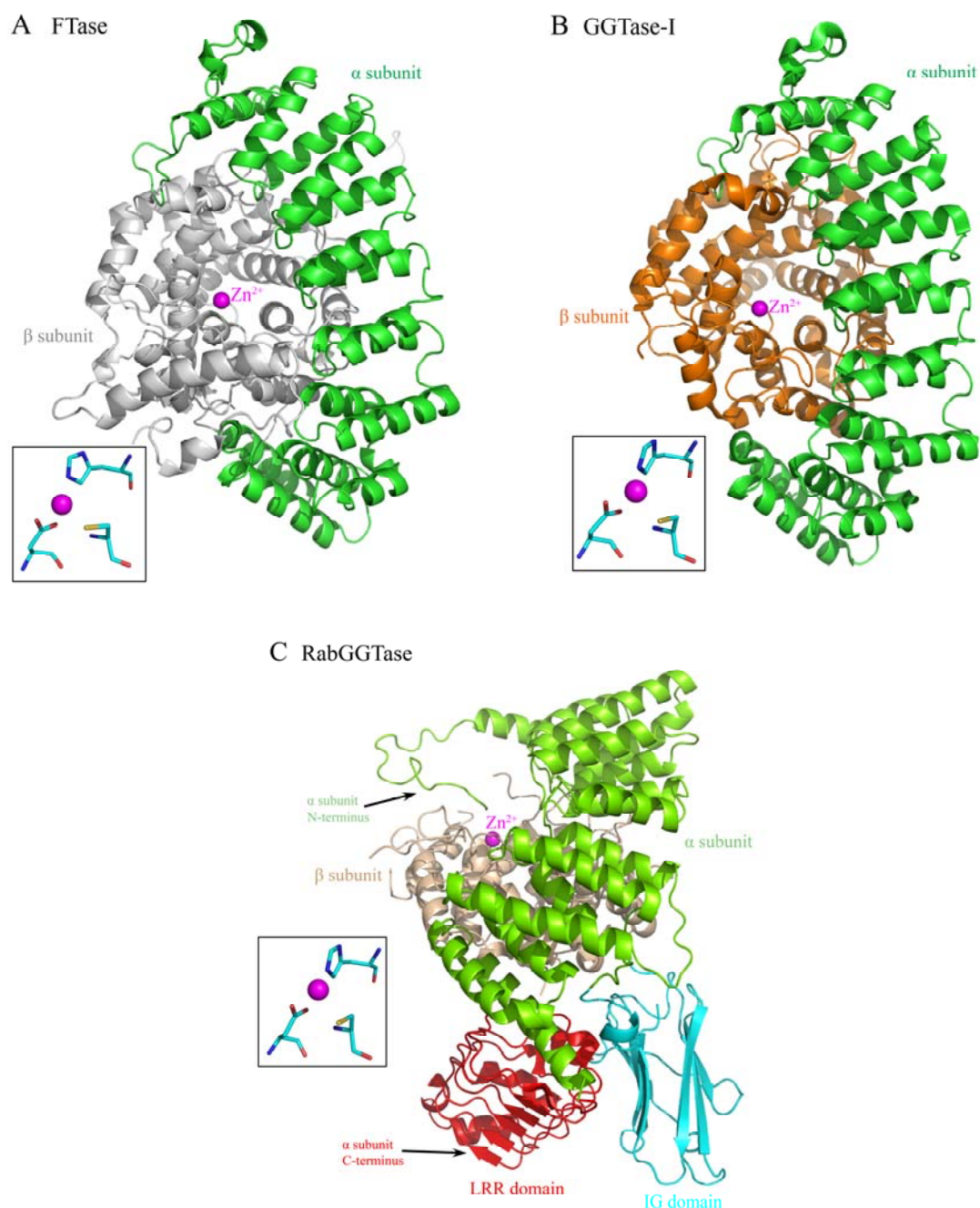


Figure 1.5: Overall structures of mammalian FTase (A), GGTase-I (B) and RabGGTase (C) and their zinc ion binding sites. Protein and zinc ion are shown as cartoons and as a magenta sphere, respectively. The zinc ion is coordinated by three conserved residues (insets): D297 β , C299 β , and H362 β in FTase; D269 β , C271 β , and H321 β in GGTase-I and D238 β , C240 β , and H290 β in RabGGTase, which are shown as stick representation. The LRR and IG domains of RabGGTase are coloured in red and cyan, respectively.

The β subunits of the three protein prenyltransferases include the major parts of the protein substrate- and isoprenoid-binding pockets. Most of the residues responsible for substrate binding are in the β subunits⁸⁹⁻⁹¹. Despite ca. 30% sequence identity among the β subunits of

the three protein prenyltransferases, they share similar overall structures. The structures of the β subunits consist of 14 α helices in FTase, 13 in GGTase-I and 12 in RabGGTase. These α helices are similarly folded into an α - α barrel containing a funnel-shaped, hydrophobic cavity lined by numerous conserved aromatic residues (Figure 1.5).

1.4.2 Zinc binding site

FTase, GGTase-I and RabGGTase are zinc metalloenzymes^{94;95}. Crystal structures of these three enzymes reveal that one Zn^{2+} ion is localized near the α/β subunit interface and is coordinated by three strictly conserved residues: Asp297 β , Cys299 β , and His362 β in FTase⁹¹; Asp269 β , Cys271 β , and His321 β in GGTase-I⁸⁹ and Asp238 β , Cys240 β , and His290 β in RabGGTase⁹⁰ (Figure 1.5). In the structures of the three enzymes a conserved hydrogen bond is formed between the zinc-coordinated histidine residue and an aspartic acid residue (Asp359 β in FTase, Asp318 β in GGTase-I; and Asp287 β in RabGGTase). This coordination possibly has a stabilizing effect on zinc binding motif.

1.5 Substrate specificity

1.5.1 Isoprenoid diphosphate substrate specificity

The structures of FTase and GGTase-I in complex with their respective isoprenoid substrate (FPP and GGPP) have been determined (PDB code: 1FT2 and 1N4P, respectively)^{89;96}. Both structures show that the lipid chain of isoprenoid inserts into the central hydrophobic funnel of the α - α barrel of the β subunit, and the diphosphate group of the isoprenoid intreracts through hydrogen bonds with a positively charged cluster formed by two lysines and one arginine. The isoprene chain of FPP and GGPP interacts with a number of conserved aromatic residues in the funnel. In the case of FPP it adopts an extended conformation and in the case of GGPP a bent conformation with an angle of ca. 90° at the C₁₅ of GGPP.

Although both FPP and GGPP bind tightly to all prenyltransferases, the transfer efficiencies are very different^{23;94;97-100}. FTase can only use FPP as a lipid donor for prenylation. In contrast, both GGTase-I and RabGGTase can prenylate their protein substrates using GGPP and FPP as lipid substrates, but with significant differences in efficiency.

1.5.2 Protein substrate specificity

As mentioned above, the recognition of protein substrates by RabGGTase is indirect and mediated by Rab escort protein (REP)^{85;86}, which occurs as two isoforms: REP-1 and REP-2. This is in harmony with the observation that RabGGTase has no pronounced sequence conservation in the C-termini of Rab proteins and RabGGTase displays no affinity for GTPases.

Both FTase and GGTase-I recognize a CA₁A₂X motif in their protein substrate. Numerous structural studies on the binding of a series of CA₁A₂X peptides towards FTase and GGTase-I reveal the mechanism and rules of protein substrate selection by CAAX protein prenyltransferases. The selection rules have been applied in the identification of novel potential protein substrates for CAAX prenyltransferases within the human genome. The CA₁A₂X peptides in the structural studies are derived from the C-terminus of protein substrates for FTase or GGTase-I and have been cocrystallized with the enzymes in the presence of an unreactive isoprenoid analogue^{88;89;101-103}.

The ternary complexes show that all CA₁A₂X motifs bind to the active sites of FTase and GGTase-I in a similar mode. In all cases, the cysteine thiol is coordinated by the catalytic Zn²⁺ ion, activating the thiol group to form the thioether linkage (see 1.6). The C-terminus of CA₁A₂X motif inserts into the funnel.

The residue A₁ is solvent-exposed and this suggests that it can be any amino acid. This conclusion is consistent with biochemical studies^{89;97;101;102}. The residue A₂ binding sites in FTase and GGTase-I are similar in nature. Although the selection of A₂ residues by both enzymes is restrained, this residue has very little effect on CAAX specificity. The residue A₂ for FTase and GGTase-I can be a variety of amino acids, such as valine, isoleucine, leucine, methionine, proline, phenylalanine, tyrosine and threonine, consistent with biochemical studies^{89;104}.

The X residue is inserted into the bottom of the hydrophobic funnel of the β subunit. The structures show that due to steric hindrance, the residue X binding site in both FTase and GGTase-I can not accommodate bulky amino acids, such as tyrosine, tryptophan, and arginine. The residue X binding site in FTase is more polar, in GGTase-I more hydrophobic. As a result, FTase and GGTase-I select CA₁A₂X motifs as their respective substrates primarily through the recognition of the X residue by enzyme residues in the active site. This selection

is achieved by polar and hydrophobic interactions between the X residue and the enzyme side chains. For FTase, the residue X is usually methionine, serine or glutamine, in some case is also can be alanine, threonine, asparagine, histidine or cysteine. In contrast, for GGTase-I, the X position is usually leucine or phenylalanine (in a few case isoleucine or valine).

1.6 Mechanism of the prenylation reaction

1.6.1 Prenylation by CAAX-prenyltransferases

Based on the biochemical results and the complex structures of both CAAX prenyltransferases along the prenylation process, a reaction pathway was proposed for FTase and GGTase-I^{88;89;98;99;105-108}. The reaction pathway of FTase mediated protein prenylation obtained from the combination of structural data is schematically represented in Figure 1.6⁸⁸.

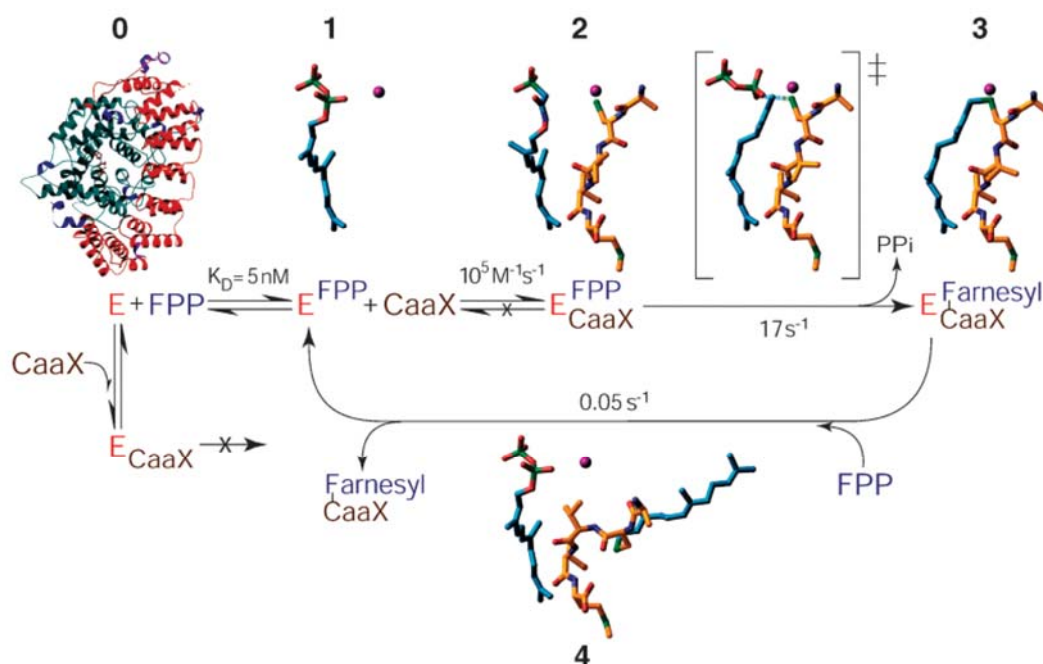


Figure 1.6: Structures along the FTase mediated prenylation reaction adopted from Long et al.⁸⁸. In all complexes^{88;89;96;102} only the substrates and products are displayed in stick representation. In the apo enzyme structure (0) (PDB code 1FT1), the α subunit and the β subunit are shown in red and blue, respectively. Firstly, FPP associates to the active site (1) (PDB code 1FT2), followed by binding of the CAAX peptide (2) (PDB code 1D8D). The resulting farnesylated peptide remains bound in the hydrophobic cavity (3) (PDB code 1KZP). The binding of a new FPP displaces the attached lipid chain from the cavity (4) (PDB code 1KZO). ‡ represents a putative transition state between 2 and 3. The isoprenoid is shown in blue, the CAAX in yellow, and the catalytic zinc ion in magenta. Kinetic constants were taken from available biochemical data^{98;99;105;106;109;110}.

Several biochemical studies reveal that the binding of substrates in CAAX prenyltransferases occurs in an ordered binding mechanism^{98;99;105-108}, first isoprenoid substrate binds to the active site of enzyme, followed by the CAAX motif (Figure 1.6, complexes 1 and 2). The ordered binding mechanism is consistent with the structural analysis. In the structure of the enzyme in complex with a CAAX peptide and an unreactive isoprenoid analogue the isoprenoid makes extensive van der Waals contacts with the CAAX peptide. The cysteine thiol is coordinated by Zn⁺ ion and thus is activated.

Following the binding of both isoprenoid substrate and CAAX peptide to the active site, a conformational change is required for the prenylation reaction. Comparison of the structure of CAAX prenyltransferase in complex with isoprenoid and CAAX peptide to the structure of the enzyme bound to the prenylated CAAX peptide reveals that the conformation and position of CAAX peptide backbone is almost identical before and after the prenylation reaction (Figure 1.7 A). Thus for the transition state it is hypothesized that the isoprenoid chain rotates at its third isoprene unit in the case of FTase or fourth in the case of GGTase-I and moves the C₁ atom of isoprenoid closer to the activated thiolate of the CAAX peptide^{88;89}. Subsequently, the prenylation reaction is carried out to form the prenylated product (Figure 1.6, complex 3). However, it is still unclear whether the reaction is through an electrophilic or a nucleophilic mechanism^{106;111;112}.

After cleavage of the bond between the C₁ atom and the α -phosphate of isoprenoid the negative charges of the diphosphate group are stabilised by residues located at the active site of the enzymes, including a lysine (Lys164 α in both FTase and GGTase-I) and a tyrosine (Tyr300 β in FTase, Tyr272 β in GGTase-I). Biochemical studies reveal that only FTase requires Mg²⁺ ion for its full catalytic activity^{78;94}. This can be explained by stabilization of the developing negative charge of the diphosphate group of FPP. Structural analysis reveals that one Mg²⁺ ion interacts with the Asp352 β of the FTase and the diphosphate group of FPP⁸⁸. The corresponding position in GGTase-I is occupancied by the residue lysine (Lys311 β), which stabilises the diphosphate group of GGPP. As a result, the catalytic activity of GGTase-I is Mg²⁺-independent. This conclusion is consistent with several mutagenesis studies, in which the enzyme activity of one mutant (FTase_{K352 β}) is Mg²⁺-independent and the other mutant (GGTase-I_{D311 β}) becomes Mg²⁺-dependent^{113;114}.

Kinetic results indicate that product release is the rate-limiting step of the prenylation and occurs via the competitive binding of new substrate(s) to the active site, particularly

isoprenoid substrate^{98;107;108;110;115;116;117}. Structural analysis of FTase and GGTase-I in complex with both isoprenoid substrate and prenylated product reveals that binding of a new isoprenoid substrate to the hydrophobic funnel shifts the attached lipid chain of the prenylated product to an ‘exit groove’ on the β subunit (Figure 1.6, complex 4, Figure 1.7 B))^{88;89}. Finally, release of the prenylated product is facilitated by the competitive binding of a new CAAX peptide.

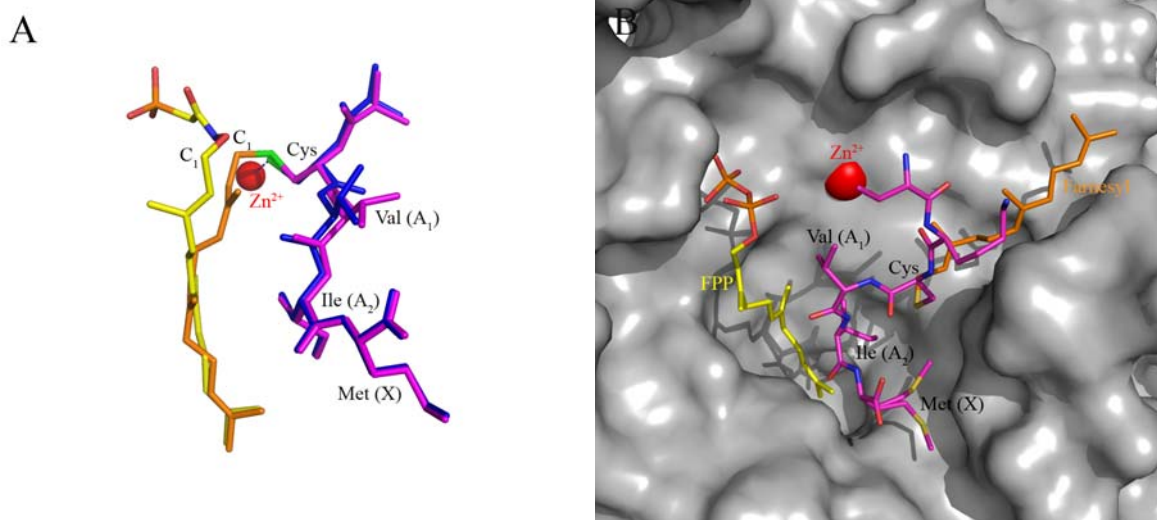


Figure 1.7: Binding of substrates and products at active site of FTase. (A) In FTase, FPP (yellow) undergoes a conformational change and brings the C₁ atom of FPP closer to the activated thiolate of the CAAX peptide (blue) (PDB code 1D8D) to form a prenylated product (orange and magenta) (PDB code 1KZP). **(B)** Binding of a fresh FPP and translocated product in FTase (PDB code 1KZO). The active site of FTase is displayed in surface representation⁸⁸. The attached lipid chain of the prenylated product is translocated to a conserved ‘exit groove’ by competitive binding of a new FPP molecule (yellow).

1.6.2 Geranylgeranylation by RabGGTase

The Rab prenylation mechanism is fundamentally different from that of the CAAX protein prenyltransferases. An additional protein factor, REP, is needed for Rab prenylation and usually Rab proteins undergo double geranylgeranylation¹¹⁸. A Rab protein, REP and RabGGTase associate as a ternary protein complex during Rab geranylgeranylation. Numerous biochemical and structural studies were focused on the process of the formation of the ternary protein complex¹¹⁹.

Based on available biochemical results two possible mechanisms were proposed for the formation of the ternary protein complex (Figure 1.8)¹²⁰⁻¹²⁶. In the ‘classical’ mechanism of

Rab prenylation, the unprenylated Rab interacts with REP first, followed by association of this complex with RabGGTase. The affinity of REP for RabGGTase is increased by the binding of either Rab or GGPP. This observation has led to proposition of an ‘alternative’ mechanism for the formation of the ternary protein complex¹²³, that REP associates with RabGGTase bound to GGPP to form a binary protein complex followed by binding to Rab protein. However, the physiological significance of the presence of these two mechanisms is still unclear⁹².

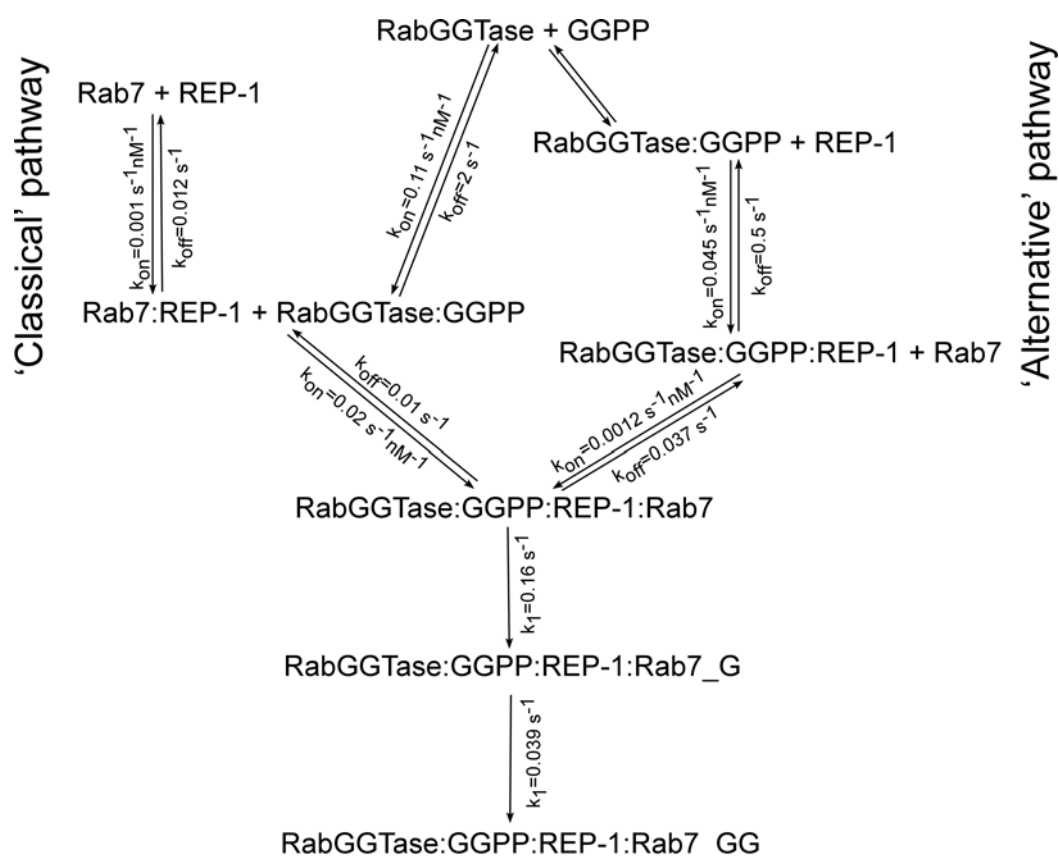


Figure 1.8: Kinetic constants for RabGGTase catalysed Rab prenylation. Based on available biochemical data two possible mechanisms (‘classical’ and ‘alternative’ mechanism) were proposed for the formation of the ternary protein complex between a Rab, REP and RabGGTase¹²⁰⁻¹²⁶.

Several years ago the structure of REP-1 in complex with RabGGTase bound to a nonhydrolyzable isoprenoid analogue⁹³ and the structures of REP-1 complexed with either un- or mono-prenylated Rab7¹²⁷ gave insight into the RabGGTase catalysed Rab geranylgeranylation mechanism. The structural analysis reveals that the complex of Rab:REP is formed by the interactions between the Rab binding platform (RBP) of REP and the effector loops of Rab and between the C-terminal binding region (CBR) of REP and the CBR interacting motif (CIM) of Rab, which is composed of two hydrophobic residues near the C-

terminus of Rab proteins^{127;128}. The association of RabGGTase with REP-1 is through the interaction of three helices of the RabGGTase α subunit and two helices of REP-1 domain II⁹³. Remarkably, the surface area buried by the interface of the complex REP-1:RabGGTase is very small, around 680 Å².

The catalytic ternary complex between Rab, REP and RabGGTase can be modeled by superimposition of the Rab:REP and REP:RabGGTase complexes (Figure 1.9). In this model, the flexible C-terminus of Rab associates with the active site of RabGGTase during the geranylgeranylation reaction. The lipid binding site of REP-1 is located in domain II formed by five helices (D, E, F, G and H) (Figure 1.9). The distance between the REP-1 domain II and the active site of RabGGTase is around 30 Å, suggesting that after prenylation the translocation of the geranylgeranylated C-terminus of Rab proteins from the active site of RabGGTase to the domain II of REP-1 is a barrier. This is supported by biochemical studies, which show that product release by RabGGTase is very slow^{124;129}.

Analysis of the RabGGTase:REP-1 complex indicates that the interaction between two residues of REP-1 (Phe279 and Arg290), which are located on helices of domain II, and the α subunit of RabGGTase is critical for the association of REP-1 towards RabGGTase^{93;122}. Following the geranylgeranylation reaction, the conjugated lipid chains are displaced from the hydrophobic funnel of the enzyme by competitive binding of a new isoprenoid substrate¹²⁴, and are translocated to the lipid binding site of REP-1. The geranylgeranyl groups insert into the hydrophobic cavity of domain II (Figure 1.9), resulting in dilation of this cavity and in conformational changes of Phe279REP-1 and Arg290REP-1. This leads to a decrease in the affinity of RabGGTase towards the prenylated Rab:REP complex and facilitates product release by the enzyme.

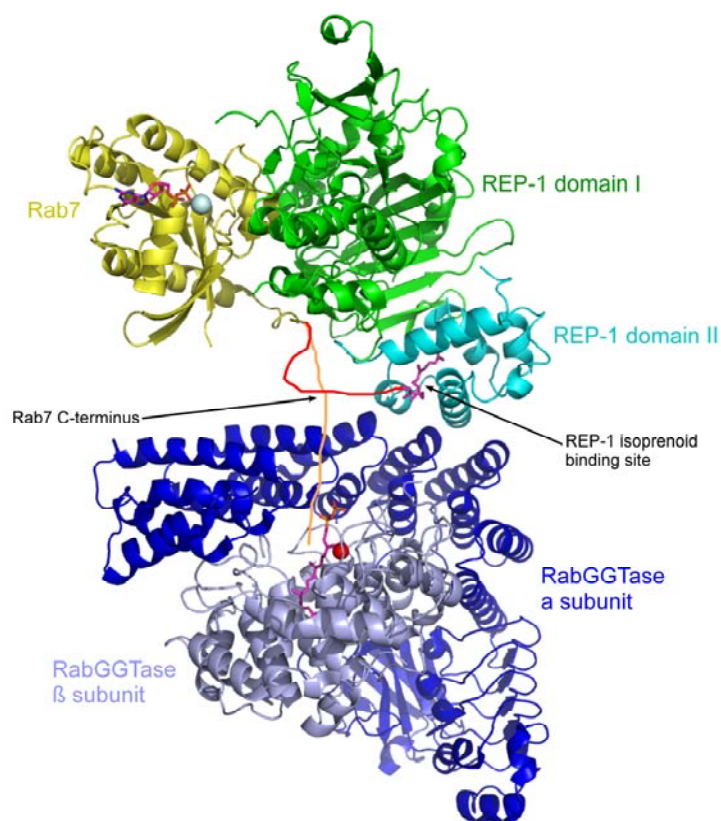


Figure 1.9: Putative model of the ternary Rab7:REP-1:RabGGTase complex. All proteins are displayed in cartoon form. Domain I and domain II of REP-1 are coloured in green and cyan, respectively; the isoprenoid binding site of REP-1 is highlighted and the geranylgeranyl lipid (magenta) bound to the domain II is shown in stick representation. The α and β subunits of RabGGTase are coloured in dark blue and light blue, respectively; GGPP (magenta) in the putative site of RabGGTase is displayed in stick form and Zn^{2+} is shown as a magenta sphere. GDP (atomic colours) and the Mg^{2+} (light cyan) bound to Rab7 (yellow) are shown in stick and sphere representation, respectively. The Rab7 C-terminus in the unprenylated complex (orange line) is expected to associate with the active site of RabGGTase. The putative position of the prenylated C terminus of Rab is shown as a red line.

1.7 Protein prenyltransferases inhibitors

Following the observation that farnesylation is required for the activity of oncogenic Ras proteins^{71;106;130;131}, the development of FTase inhibitors became an active field of research. Recently GGTase-I has been also recognized as a promising anti-cancer target¹³².

Several members of Ras subfamily are involved in human cancer, including K-Ras, N-Ras and H-Ras. Biochemical studies reveal that over 30 % of all human cancers are related to Ras mutational activation¹³³. The GTP-bound active form of Ras proteins is stabilized by the

mutations¹³⁴. Constitutively activating mutations of Ras proteins have been identified in numerous human cancers including pancreatic cancer, non-small-cell lung cancer, colorectal cancer, melanoma, hepatocellular cancer, myelodysplastic syndrome and acute myelogenous leukaemia, follicular and undifferentiated papillary thyroid cancer, bladder cancer and renal cell cancer¹³⁴⁻¹³⁶.

Human cancers are also related to the deregulation of Rho proteins, including breast cancer, colon cancer, lung cancer, bladder cancer, testicular germ cell cancer, melanoma cancer¹³⁷⁻¹⁴⁰. Unlike the Ras subfamily, so far, only one Rho subfamily member, RhoH, has been observed to be altered genetically in human cancer^{137;141;142}. Usually the deregulation of Rho proteins is related to overexpression of Rho proteins and their regulators, or is related to mutations of their regulators. These regulators include GEFs^{143;144}, GAPs^{145;146} and GDIs^{147;148}.

Recent studies demonstrates that the Rab proteins are also involved in human cancer^{136;149}. One example is Rab25, which is overexpressed at the RNA level in human ovarian and breast cancer¹⁵⁰. Overexpression of Rab25 induced an increase in cell proliferation and prevention of apoptosis. The other examples include the overexpression of Rab5a and Rab7 in thyroid adenomas¹⁵¹ and the upregulation of Rab1b, Rab4b, Rab10, Rab22a, Rab24 and Rab25 in hepatocellular carcinomas and cholangiohepatomas¹⁵².

A number of FTase inhibitors and GGTase-I inhibitors have been developed over the past decade¹⁵³⁻¹⁵⁶. Based on their inhibitory mechanism these inhibitors can be divided into different classes. For example, some inhibitors inhibit prenyltransferases by competitive binding with either isoprenoid substrate or CAAX peptides, in some cases with both substrates. One another class of inhibitors coordinates the catalytic zinc ion to inhibit the enzyme activity. Some of the identified FTase or GGTase-I inhibitors are being evaluated in clinical trials as anticancer¹⁵⁷⁻¹⁶¹, antiparasitic¹⁶²⁻¹⁶⁴, antifungal^{165;166}, and antiviral^{167;168} therapeutic agents. Several FTase inhibitors displaying high inhibitory activity, such as R115777 (tipifarnib), SCH66336 (lonafarnib) and BMS214662 are currently as anticancer candidates in clinical phase II or III studies¹⁶⁹. A few effective and specific inhibitors of GGTase-I have also been developed¹⁷⁰. However, till now only one specific but weak phosphonocarboxylate inhibitor of RabGGTase, NE10790, has been identified¹⁷¹.

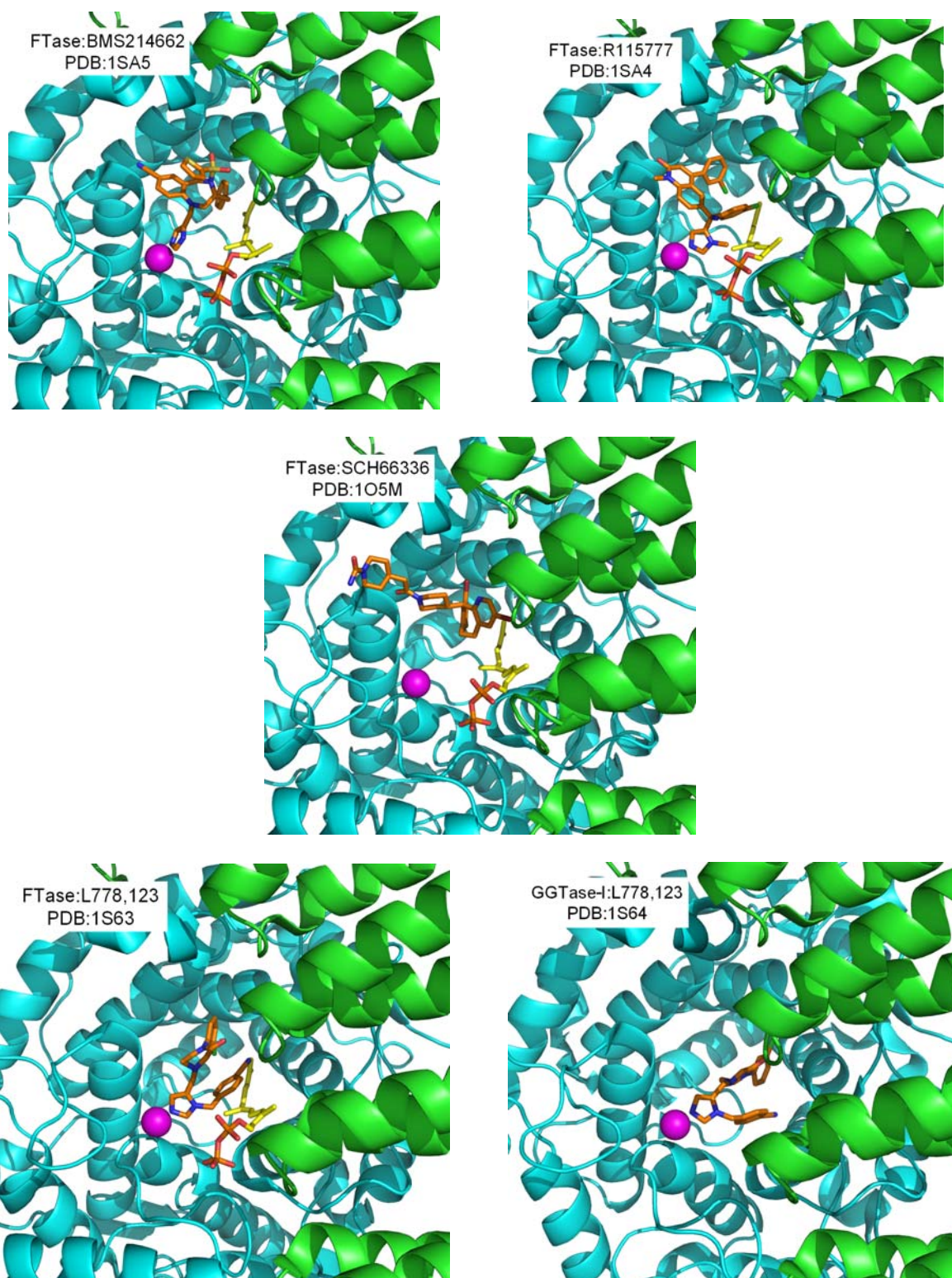


Figure 1.10: FTase or GGTase-I in complex with inhibitors currently evaluated in anticancer clinical trials. The α subunit (green) and β subunit (cyan) of FTase or GGTase-I are in cartoon representation, Zn^{2+} is shown as a magenta ball. Inhibitors and FPP are represented in atomic colours. The complex structures revealed a molecular basis for the inhibitory activities of the inhibitors.

The crystal structures of FTase or GGTase-I in complex with several inhibitors have been determined^{154;155;172} (Figure 1.10). Analysis of these complexes reveals the inhibitory mechanism of the inhibitors. The availability of such structures should facilitate the development of more effective and selective inhibitors by structure-guided ligand design.

Many developed inhibitors display dual specificity. For example, compound L-778,123 inhibits both FTase and GGTase-I¹⁵⁴. Remarkably, the crystal structures of FTase and GGTase-I in complex with this inhibitor indicate that it inhibits the enzymes through different mechanisms (Figure 1.10). In the case of FTase this inhibitor is competitive with the CAAX motif, whereas in the case of GGTase-I it is competitive with the isoprenoid substrate. The Bristol-Myers Squibb compounds, such as BMS1, BMS2, BMS3 and BMS4, are also inhibitors with dual-specificity and inhibit both FTase and RabGGTase¹³¹.

During the development of BMS inhibitors, several compounds displayed proapoptotic activity in human cancer cells. However, the activity was not induced by inhibition of either FTase or GGTase-I¹⁷³. Similar proapoptotic effects were observed by knockdown of RabGGTase gene and specific Rab protein genes^{131;174-176}. Several biochemical and genetic studies indicate that the proapoptotic activity of the BMS compounds is related to their inhibition of RabGGTase^{131;176}. These studies demonstrate that inhibition of RabGGTase can induce apoptosis in human cancer cells, and suggest that RabGGTase is a promising anti-cancer target.

2 Aims of the project

Despite significant progress, RabGGTase remains the least studied prenyltransferase and the exact mechanism of substrate selection and product release remains unclear. The lack of structural information is in part due to difficulties in obtaining high quality crystals of RabGGTase.

This project firstly aims to address the mechanism of REP mediated Rab geranylgeranylation by determination of the structures of RabGGTase in the apo form and in complex with phosphoisoprenoids, including the native lipid donor GGPP, as well as FPP, GGMP and GGTP. Such structures would give mechanistic insights into lipid substrate specificity of RabGGTase, the mode of isoprenoid binding to RabGGTase, explain the large difference in affinity of the farnesyl and geranylgeranyl moieties and complete the pictures of substrate:enzyme complexes for the protein prenyltransferase family.

Secondly, the structure of RabGGTase in complex with both the intermediate and the final product, namely mono- and di-prenylated peptides mimicing the mono- and di-prenylated Rab, should increase our understanding of the Rab prenylation reaction pathway.

More recent studies validated RabGGTase enzyme as a promising target for anti-cancer therapy¹³¹. To study the role of RabGGTase in cancer, as well as the biological function of Rabs, potent and selective inhibitors of the enzyme with activity in cells would be invaluable. In addition, specific inhibitors of RabGGTase may have potential medical application. However, currently such compounds are not available¹³¹. Thus the third aim of this project is the structural determination of RabGGTase in complex with potential inhibitors. Such structures would reveal the molecular basis for the inhibition, potentially allowing development of more effective and selective inhibitors for RabGGTase by structure-guided ligand design.

3 Materials and methods

3.1 Materials

3.1.1 Bacterial strains

E. coli Strain	Genotype	Company
BL21 CodonPlus (DE3) RIL	<i>B F ompT hsdS(rB⁻ mB⁻) dcm+Tet^r E. coli gal λ (DE3) endAHte [argU ileY leuWCamr]</i>	Stratagene
XL1 Blue	<i>recA1, endA1, gyrA96, thi-1, hsdR17, supE44, relA1, lac [F', proAB, lacIqZΔM15, Tn10 (Tetr)]</i>	Stratagene

3.1.2 Media and antibiotics

LB (Luria-Bertani) medium	10 g/l tryptone
	10 g/l NaCl
	5 g/l yeast-extract
LB Plattenagar	10 g/l tryptone
	10 g/l NaCl
	5 g/l extract
	20 g/l agar
TB (terrific broth) medium	12 g/l tryptone
	24 g/l yeast-extract
	0.4% (v/v) glycerol
	2.31 g/l KH ₂ PO ₄
	12.54 g/l K ₂ HPO ₄

Antibiotics

Ampicillin 125 mg/l medium

Kanamycin 50 mg/l medium

Chloramphenicol 35 mg/l medium

3.1.3 Biochemicals and chemicals

Unless otherwise noted all chemicals were purchased from Aldrich (Steinheim), Amersham-Pharmacia (Freiburg), Boehringer Mannheim (Mannheim), Fluka (Neu-Ulm), Merck (Darmstadt), Roche (Mannheim), GERBU (Gaiberg), Serva (Heidelberg), Invitrogen (Karlsruhe), Qiagen (Hilden), Roth (Karlsruhe), Serva (Heidelberg), Sigma-Aldrich (Deisenhofen) and Jena Bioscience (Jena).

Protein Standard

SDS-6 97 / 66 / 45 / 30 / 20 / 14 kDa Amersham (Freiburg)

DNA Standard

GeneRuler™ Fermentas (St. Leon-Rot)

Chromatography Columns and Material

Hi-Load™ Superdex S75/S200 GE-Healthcare (Freiburg)

HiTrap Chelating HP GE-Healthcare (Freiburg)

Synthesized Chemicals

NBD-FPP

Ser-Cys-Ser-Cys(GG) Synthesized und provide by Prof.
 Ser-Cys(GG)-Ser-Cys Waldmann's group with high purity

Ser-Cys(GG)-Ser-Cys(GG)

RabGGTase inhibitors

MT650

MT670

KT90102

Synthesized und provide by Prof.
Waldmann's group with high purity

BMS3

Psoromic acid

Indofine Chemical company(Hillsborough)

Vectors

pET27b(+)

Novagen

pET28a

Novagen

pET30a

Novagen

pGATEV

Department III / AG Alexandrov

Oligonucleotide primers

All Oligonucleotide primers were purchased from Sigma-Aldrich (Deisenhofen) or MWG-Biotech (Ebersberg).

Primer 1	5`-CAGCAAGTATATAGCATGGCCTTT-3`
Primer 2	5`-GGTCGACGAATTCTCAAGCGTACTCCATCTTGAGAACAC-3`
Primer 3	5`-GGTTCTATCACCGCTGGCTCCTGGGTGCCGGTCCGGCAGGTGT GAGCTGTCAGTGGAAAAG-3`
Primer 4	5`-GCTAGTTATTGCTCAGCGG-3`
Primer 5	5`-GGAGATATAACCATGGCTTCTTCGAGTTCCTTCACCTATTATTG-3`
Primer 6	5`-GTTTGATCTCGAGTCATTCGCATTCCTCAAAGCCTGGGAC-3`
Primer 7	5`- CCCGTTTGATCTCGAGTCACTTCTGCAGAAAGTGTGTGGTGG-3`

3.1.5 Equipments

ABI PRISM 3700 DNA Analyzer	Applied Biosystems (Langen)
Analytical balance	Sartorius (Göttingen)
Benchtop Centrifuge, Eppendorf 5415C/D	Eppendorf (Cologne)
Benchtop Centrifuge, Avanti J20-XP	Beckman (München)
Bio-imaging System FLA-5000	FujiFilm (Germany)
Biorad Mini-Protean II system	BioRad (München)
Dialysis tube	Schleicher and Schuell (Dassel)
Electroporation cuvette	BioRad (München)
Finnigan LCQ Advantage Max	Thermo Electron Corporation (Dreieich)
Formulatrix	The Scripps Research institute (USA)
FPLC Äkta Prime	Amersham Pharmacia (Freiburg)
FPLC Pharmacia Biotech GradiFrac	GE Healthcare (Uppsala)
Infors-HT Shakers	Infors AG (Bottmingen)
Leica MZ16/M165C	Leica Microsystems (Wetzlar)
Magnetic Stirrer RCT basic	IKA Labortechnik
MALDI-TOF-MS	Applied Biosystems (USA)
METTLER PM 480 Delta Range	Mettler-Toledo-GmbH (Giessen)
Microbiological Incubator	WTC binder (Tuttlingen)

Microfluidizer	Microfluidics Corporation
MJ Research PTC-200	MJ Research (Watertown, USA)
Mosquito Pipetting Station	TTP Labtech (UK)
Nanodrop Spectrophotometer ND-1000	PeQLab (Erlangen)
Olympus CX40	Olympus Optical Co., LTD. (Japan)
pH-Meter 761	Calimatic Knick (Berlin)
Rigaku MicroMax TM -007HF	Rigaku (UK)
Rotors (JA 10-17, 30.50)	Beckman (München)
Spectro Fluorimeter FluoroMax 3	Spex Instruments Inc. (Edison, USA)
Thermomixer Comfort	Eppendorf (Hamburg)
Ultracentrifuge, Beckman Optima L-70K	Beckman (München)
UV/VIS-Spectrometer DU 640	Beckman Coulter (USA)

3.2 Molecular biological methods

3.2.1 Agarose gel electrophoresis

Agarose gels were prepared and run according to standard procedures¹⁷⁷. Agarose gel electrophoresis was used for analytical and preparative separation of DNA fragments. The method is based on the migration of the negatively charged DNA towards the anode in an electric field. The rate of migration of a DNA fragment through the agarose gel is inversely proportional to the logarithm (\log_{10}) of the number of base pairs. DNA bands were visualized by staining with the intercalating fluorescent dye Ethidium bromide and subsequent illumination under UV light. A DNA-molecular weight standard GeneRuler™ (Fermentas, St. Leon-Rot) was used to determine the DNA-fragment size. To cast the gel, 0.8 to 2% (w/v) agarose was melted in TAE buffer (0.2 M Tris, 5 mM EDTA, pH adjusted to 8 with acetic acid) and supplemented with 0.5 $\mu\text{g/ml}$ Ethidium bromide and poured into a casting tray of the desired size. The gel was placed in an electrophoresis tank and submerged in TAE buffer. The DNA probes were mixed with 1/2th volume equivalent DNA loading buffer and the gels were run at 12 V/cm.

3.2.2 Preparation of plasmid DNA

Plasmid DNA was isolated from bacteria cultures by alkaline lysis of the bacterial cells using the plasmid Mini-prep Kit (peQLab Biotechnology GmbH) according to the protocols of manufacturer.

To amplify the plasmid of interest *in vivo*, a small culture (10 ml) of bacteria (*E. coli* XL1 Blue) was incubated with the appropriate antibiotic(s). The bacteria were harvested by centrifugation at 5000 \times g for 5 min and lysed by alkaline/SDS treatment. Chromosomal DNA, lipids and protein were precipitated and subsequently removed by centrifugation for 10 minutes at 5000 \times g while the plasmid DNA was left in supernatant. The supernatant was filtrated through the spin column by centrifugation at 5000 \times g for 1 minute, followed by a washing step. Plasmid DNA was eluted using 50 μl sterile buffer (10mM TrisHCl pH 8.0) or deionized water.

3.2.3 Polymerase chain reaction (PCR)

Amplification of DNA fragments was carried out using High Fidelity Expand Polymerase mix from Roche (Mannheim) according to standard procedures^{177;178}.

In brief, a 50 µl reaction mixture contained 1 – 10 ng of template DNA, 10 pM of upstream and downstream primers, 100 µM of dNTP mix, 2 – 4 units of High Fidelity Expand Polymerase mix from Roche (Mannheim) as well as the corresponding reaction buffer. The PCR-reaction was performed with a MJ Research PTC-200. Firstly, a denaturation step was performed for 1 min at 96 °C, followed by annealing for 30 sec at 55 – 65 °C depending on primer length and GC content. The extension step occurred at 72 °C for 2 – 3 min, depending on the length of the amplified DNA fragment. In general, ca. 20 cycles were performed for amplification. Prior to further use, the salts in the reaction buffer were removed from the PCR reaction mixture using the Cycle-Pure Kit from PeQLab (Erlangen).

3.2.4 DNA digestion

DNA was digested using restriction enzymes and buffers from New England Biolabs (Beverly) or Fermentas (St. Leon-Rot) according to the protocols of manufacturer.

The reaction mixture was incubated at the appropriate temperature and stopped by addition of DNA loading buffer after 1-2 h. The digested fragments were separated using agarose gel electrophoresis (see 3.2.1), which was followed by isolation (see 3.2.2) using the Gel Extraction Kit from PeQLab (Erlangen).

3.2.5 Ligation

For ligation ca. 100 ng of linearised vector was mixed with a five fold molar excess of insert DNA in reaction buffer using 10U T4-DNA ligase from New England Biolabs (Beverly) for 1 – 2 h at 25 °C.

3.2.6 Preparation of competent cells

Competent expression (*E. coli* BL21 CodonPlus (DE3) RIL) or amplification (*E. coli* XL1 Blue) cells were prepared as follows¹⁷⁹: 5ml LB media was inoculated with a single colony of *E. coli* cells and incubated overnight at 37°C with shaking. 2.5 ml of this preculture was mixed with 250 ml LB media and grown to an optical density (OD600) of 0.8. The cells were

harvested by centrifugation for 10 minutes at 4°C and 2000×g. The pellet was washed with 250 ml sterile H₂O at 4°C, twice, and then mixed with 5 ml 10% (v/v) glycerol and centrifuged. The cell pellet was resuspended in approximately 2.5 ml GYT media (10% (v/v) glycerol, 0.125% (w/v) yeast extract, 0.25% (w/v) tryptone), aliquoted into 70 µl portions, flash frozen in liquid nitrogen and stored at -80°C.

3.2.7 Transformation

Electrotransformation was performed by applying a high voltage pulse using the *E. coli* Pulser from Biorad at 25 µF, 200 Ω and 2.5 kV¹⁷⁷.

Briefly, ca. 1 ng of ligated DNA fragment was mixed with the competent cell suspension in an electroporation cuvette on ice. After electrotransformation 1 ml of LB medium was added to the cell suspension and the culture incubated at 37 °C for 1h. Transformed cells were selected on agar plates containing the appropriate antibiotics.

Ligated DNA was initially transformed in *E. coli* XL1 Blue, amplified and purified. The purified DNA was transformed in *E. coli* BL21 CodonPlus (DE3) RIL expression bacteria.

3.2.8 Bacteria storage

Glycerol stocks of transformed bacteria were made by adding an equivalent volume of 50% sterile glycerol to an overnight culture. Stocks were stored at -80 °C.

3.2.9 DNA sequencing

DNA sequencing was carried out according to¹⁸⁰ using the BigDyeDesoxy terminator cycle sequencing kit (Applied Biosystems, Weiterstadt). A sequencing reaction mixture typically included 500 ng DNA, 4 µl terminator mix, 3.2 pmol sequencing primer in a volume of 10 µl. The sequencing PCR and DNA precipitation was carried out according to the protocols of manufacturer. Analysis of the sequencing products was performed on an ABI PRISM 3700 DNA Analyzer (Applied Biosystems, Langen).

3.3 Expression and purification of proteins

3.3.1 Growth and harvest of bacteria expressing prenyltransferases

The α and β subunit of all prenyltransferase variants were co-transformed into *E.coli* BL21CodonPlus(DE3) RIL cells. Cells were grown in a 37°C shaker at 200 rpm to an A600 of 0.7-0.8. The α subunits of FTase or RabGGTase were expressed as an N-terminal 6 \times His- and GST-Tag fusion protein and the β subunit of FTase or RabGGTase was expressed as the wild-type protein. Expression was induced with 100 μ M isopropyl- β -D-thiogalactoside at 37°C for FTase or 16°C for RabGGTase. After cell growth, the cells were pelleted at 5000 \times g for 15 min at 4°C; the cells were re-suspended in lysis buffer (50 mM Na₂HPO₄, pH 8.0, 0.3 M NaCl and 2 mM β -mercaptoethanol) and were frozen at -80°C¹⁸¹.

3.3.2 Nickel-NTA affinity chromatography

The frozen cell pellet was resuspended in ice-cold lysis buffer (see 3.3.1) containing 1 mM protease inhibitor PMSF (phenylmethylsulfonyl fluoride). The cells were lysed using a microfluidizer (Microfluidics Corporation, USA) at a pressure of 950 kPa. The cell debris was removed from the lysate by centrifugation at 90,000 \times g at 4°C for 30 min and the supernatant was filtered. The lysate was loaded onto a Ni-NTA column (HiTrap Chelating HP, GE-Healthcare) equilibrated in lysis buffer (see 3.3.1). After washing with 3-5 column volumes with lysis buffer (see 3.3.1), the bound N-terminal hexa-histidine and GST fusion α subunit in complex with β subunit were eluted on a 5-200 mM imidazole gradient. Protein containing fractions were identified by analysis on 15% SDS-PAGE and pooled.

3.3.3 Removal of 6 \times His-tag and size exclusion chromatography

To remove the histidine- and GST-Tags from the α subunit of FTase or RabGGTase, TEV protease was added at a 1:40 molar ratio and the sample was dialyzed against 25 mM Na₂HPO₄, pH 8.0, 1 mM EDTA and 2 mM β -mercaptoethanol at 4°C. The progression of the cleavage reaction was determined by SDS-PAGE. TEV protease and 6 \times His-GST-Tag were removed by passing the dialysed sample over a Ni-NTA column (HiTrap Chelating HP, GE-Healthcare). The flowthrough was concentrated and then loaded on a Superdex S200 size exclusion column (GE-Healthcare) pre-equilibrated with gel-filtration buffer (25 mM HEPES pH 7.2, 40 mM NaCl, 5 mM β -mercaptoethanol) as a further purification procedure to obtain

pure protein for crystallisation purposes. The fractions containing pure protein were identified using SDS-PAGE and pooled.

3.3.4 Concentrating proteins by ultra-filtration

The pooled pure fractions were concentrated to ca. 20 mg/ml by a centrifugal concentrator or Amicon chamber (Vivascience, Lincoln, USA) with a 30 kDa cut off filter by centrifugation at 3000×g at 4°C. Aliquots were flash-frozen in liquid nitrogen and were stored at –80° C.

3.3.5 SDS-PAGE

For the analysis of proteins, one-dimensional gel electrophoresis was carried out using denaturing 15% SDS-polyacrylamide gel electrophoresis (SDS-PAGE) according to the standard protocol¹⁷⁷.

3.4 Biochemical and biophysical methods

3.4.1 Determination of protein concentration

Protein concentrations were determined using the Biorad protein assay solution¹⁸². This solution was calibrated prior to use by bovine serum albumin (BSA).

3.4.2 Fluorescence spectroscopy

Fluorescence is highly sensitive to the environment around fluorophore, what makes it very valuable for kinetic and other investigations of molecular interactions.

NBD-FPP is a fluorescent analogue of geranylgeranyl pyrophosphate that binds to RabGGTase competitively to its natural lipid substrate^{92;183}. The fluorescent NBD fluorophore serves as a read-out for interactions between RabGGTase and isoprenoids, as well as between RabGGTase and mono- or di-prenylated Rab7 C-terminal peptides.

To determine the affinities between RabGGTase and mono- or di-prenylated Rab7 C-terminal peptides, competitive titration¹²⁵ was carried out using a Fluoromax 3 Spectro fluorimeter (SPEX instruments S.A., Inc., Edison, USA) in 0.4 x 1 cm² cuvettes at 25°C. 200 nM NBD-FPP was mixed with 1 µM prenylated peptide in 50 mM Hepes pH 7.2, 50 mM NaCl, 2 mM MgCl₂, 5 mM DTE and 2% DMSO. The mixture was titrated with increasing concentrations of RabGGTase. NBD-FPP was excited at 487 nm and fluorescence was monitored at 550 nm. The decrease in fluorescence upon addition of protein was measured, and at each step the values were averaged after equilibrium. K_d-values were obtained by fitting data using the program Scientist 2.0 as described by Thoma et al. (2000).

3.5 Crystallographic methods

3.5.1 Crystallisation

Initial protein crystallisation is a trial-and-error procedure in which the protein is slowly precipitated from its solution. Usually, crystallogenesis falls into two separate phases. The first is the screening of crystallisation conditions to obtain the first crystalline material, the second is the optimising of the identified conditions to improve the size and quality of the crystal. The classical procedure for slowly precipitating proteins from solution to form a crystal is to gradually increase the level of saturation by addition of a precipitant. The typical precipitating agents include salts (such as ammonium sulphate), organic solvents (such as glycerol and methylpentanediol (MPD)), and highly soluble synthetic polymers (such as polyethylene glycol (PEG)).

3.5.2 Crystallisation by vapour diffusion methods

Vapour diffusion was first used for the crystallization of tRNA¹⁸⁴ and now it is the most widely used method for protein crystallisation. A drop containing the protein to crystallise with buffer, precipitating agent with appropriate ions, is equilibrated against a reservoir of precipitating agent in a sealed container. Equilibration occurs by diffusion of water molecules until the vapour pressure in the drop equals that in the reservoir. During equilibration the concentration of all constituents in the drop increases, which in turns lead to nucleation in the drop. In this work, two variations of vapour-diffusion, ‘hanging drop’ and ‘sitting drop’ methods, are used. The details of protein crystallizations are described in the results and discussion (see 4.5 and 4.6).

3.5.3 Co-crystallisation and crystal soaking

Co-crystallisation and soaking are two common approaches used in seeking structures of proteins in complex with small molecules, such ligands and inhibitors.

In the soaking approach, the compound is incubated with protein crystals, which have been crystallized in the absence of ligands or inhibitors. The soaked ligand or inhibitor is expected to diffuse into the crystals and to associate with their binding site of the protein, such as the active site of enzyme. Protein crystals typically have a high solvent content, ranging from 30 to 80%¹⁸⁵. This solvent forms channels through the crystals, typically from 20 to 100 Å in

diameter¹⁸⁶, and allows the diffusion of small molecules. Ideally, the protein in the crystal should have sufficient freedom to undergo conformational changes induced by binding to the small molecules.

In the co-crystallisation approach, the ligands or inhibitors are incubated with the protein prior to crystallisation and the complex is then crystallized. In some cases conditions for co-crystallisation of a protein in complex with ligands or inhibitors may differ from that of the apoenzyme or of other compound complexes.

3.5.4 Cryo-crystallography

In many cases, protein crystals are prone to radiation damage over the time caused by the formation of solvent-derived free radicals in the crystals. Cryo-crystallography (at 100K) is a powerful means to overcome such hurdles, since the low temperatures can slow-down the process of radical formation by preventing the heating of the crystals when exposed to x-rays.

Cryo-crystallography enables the measurement of a complete data set from a single crystal. In some cases it provides higher resolution than room temperature measurement, it is suggested that cooling may increase the internal order of the parts of the protein which are mobile at room temperature¹⁸⁷. For cryo-crystallography, the crystals are transferred into a suitable cryo-protectant solution and mounted on a cryo-nylon loop. The crystals are then flash-frozen in liquid nitrogen. To prevent the formation of ice crystals, the cryo-protectants commonly contain appropriate concentrations of glycerol, ethelene glycol, MPD, PEGs or sugars.

3.5.5 Data collection

All cryoprotected crystals were first tested on an in-house source, which used a copper rotating X-ray anode with an Osmic mirror ($\lambda = 1.5419 \text{ \AA}$, 50 kV, 100 mA, 0.1 mm collimator). Usually, the final datasets were collected at beamline PXII at the Swiss Light Source, Villigen, Switzerland. Data processing, including indexing, integration and scaling, was carried out using the program XDS¹⁸⁸. The quality of the datasets were validated based on the I/σ (signal to noise ratio) where generally a cut-off of 3 is widely accepted, and also by calculating R_{symm} which compares symmetry related reflections according to Equation 1.

$$R_{\text{symm}} = \frac{\sum_{hkl} \sum_i |I_i - \langle I \rangle|}{\sum_{hkl} \sum_i |I_i|} \quad \text{Equation 1}$$

h, k, l – indices of independent reflections with the average intensity $\langle I \rangle$

I_i – intensities of independent reflections.

3.5.6 Matthews coefficient and solvent content analysis

Based on the volume of the asymmetric unit and the molecular weight of the protein, the number of protein molecules present in a unit cell can be estimated¹⁸⁹. The Matthew coefficient V_M is described by Equation 2.

$$V_M = \frac{V}{Mw \cdot Z} \quad \text{Equation 2}$$

V – Volume of the asymmetric unit in \AA^3

Mw – Molecular weight of the monomer in Dalton

Z – Number of molecules in the asymmetric unit

The average Matthew coefficient of a protein crystal is $2.5 \text{ \AA}^3/\text{Da}$ which corresponds to a solvent content of 50%¹⁸⁹.

3.5.7 Phase determination

During data collection, the intensities of waves scattered from planes (denoted by h, k and l) in the crystal are measured. To calculate the electron density at a position (xyz) in the unit cell of a crystal requires a summation over all the hkl planes, which is mathematically expressed in Equation 3.

$$\rho(x, y, z) = \frac{1}{V} \sum_h \sum_k \sum_l |F_{hkl}| \cdot e^{-2\pi i(hx+ky+lz-\alpha'_{hkl})} \quad \text{Equation 3}$$

V – Volume of the unit cell

α_{hkl} – Phase associated with the structure factor amplitude $|F_{hkl}|$

F_{hkl} is a periodic function and possesses amplitude, frequency and phase (α_{hkl}). This is diffracted and thus has the same frequency as that of the x-ray source. The amplitude of F_{hkl} is proportional to the square root of the reflection intensity (I_{hkl}) measured on the detector.

However, the phases are lost during measurement, as there is no formal relationship between amplitudes and phases. Thus phases can be not directly obtained from a single measurement of reflection intensities. The only relationship is via the molecular structure or electron density. Therefore, the values of phases can be evaluated, if there is some prior knowledge of the structure or electron density. This is the basis for all phasing methods (Table 3.1). A detailed description of phase problem is described elsewhere¹⁹⁰. In this work molecular replacement (MR) has been used.

Table 3.1: Different phasing methods, modified from Garry Taylor *Acta Cryst.* (2003).

Phasing Method	Necessary Prior Knowledge
Direct methods	$\rho \geq 0$, discrete atoms
Isomorphous replacement	Heavy-atom substructure
Anomalous scattering	Anomalous atom substructure
Molecular replacement	Homology model
Density Modification (Phase Improvement)	Solvent content, Phase extension, Non-crystallographic symmetry etc.

3.5.8 Phase determination using molecular replacement (MR)

If a homology model is available, molecular replacement can be successfully employed to obtain phase information, as first described by Rossmann & Blow¹⁹¹. In this method, the values of phases for the unknown structure can be evaluated from the coordinates and the structure factor amplitudes (F_{Calc}) of the known structure. In general the space group and the orientation of the unknown structure differ from those of the known structure, thereby the known structure as a search model is required to be reoriented in the new unit cell appropriately. This is achieved by comparing the Patterson functions, which are obtained from the structure factor amplitude (F_{Obs}) of the measured intensities and from the search model (F_{Calc})^{192;193}.

3.5.9 Refinement

After obtaining proper phase information the initial structural model can be built. It contains errors that can be minimised through iterative model refinement. During refinement the

atomic coordinates of the current model were adjusted in order to minimise the difference between experimentally observed structure factor amplitudes (F_{Obs}) and those calculated from the model (F_{Calc}). The quality of the model was evaluated using the crystallographic index ‘R-factor’ and ‘R-free’. The R factor is described by equation 4.

$$R - factor = \frac{\sum_{hkl} \|F_{Obs} hkl\| - \|F_{Calc} hkl\|}{\sum_{hkl} \|F_{Obs} hkl\|} \quad \text{Equation 4}$$

However if the crystallographic data are over-weighted, the R-factor can be artificially lowered at the expense of the stereochemistry of the model. To overcome this over-fitting, 5% of the data (a test set of reflections ‘T’) are isolated from the remainder (the working set) and not used for the purposes of refinement¹⁹⁴. The working set is used for the calculation of the R-factor as described by the equation 4, whereas the test set for the calculation of a new parameter, R-free, which is defined similarly to R factor.

$$R - free = \frac{\sum_{hkl \in T} \|F_{Obs} hkl\| - \|F_{Calc} hkl\|}{\sum_{hkl \in T} \|F_{Obs} hkl\|} \quad \text{Equation 5}$$

The R-free parameter is a sensitive indicator of over-fitting. It is expected, that the value of the R-factor is slightly lower than that of the R-free.

The program REFMAC5¹⁹⁵ was used for refinement and the models were built and adjusted manually using the software COOT¹⁹⁶. The model was validated by the program Procheck¹⁹⁷.

3.5.10 Representation of structures

All figures were generated using the program PYMOL (www.pymol.org, DeLano Scientific LLC) and the final figures were prepared with the help of Photoshop (Adobe Corporation) or Canvas (ACD System Inc.).

4 Results and discussions

Section I

Engineering, cloning and purification of RabGGTase and FTase from *E. coli*

4.1 Engineering of rat RabGGTase mutants

The structural analysis of RabGGTase is hampered by difficulties in reliably obtaining well diffracting crystals. Although RabGGTase has previously been crystallized in the apo form as well as in complex with REP-1 and a farnesyl moiety, in both cases the search for well diffracting crystals required considerable effort^{90;93}. In contrast, both GGTase-I and FTase could be crystallized and a large number of structures in complex with substrate analogues and inhibitors are known^{88;89;198}. Comparing the RabGGTase structure to FTase and GGTase-I, the most striking difference is the presence of two additional domains in the α subunit of RabGGTase, the LRR (Leucine-rich repeat) domain and the IG (Ig-like domain) domain (Figure 4.1). The LRR and IG domains of RabGGTase do not make contacts with the β subunit. Since the LRR (residue 442 to residue 567) and IG (residue 238 to residue 352) domains of mammalian RabGGTase are not involved in its catalytic activity⁹³, we decided to engineer versions of the enzyme in which these domains were deleted. Mutant variants of the α subunit gene lacking sequences for either the LRR or IG domain or both were created. The overall shape of the RabGGTase mutant lacking both LRR and IG domains is expected to be similar to that of FTase or GGTase-I, which could make it more amenable to crystallisation than the parental enzyme. While deletion of the C-terminally located LRR domain is trivial from the protein engineering point of view, removing the IG domain inserted into the middle of the molecule is less obvious. A linker Ala-Gly-Ser-Gly connecting helices 11 and 12 (residues 237 and 353) was designed based on the alignment of yeast and mammalian RabGGTase.

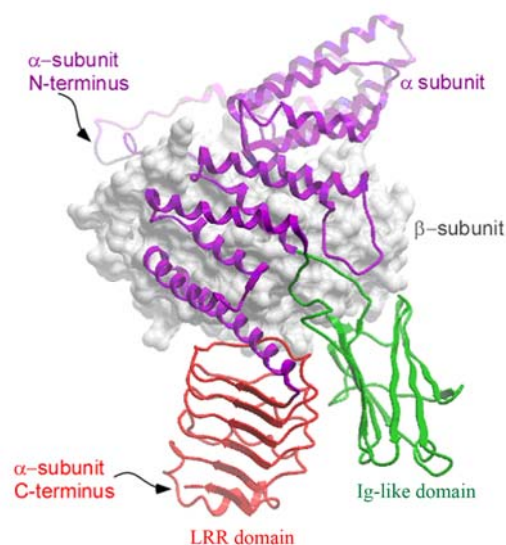


Figure 4.1: Engineering of rat RabGGTase. Structure of wild type mammalian RabGGTase. The α subunit is displayed in ribbon representation and domains are coloured while the β subunit is shown as a molecular surface.

The vectors for *E. coli* expression of mutants of the α subunit of RabGGTase were constructed as follows: pGATEV-RabGGTase_ $\alpha\Delta$ LLR was constructed by a PCR amplification of the RabGGTase α subunit gene with the direct primer 1 (see 3.1.3) annealing to GST tag and the reverse primer 2 (see 3.1.3) using pGATEV-RabGGTase_ α as a template¹⁸¹. The resulting PCR fragment was digested with NdeI and EcoRI and cloned into the pGATEV vector pre-digested with the same enzymes.

pGATEV-RabGGTase_ $\alpha\Delta$ IG was constructed by a two step PCR. In the first step a 5' fragment of the α subunit was PCR amplified using the above described template with specific forward primer 3 and reverse primer 4 (see 3.1.3) annealing to the T7 terminator. The resulting 600bp product was gel purified and used in the second round of PCR as a reverse primer in combination with the direct primer 1 (see 3.1.3) annealing to GST tag. Cloning into the pGATEV vector was performed as described above.

pGATEV-RabGGTase_ $\alpha\Delta$ LLR Δ IG was obtained as described for pGATEV-RabGGTase_ $\alpha\Delta$ LLR but using pGATEV-RabGGTase_ $\alpha\Delta$ IG as a template for the PCR reaction.

In all cases the integrity of open reading frame was determined by sequencing.

4.2 Purification of engineered RabGGTases from *E. coli*

Genes for mutant α and wild type β subunits of RabGGTase were co-expressed in *E. coli* as described in Material and Methods (see 3.3)¹⁸¹ and analyzed for expression level and solubility. Soluble recombinant proteins were observed in the case of the α subunit lacking either the LRR domain or both LRR and IG domains. In both cases the α/β -heterodimer remained stable throughout purification on Ni-NTA and gel filtration columns and could be purified to near homogeneity. As can be see in Figure 4.2, in both mutants the subunits were present at 1:1 stoichiometry, indicating that engineering does not affect the structural integrity of the α subunit (Figure 4.2).

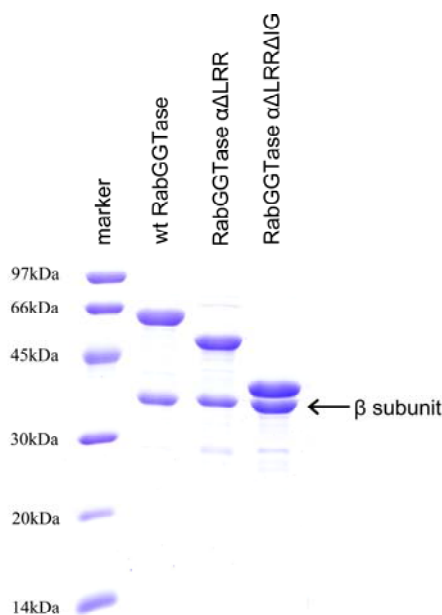


Figure 4.2: Purification of wild type and mutants of rat RabGGTase. SDS-PAGE analysis of recombinantly produced wild type and deletion mutants of RabGGTase.

To confirm that the obtained mutants were catalytically active, a recently described fluorescent *in vitro* Rab prenylation assay¹⁸³ was performed by Yaowen Wu. Briefly, in the *in vitro* prenylation assay 4 μ M Rab7, 4 μ M REP-1, 4 μ M wild type or mutant RabGGTase and 40 μ M NBD-FPP were mixed in a buffer containing 50 mM Hepes pH 7.2, 50 mM NaCl, 2 mM MgCl₂ and 5 mM DTE at room temperature. In control reactions, REP-1 was omitted. The progression of the reaction was monitored by changes in NBD fluorescence. In summary, both mutants were able to prenylate Rab7 with an efficiency comparable to that of wild type enzyme¹⁹⁹ (Figure 4.3). This directly confirms the earlier proposal that IG and LRR domains

of mammalian RabGGTase are not involved in the prenylation reaction and perform an as yet unidentified function⁹².

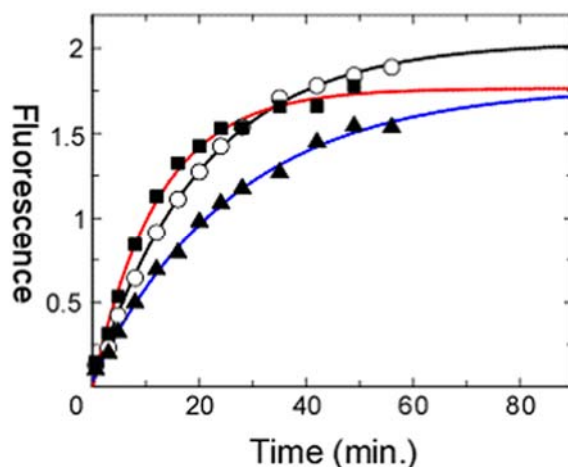


Figure 4.3: Functional analysis of wild type and mutants of rat RabGGTase¹⁹⁹. In the *in vitro* prenylation Rab7 was mixed with wild type and mutants of RabGGTase using NBD-FPP as a substrate. Incorporation of NBD-F into Rab7 was measured as described in Wu, 2006 1640 and plotted against time. Open circles – RabGGTase_αALLRΔIG enzyme, open triangles RabGGTase_αΔIG, filled triangles - wild type enzyme.

4.3 Engineering of rat FTase mutants

Recombinant rat FTase obtained from the insect cell (Sf9)/baculovirus expression system^{95;200}, an expression system with relatively low FTase levels, has been successfully utilized to solve the FTase crystal structure^{91;198}. In this crystal form, the enzyme active site is partially occupied by C-terminal residues of the β subunit from an adjacent molecule in the crystal lattice. This steric obstruction could hinder enzyme ligands from binding to the active site, cause local conformational changes and substantially reduce crystal diffraction resolution⁹⁶. Recently, Weber's group crystallized a β subunit C-terminal truncation mutant and solved its structure at high resolution²⁰¹. The new FTase crystal form contained an open active site. The FTase mutant was obtained by recombinant expression in *E. coli*. It was truncated at the C-terminus of β subunit by 10 amino acid residues and contained an extra 20 amino acid residues including a His-tag at the N-terminus of the α subunit of FTase.

To facilitate the purification of large quantities of protein for crystallographic and thermodynamic studies of FTase:inhibitor interactions and provide a system for the rapid production of site-directed mutants, an *E. coli* expression system for FTase was used in our

research. Analysis of the FTase crystal structure^{91;201} revealed that the β subunit C-terminal tail, primarily the last five amino acid residues, interacts with the active site through a combination of hydrogen bonds and hydrophobic interactions (Figure 4.4). The active site residues involved in the binding were mainly from the β subunit, including residues Trp102 β , His248 β , Lya264 β , Arg291 β , Tyr300 β , Cys345 β , Ser357 β and two α subunit residues Tyr166 α and Asp196 α . Based on this analysis, two β subunit C-terminal truncation mutants, $\Delta 10$ and $\Delta 19$, were designed to eliminate the C-terminal tail from the active site. The $\Delta 10$ truncation would remove the majority of the interaction, while the $\Delta 19$ would further eliminate the binding residues of the C-terminal tail.

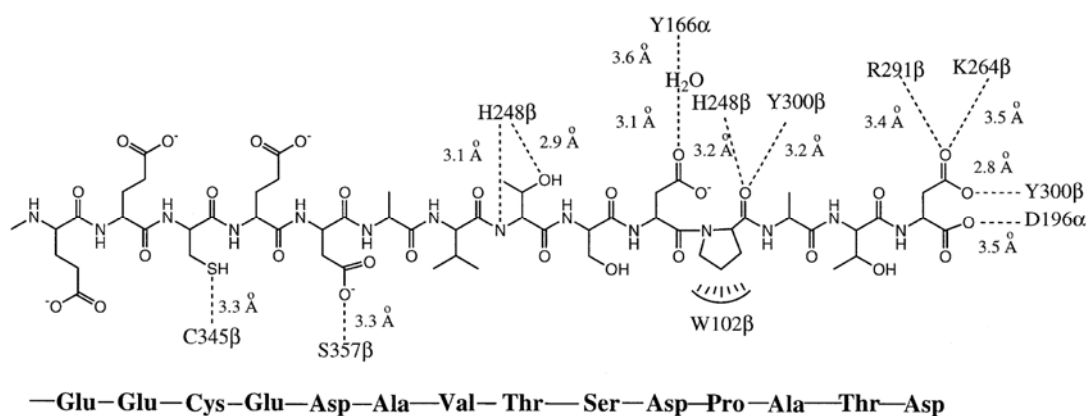


Figure 4.4: Hydrogen bonding and hydrophobic interactions between the β subunit C-terminal tail and the FTase active site residues mapped from the FTase structure (PDB code: 1FT1)⁹¹.

The vectors for *E. coli* expression of β subunit mutants of FTase were constructed as follows: pET27b(+) $\beta\Delta 10$ was constructed by a PCR amplification of the FTase β subunit gene with the forward primer 5 and the reverse primer 6 (see 3.1.3) using pET28a-FTase β as a template. The resulting PCR fragment was digested with NcoI and XhoI and cloned into the pET27b(+) vector pre-digested with the same enzymes.

The vectors pET27b(+) $\beta\Delta 19$ was obtained as described for pET27b(+) $\beta\Delta 10$ but using the forward primer 5 and the reverse primer 7 (see 3.1.3) for the PCR reaction.

In addition, the N-terminal domain (~50 amino acids) of α subunit is disordered in FTase. To improve the chance of FTase crystallisation an α -subunit N-terminal truncation mutant ($\Delta 50$) was designed to eliminate the flexible N-terminal tail.

The vectors for *E. coli* expression of mutant of α subunit of FTase were constructed as follows: pGATEV $\alpha\Delta 50$ was constructed by a PCR amplification of the FTase α subunit

gene with the forward primer 8 and the reverse primer 9 (see 3.1.3) using pGATEV-FTase $_{\alpha}$ as a template. The resulting PCR fragment was digested with NcoI and XhoI and cloned into the pGATEV vector pre-digested with the same enzymes.

In all cases the integrity of open reading frame was determined by sequencing.

4.4 Purification of wild-type and engineered FTases from *E. coli*

Genes for α and β subunits (wild-type or mutant) of FTase were co-expressed in *E. coli* as described in Material and Methods (3.3)¹⁸¹. Soluble recombinant protein could be obtained and the α/β -heterodimer remained stable throughout purification on Ni-NTA and gel filtration columns and could be purified to near homogeneity in all cases. In all mutants the subunits were present in 1:1 stoichiometry indicating that engineering does not affect the structural integrity of the heterodimer (Figure 4.5).

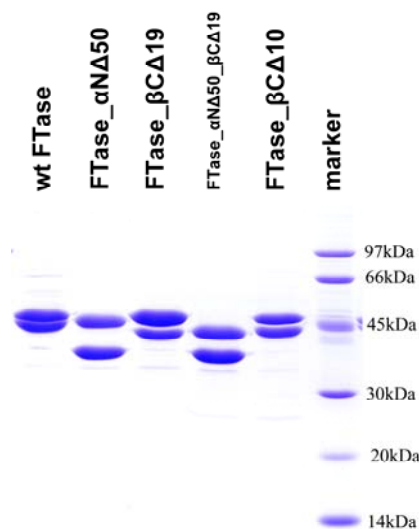


Figure 4.5: Purification of wild type and mutants of rat FTase. SDS-PAGE analysis of recombinantly produced wild type and truncation mutants of FTase.

To confirm that the obtained variants of FTase were catalytically active, a recently described fluorescent in vitro prenylation assay^{202;203} was performed. In this assay Ypt7 was used and expressed in *E. coli* with the C-terminal extension TKCVIM, derived from a mammalian K-Ras protein. Briefly, in the prenylation reaction 15 μ M Ypt7_TKCVIM, 3 μ M variants of FTase and 45 μ M fluorescent isoprenoid substrates NBD-GPP were mixed in a buffer

containing 50 mM Hepes pH 7.2, 50 mM NaCl, 2 mM MgCl₂ and 5 mM DTE. Control samples were supplemented with an excess of FPP (225 μM) that would compete with the fluorescent analogues and thus yield non-fluorescently prenylated Ypt7_TKCVIM. The reaction proceeded for 2 h at room temperature and was quenched by addition of SDS-PAGE sample buffer, after which the samples were resolved on a 15% SDS-PAGE gel and scanned for fluorescence using a fluorescent image reader followed by Coomassie blue staining.

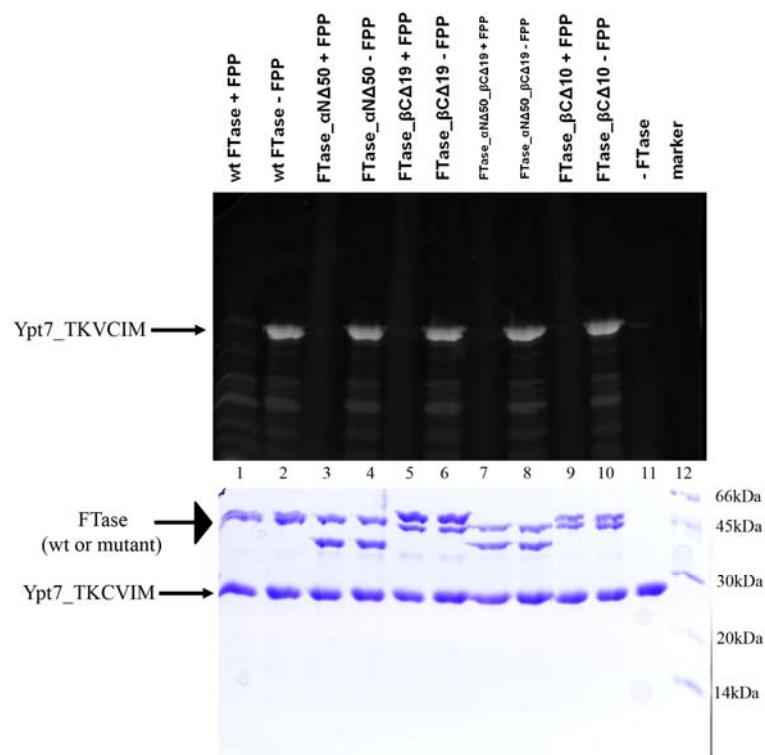


Figure 4.6: Functional analysis of wild type and mutants of rat FTase. SDS-PAGE gels of the fluorescently labeled Ypt7_TKCVIM proteins after prenylation with NBD-GPP mediated by variants of FTase. The control reactions were supplemented with a 5-fold excess of FPP over the fluorescent isoprenoid. Upper panels represent the fluorescent scans of the gels, while the lower panels show the same gels stained with Coomassie blue. Under these conditions incubation of all variants of FTase with protein substrate Ypt7_TKCVIM led to emergence of fluorescent bands with comparable intensities corresponding to prenylated Ypt7_TKCVIM. No fluorescent product was generated when FTase was omitted.

As can be seen in Figure 4.6 under these conditions incubation of all variants of FTase with protein substrate Ypt7_TKCVIM led to emergence of fluorescent bands with comparable intensities corresponding to prenylated Ypt7_TKCVIM. No fluorescent product was generated when FTase was omitted (Figure 4.6). In summary, all mutants were able to prenylate Ypt7_TKCVIM with an efficiency comparable to that of wild type enzyme.

Section II

Crystallisation and structural determination of protein prenyltransferases

4.5 Crystallisation and structural determination of RabGGTase_ α Δ LRR Δ IG mutant

Initial crystallisation conditions were found at 20 °C using 100 nl of the Classics, PEG, PEG II, JCSG, PACT and protein complexes suites from Qiagen plus 100 nl of protein solution of RabGGTase mutants (RabGGTase_ α Δ LRR Δ IG or RabGGTase_ α Δ LRR) in sitting drops, set up against a 50 μ l reservoir using a Mosquito nanolitre dispensing robot (Molecular Dimensions Limited). Crystals were observed only with the enzyme in which the α subunit lacked both LRR and IG domains (Figure 4.7, left).

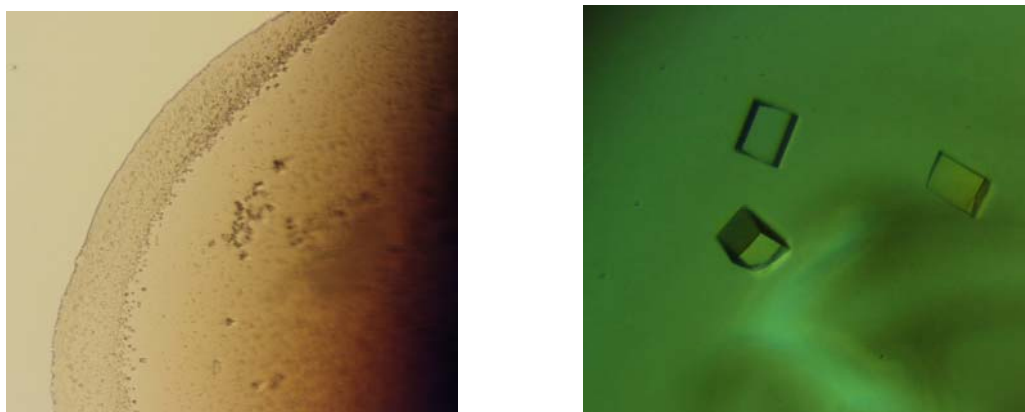


Figure 4.7: Crystals of the RabGGTase_ α Δ LRR Δ IG mutant obtained during the initial crystallisation screening (left) and after optimization of crystallisation condition (right).

Promising conditions were optimized with respect to precipitant composition, pH, temperature and protein concentration, changing the setup to hanging drops, prepared by mixing 1 μ l of protein solution with 1 μ l of precipitant mixture. The crystals for data collection were obtained at 12°C with a reservoir consisting of 14% (w/v) PEG 3350, 0.2 M CaAc₂, 0.1 M HEPES pH 7.2. The protein was supplied at 14 mg/ml in a buffer containing 25 mM HEPES pH 7.2, 40 mM NaCl, 5 mM β -mercaptoethanol. The observed crystals formed in a cubic shape and grew to a size of approximately 60*60*60 μ m within 1 day (Figure 4.7, right).

Prior to flash-cooling in liquid nitrogen, the crystals were briefly washed in 20% (w/v) PEG 3350, 5% (v/v) glycerol, 0.2 M CaAc₂, 0.1 M HEPES pH 7.2. Diffraction data were collected at 100 K, at station X10SA of the Swiss Light Source (SLS Villigen, Switzerland). The data were processed with XDS¹⁸⁸. The crystals belong to the orthorhombic space group P212121, contain one RabGGTase_αΔLRRΔIG complex in the asymmetric unit, and diffract to 1.8 Å resolution.

Initial phases were determined by molecular replacement with PHASER²⁰⁴ of the CCP4 suite²⁰⁵, using coordinates of RabGGTase in the RabGGTase:REP-1 complex (PDB code 1LTX)⁹³ from which the IG and LRR domains had been deleted. The model was then corrected by alternating rounds of refinement in REFMAC5¹⁹⁵ and manual adjustment in COOT¹⁹⁶. Full data collection and refinement statistics are given in Table 4.2. Coordinates and structure factors have been deposited in the Protein Data Bank PDB²⁰⁶ with entry code xxxx.

The structure of the RabGGTase mutant was determined to 1.8 Å resolution by molecular replacement. The final model of RabGGTase_αΔLRRΔIG contains 394 water molecules, one Zn²⁺ ion and two Ca²⁺ ions. The structure is refined to an R-factor of 18.5 % and R_{free} of 21.8 %. The model of the RabGGTase mutant contains an α/β heterodimer in the asymmetric unit. Of the total residues for the RabGGTase mutant structure, 90.8 % lie in the most favoured region of the Ramachandran plot (PROCHECK¹⁹⁷). Most of the residues with poorer electron density are located in the additionally allowed regions, with no residue in the disallowed region.

Figure 4.8 A shows a cartoon representation of the engineered molecule, which bears the typical hallmarks of a prenyltransferase: a crescent-shaped α-subunit formed by seven successive pairs of helical hairpins wrapped around the β subunit. The β subunit folds into an α-α barrel consisting of six core and six peripheral helices.

As expected the overall structure of the engineered enzyme changed very little compared to the wild type protein with an overall C_α RMS-deviation of 0.85 Å for 602 residues (Figure 4.8 B). Most of the changes are represented by shifts in the position of α-helices in the α subunit while the β subunit is essentially unchanged with a C_α RMS-deviation of 0.35 Å. Electron density is missing for the flexible 18 N-terminal amino acids and for the loop region between helices 9 and 10. The engineered link between helices 11 and 10, on the other hand,

is visible in the electron density (Figure 4.8 A), indicating that the chosen length and sequence were appropriate to create a defined structure.

Similar to the native enzyme the mutant contains the catalytic Zn^{2+} ion at the top of the active site funnel in the β subunit. The Zn^{2+} ion is coordinated by Asp238 β , Cys240 β and His290 β (Figure 4.8 A) in a fashion identical to that observed in wild type RabGGTase.

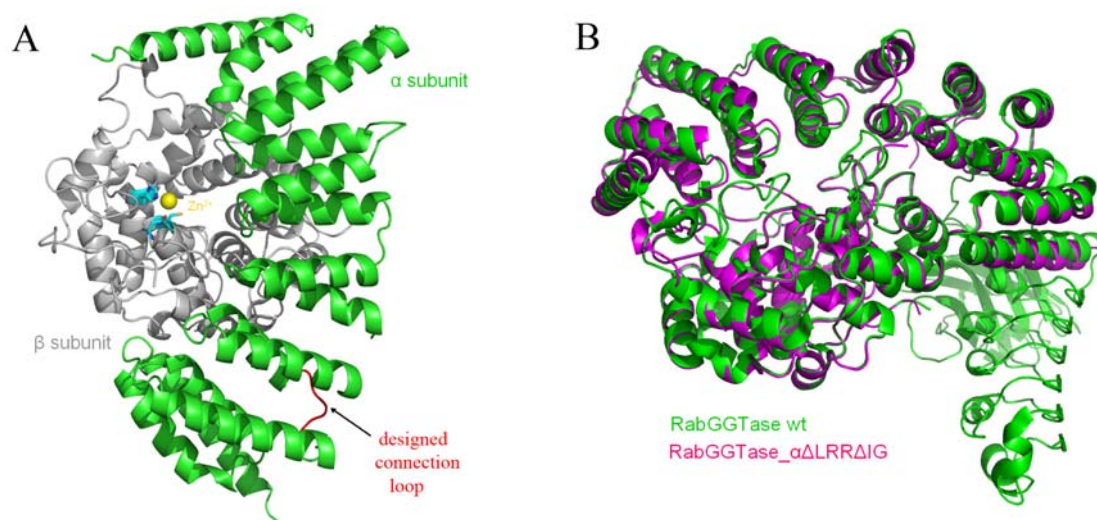


Figure 4.8: Overall structure of RabGGTase_αΔLRRΔIG mutant and Zn^{2+} binding site. (A) The α (green) and β (gray) subunits are displayed in cartoon and Zn^{2+} (yellow) in sphere representation. The designed connection loop Ala-Gly-Ser-Gly is coloured in red. The residues coordinated with Zn^{2+} (D238 β , C240 β and H290 β) are displayed in stick representation. (B) Superposition of wild type RabGGTase (green, PDB code: 1DCE)⁹⁰ and the RabGGTase_αΔLRRΔIG mutant (magenta) demonstrates the structural similarity. The α and β subunits of the both proteins are displayed in cartoon and Zn^{2+} in sphere representation.

4.6 Crystallisation and structural determination of FTase mutants

Initial crystallisation screening experiments were performed as described above (4.5) using wild type and engineered FTase from *E. coli*. A number of distinct crystal shapes was observed using the different FTase mutants in various conditions. After optimization of the crystallisation conditions, crystals of sufficient size could be obtained (Figure 4.9). Diffraction to a high resolution shell, however, was observed only in the case of the construct FTase_α_βCΔ10 (lacking 10 amino acids at the C-terminus of β subunit).

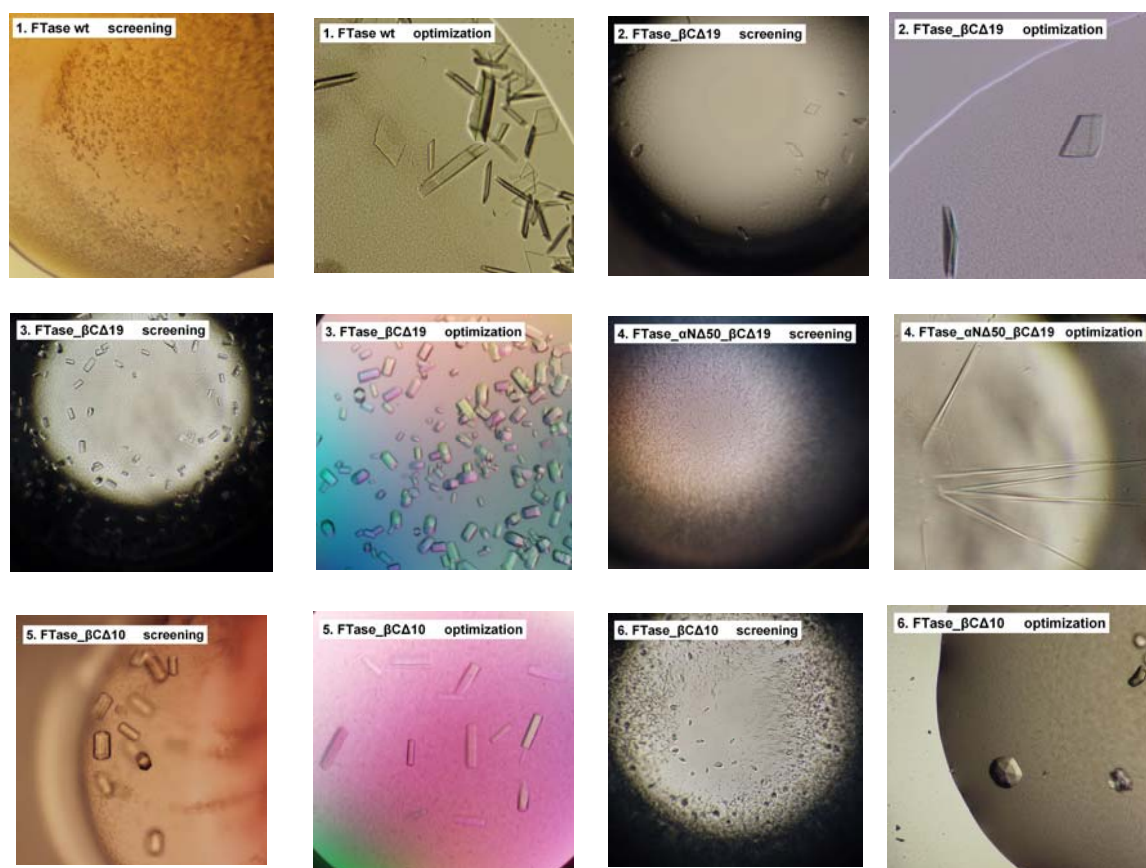


Figure 4.9: Crystals of FTase wt and mutants obtained during initial crystallisation screening and after optimization of crystallisation conditions.

High resolution crystals (images numbered 6 in Figure 4.9) of FTase_α_βΔ10 were obtained at 20°C with the hanging drops method by mixing 1 μl of protein solution with 1 μl of precipitant mixture consisting of 20% (w/v) PEG 4000, 0.2 M MgCl₂, 0.1 M Tris pH 7.5. The protein was supplied at 10 mg/ml in a buffer containing 25 mM HEPES pH 7.2, 40 mM NaCl, 5 mM β-mercaptoethanol. The crystals (6 in Figure 4.9) had a hexagonal shape and grew to a size of approximately 60*60*20 μm within 1 week.

Prior to flash-freezing in liquid nitrogen, the crystals were washed in 20% (w/v) PEG 3350, 5% (v/v) glycerol, 0.2 M MgCl₂, 0.1 M Tris pH 7.5. Data sets were collected at 100 K, at station X10SA of the Swiss Light Source. The data were processed as described above (4.5). The crystals belong to the hexagonal space group P61, contain one FTase_α_βΔ10 complex in the asymmetric unit and diffract to 2.8 Å resolution.

Initial phases were determined by molecular replacement with PHASER of the CCP4 suite, using coordinates of FTase (PDB code: 1FT1)⁹¹ without 10 amino acids at the C-terminus of

the β subunit as search model. The model was then corrected by alternating rounds of refinement in REFMAC5 and manual adjustment in COOT. Full data collection and refinement statistics are given in Table 4.2.

The structure of the FTase_ α _ β C Δ 10 mutant was determined at 2.8 Å resolution. The final model of the FTase_ α _ β C Δ 10 mutant structure contains 54 water molecules and one Zn²⁺ ion. And the structure is refined to an R-factor of 17.7 % and R_{free} of 23.2 %. The model of the FTase mutant contains one α/β heterodimer in the asymmetric unit. Of the total residues for the FTase mutant structure, 86.5 % lie in the most favoured region of the Ramachandran plot (PROCHECK). Most of the residues with poorer electron density are located in the additionally allowed regions.

The secondary structure of both the α and β subunits is largely composed of α helices (Figure 4.10 left). Helices of the α subunit are folded into seven successive pairs that form a series of right-handed antiparallel coiled coils. These “helical hairpins” are arranged in a double-layered, right-handed superhelix resulting in a crescent shaped subunit that envelops part of the β subunit. Twelve α helices of the β subunit are folded into an α - α barrel (Figure 4.10 left). A core of six parallel helices forms the inner portion of the barrel. The other six additional helices interconnect the inner core of helices and form the outside of the helical barrel. The N-terminal domain (~50 amino acids) is disordered in the structure of the FTase mutant (similar with wild type FTase). In addition, two C-terminal amino acids of the β subunit are invisible in the structure.

As expected the structure of the engineered enzyme contains an open active site and is almost identical with the structure of wild type FTase (PDB code: 1FT1)⁹¹ expressed in insect cells, with a C $_{\alpha}$ RMS-deviation of 0.65 Å for 709 residues (Figure 4.10 right). The catalytic zinc ion is located at the top of the active site funnel in the β subunit, which is coordinated by residues Asp297 β , Cys299 β and His362 β (Figure 4.10 left).

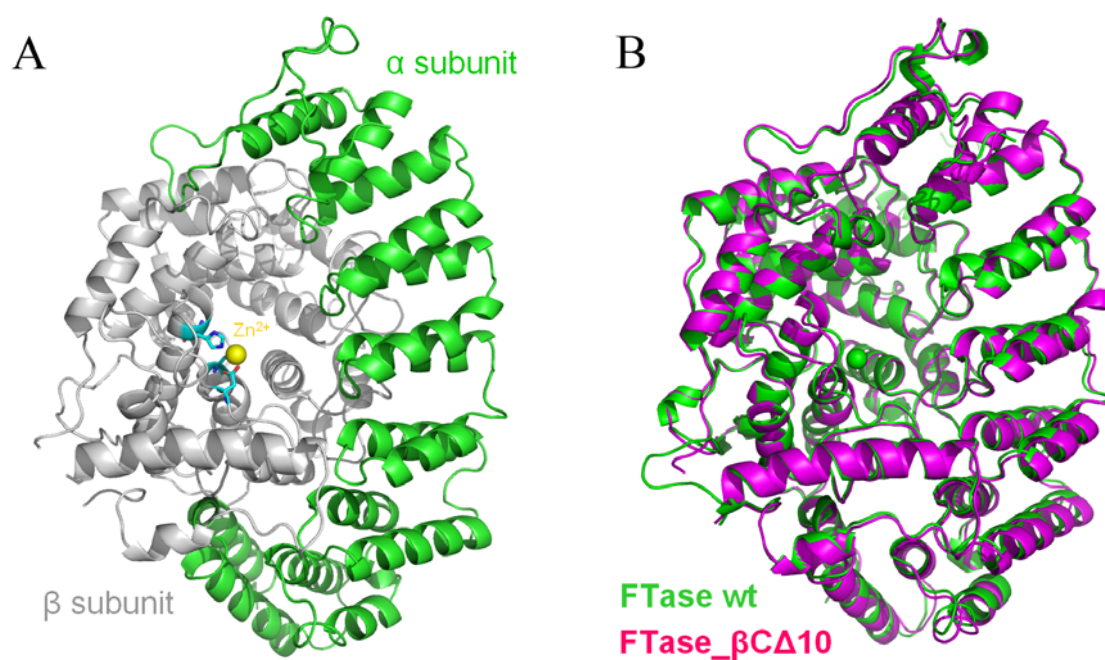


Figure 4.10: Overall structure of FTase_{α_βCΔ10} mutant and Zn²⁺ binding site. (A) The α (green) and β (gray) subunits are displayed in cartoon and Zn²⁺ (yellow) in sphere representation. The residues coordinated with Zn²⁺ (D297β, C299β and H362β) are displayed in stick representation. (B) Superposition of wild type FTase (green, PDB code: 1FT1)⁹¹ and the FTase_{α_βCΔ10} mutant (magenta) demonstrates the structural similarity. The α and β subunits of both proteins are displayed in cartoon and Zn²⁺ in sphere representation.

Section III

Structural Analysis of the protein prenyltransferase bound to phosphoisoprenoids

4.7 Structure of RabGGTase_{αΔLRRAIG} in complex with its lipid substrate GGPP

The availability of a RabGGTase construct displaying robust crystallisation behavior and near native biochemical properties prompted us to attempt to solve the structure of RabGGTase with its native substrate geranylgeranyl pyrophosphate (GGPP). The availability of such a structure would complete the picture of enzyme:substrate complexes for the protein prenyltransferase family and give mechanistic insights into lipid substrate specificity of protein prenyltransferases.

The co-crystallisation approach (3.5.3) was used to obtain enzyme:isoprenoid complex structures, which were prepared as follows. 1 µl of 2 mM isoprenoid GGPP in methanol were applied to a glass cover slip. After evaporation of the organic solvent, 1 µl of protein solution (12 mg/ml protein in 40 mM NaCl, 5 mM β-mercaptoethanol, 25 mM HEPES pH 7.2) and 1 µl of reservoir containing 14% (w/v) PEG3350, 0.2 M CaAc₂, 0.1 M HEPES pH 7.2 were added. The drop was equilibrated in a hanging drop setup at 12°C against 500 µl reservoir. The crystals had a rectangular shape and grew to a size of approximately 40*40*100 µm within 1 day (Figure 4.11). The rectangular shape of complex crystals is different from the cubic shape observed in the case of the apo enzyme.

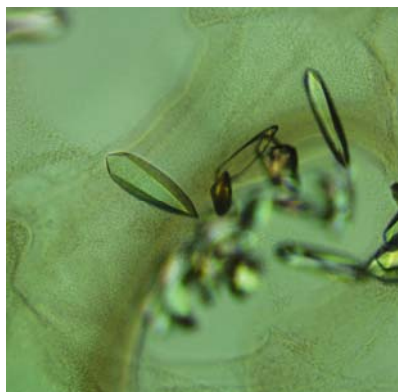


Figure 4.11: Crystals of RabGGTase_αΔLRRΔIG mutant in complex with GGPP obtained by a co-crystallisation approach.

Cryoprotection was achieved by washing crystals briefly in 20% (w/v) PEG3350, 5% (v/v) glycerol, 0.2 M CaAc₂, 0.1 M HEPES pH 7.2 supplemented with 2 mM GGPP prior to flash-cooling in liquid nitrogen. Diffraction data were collected at 100 K on beamline X10SA of the Swiss Light Source (Villigen, Switzerland) and processed with the XDS package. The crystals belong to orthorhombic space group P212121 and contain one copy of the RabGGTase_αΔLRRΔIG:GGPP complex in the asymmetric unit.

The structures were solved by molecular replacement with PHASER software using the apo-form of RabGGTase_αΔLRRΔIG as a search model. The structures were refined in REFMAC5 and COOT. The complex structure was determined to 1.85 Å resolution. Initial difference density electron maps (fofc-map) showed strong positive density in the hydrophobic cavity of the α-α barrel of the β subunit (Figure 4.12).

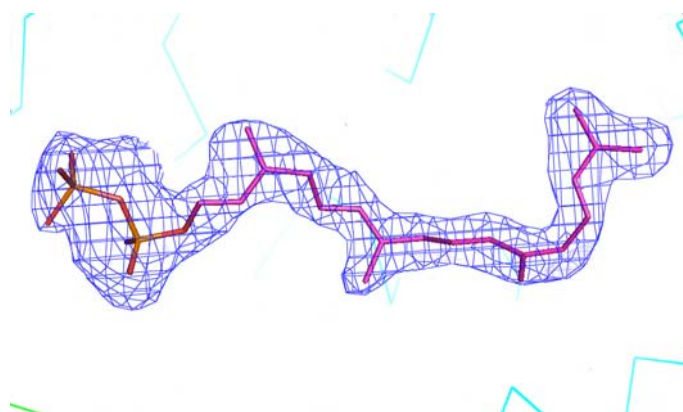


Figure 4.12: Difference electron density of GGPP displayed at 2.5 σ . The electron density (fofc-map) was calculated before incorporation of the ligand into the model. The truncated RabGGTase and GGPP molecule are displayed in ribbon and stick, respectively.

The isoprenoid substrate GGPP was added in the final rounds of refinement, using a restraints library generated with PRODRG²⁰⁷. Full data collection and refinement statistics are summarized in Table 4.2. Structure factors and coordinates will be deposited in the Protein Data Bank with entry code xxxx (RabGGTase_αΔLRRΔIG:GGPP).

The quality of the final electron density map together with a comparison of the refined temperature factors of GGPP (~40 Å²) and the surrounding protein residues (~35 Å²) suggest that the occupancy of GGPP is approximately 85%.

The final model of the RabGGTase_αΔLRRΔIG:GGPP complex contains 127 water molecules, one GGPP molecule, one Zn²⁺ ion and two Ca²⁺ ions. The structure is refined to an R-factor of 21.3 % and R_{free} of 25.0 %. The model of the complex contains one α/β heterodimer in the asymmetric unit. 91.0 % of all residues of the complex structure lie in the most favoured region of the Ramachandran plot (PROCHECK). Most of the residues with poorer electron density are located in the additionally allowed regions.

Similar to structures of other prenyltransferases the hydrophobic tail of GGPP is held in the hydrophobic binding cleft formed by conserved predominantly aromatic residues Tyr51β, Trp52β, Phe147β, Tyr195β, Tyr241β, Trp243β, Trp244β, Phe289β, Phe293β, Phe143α and Tyr107α (Figure 4.13 A). Binding of GGPP to RabGGTase leads to several minor changes in the structure of the active site mostly involving rotation or displacement of side chains of the hydrophobic residues Phe293β, Tyr241β, Trp244β and Tyr195β (Figure 4.13 B).

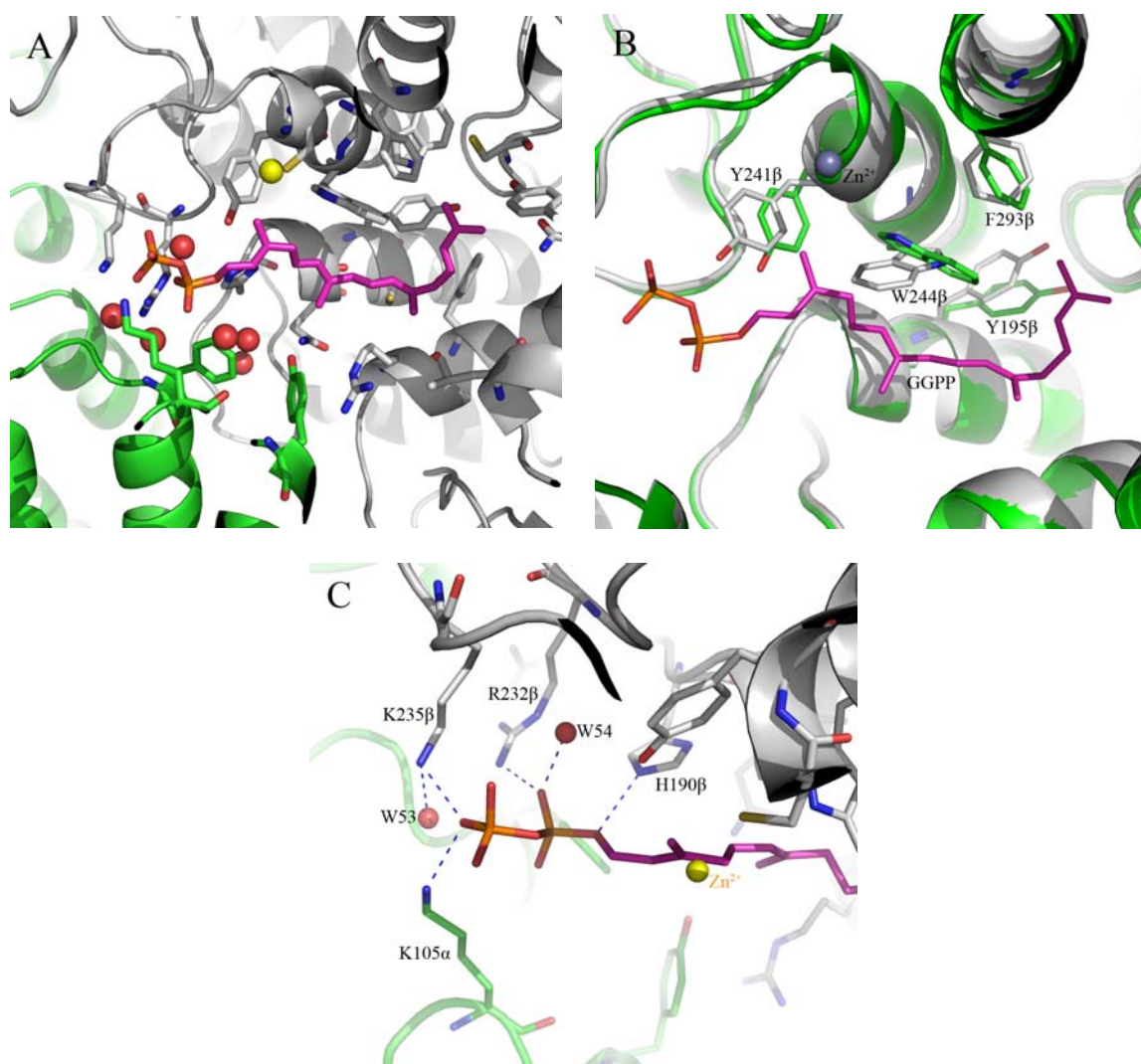


Figure 4.13: Structure of RabGGTase_αΔLLRAIG mutant in complex with GGPP. (A) The α (green) and β (gray) subunits are displayed in cartoon forms. The GGPP molecule (magenta) and the residues (Y51β, W52β, F147β, Y195β, Y241β, W243β, W244β, F289β, F293β, F143α, Y107α), which line along the central cavity, are displayed in stick representation. The Zn²⁺ ion and water molecule are shown as yellow and red balls, respectively. **(B)** Superposition of apo RabGGTase mutant (gray) and its complex with GGPP (green) demonstrates the structural conformational change upon binding of GGPP. The α and β subunits of both proteins are displayed in cartoon and Zn²⁺ in sphere representation. The Binding of the GGPP to RabGGTase results in the rotation or displacement of side chains of the residues F293β, Y241β, W244β and Y195β, which are shown in stick representation. **(C)** Hydrogen bonding of the diphosphate moiety of GGPP is displayed in the stick representation. Residues of the α and β subunits are coloured in green and gray, respectively. Hydrogen bonds are shown as blue dashed lines.

The diphosphate moiety of the GGPP molecule binds in a positively charged cluster at the subunit interface, which is formed by Arg232β, Lys235β and Lys105α, and is close to the catalytic zinc ion (Figure 4.13 A and B). The resolution of the structure allows

unambiguously determination of residues that form hydrogen bonds with the diphosphate moiety of the GGPP molecule. One oxygen atom of the β -phosphate forms two 2.6 Å hydrogen bonds with residues Lys235 β and Lys105 α (Figure 4.13 C), while one oxygen atom of the α -phosphate forms 2.7 Å and 2.5 Å hydrogen bonds with Arg232 β and a water molecule and the other oxygen atom of the α -phosphate forms a 3.0 Å hydrogen bond with His190 β (Figure 4.13 C).

The most interesting aspect of the obtained structure is its comparison with the structure of the GGTase-I:GGPP complex⁸⁹. Carbons 1-7 of GGPP adopt different conformations and are located much closer to the Zn²⁺ atom in RabGGTase than in GGTase-I (Figure 4.14). The carbon atoms 8-15 superimpose very well while the last portions of the isoprenoids are positioned differently. The binding sites can be divided into two halves based on their conservation. The part of the binding site harboring phosphate groups and carbons 1-12 of the isoprenoid chain are invariant and adopt very similar positions in both enzymes. However the bottom of the binding site appears to be less conserved. While some substitutions, such as Phe53 β (GGTase-I) to Trp52 β (RabGGTase), Phe52 β (GGTase-I) to Tyr51 β (RabGGTase), do not lead to significant changes in the shape of the binding site or its hydrophobicity, several other substitutions such as Leu320 β (GGTase-I) to Phe289 β (RabGGTase), Tyr323 β (GGTase-I) to Leu292 β (RabGGTase), Tyr126 β (GGTase-I) to Leu99 β (RabGGTase) and Asn345 β (GGTase-I) to Cys314 β (RabGGTase) change both properties of the active site. Compared to GGTase-I the lipid binding site of RabGGTase is expanded at the bottom, primarily due to the substitution of Tyr323 β (GGTase-I) and Tyr126 β (GGTase-I) to Leu292 β (RabGGTase) and Leu99 β (RabGGTase), respectively (Figure 4.14). These substitutions are responsible for the bend in the last 5 carbon atoms of GGPP associated with RabGGTase.

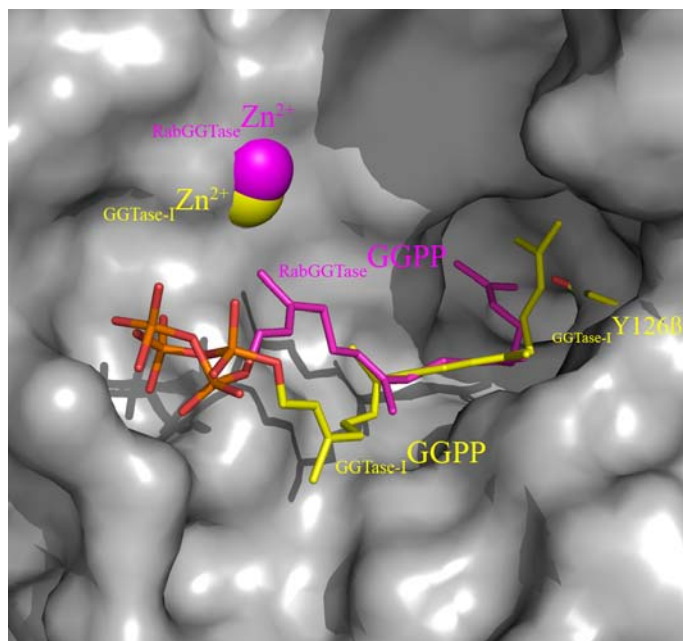


Figure 4.14: Comparison of the RabGGTase:GGPP structure with the structure of GGTase-I:GGPP complex (1N4Q)⁸⁹ by superposition. The active site of RabGGTase is displayed in surface representation while the residues of the active site of GGTase-I are displayed in stick representation. GGPP bound to RabGGTase is coloured in magenta and bound to GGTase-I in yellow, while the zinc ion is shown as a sphere.

4.8 The structures of RabGGTase_αΔLRRΔIG in complex with FPP, GGMP and GGTP

The affinities of the isoprenoids farnesyl pyrophosphate (FPP), geranylgeranyl monophosphate (GGMP), geranylgeranyl pyrophosphate (GGPP) and geranylgeranyl triphosphate towards RabGGTase had been determined by Yaowen Wu using a previously established assay, in which binding of isoprenoid to prenyltransferase can be monitored by the influence of the former on the interaction of prenyltransferase with a fluorescent isoprenoid analogue (mant-FPP or NBD-FPP)²⁰⁸. Remarkably, although FPP binds to RabGGTase with an affinity of ca. 90nM, i.e. >100 times weaker than the native substrate GGPP, all three phosphorylated forms of geranylgeraniol (GGMP, GGPP and GGTP) bind with comparably high affinities to RabGGTase (3 nM, 0.8 nM and 1 nM, respectively)¹⁹⁹.

The ability of the isoprenoids to bind tightly to RabGGTase prompted us to test whether phosphoisoprenoids other than the native substrate could be lipid donors in the Rab prenylation reaction. Two *in vitro* Rab prenylation assays described by Rak et al¹²⁷ and in by

Wu et al¹⁹⁹ were performed by Yaowen Wu¹⁹⁹. Briefly, these data suggest that FPP still served as a lipid substrate and that in contrast GGMP, GGTP and FTP could not serve as lipid donors in the Rab prenylation reaction.

In order to gain further insight into the mode of isoprenoid binding to RabGGTase and the basis for the large difference in binding strength and in transfer efficiency the complex structures of the truncated RabGGTase in complex with FPP, GGMP or GGTP have been determined and are described as follows.



Figure 4.15: Crystals of RabGGTase_αΔLRRΔIG mutant in complex with FPP (left), GGMP (middle) or GGTP (right) obtained by a co-crystallisation approach.

The preparation of the crystals of RabGGTase_αΔLRRΔIG in complex with FPP, GGMP or GGTP, as well as the collection of diffraction data, the subsequent processing and the final structural determination were performed as described in the structural determination of the truncated RabGGTase in complex with GGPP by the co-crystallisation approach. All crystals appeared within 1 day, with a rectangular shape and a size of approximately 40*40*100 μm (Figure 4.15). The shape of the complex crystals is different from the shape in the case of the apo enzyme, while it is similar to the enzyme:GGPP complex. All crystals belong to space group P212121 and contain one copy of the RabGGTase_αΔLRRΔIG complex in the asymmetric unit. Full data collection and refinement statistics are summarized in Table 4.2. Structure factors and coordinates will be deposited in the Protein Data Bank with entry codes xxxx (RabGGTase_αΔLRRΔIG:FPP), yyyy (RabGGTase_αΔLRRΔIG:GGMP) and zzzz (RabGGTase_αΔLRRΔIG:GGTP).

The complex structures of the truncated RabGGTase in complex with FPP, GGMP and GGTP were determined at 1.85 Å, 2.55 Å and 2.0 Å, respectively by molecular replacement. Initial difference density electron maps (fofc-map) showed strong positive density in the hydrophobic cavity of the α-α barrel of the β subunit (Figure 4.16).

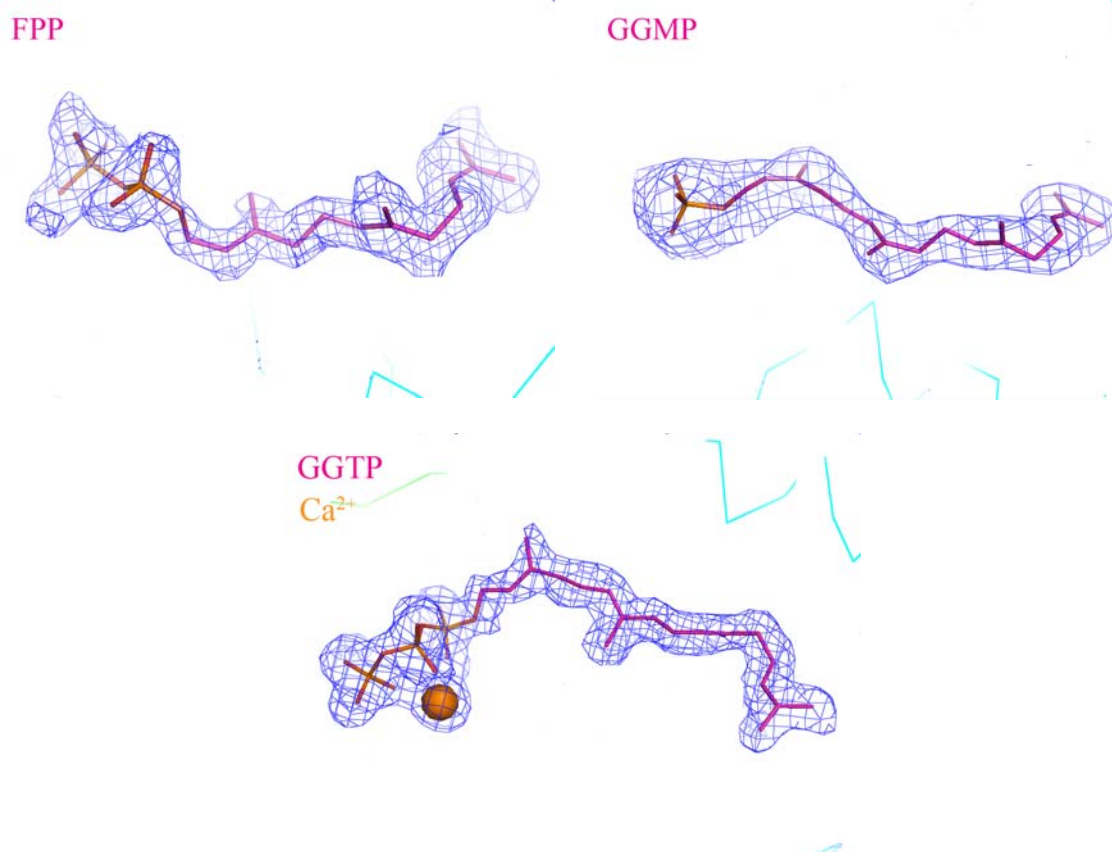


Figure 4.16: Difference electron density of FPP (upper, left) , GGMP (upper, right) and GGTP (bottom) displayed at 2.5σ . The electron density (fofc-map) was calculated before incorporation of the phosphoisoprenoids into the model. The truncated RabGGTase and phosphoisoprenoid molecules are displayed in ribbon and stick, respectively. In the case of GGTP, one Ca^{2+} ion (orange) was modeled into the structure.

One molecule of respective phosphoisoprenoid was modeled into the density observed and final rounds of refinement were performed using a restraints library generated with PRODRG. The quality of the final electron density map together with a comparison of the refined temperature factors of phosphoisoprenoids (FPP $\sim 40 \text{ \AA}^2$; GGMP $\sim 40 \text{ \AA}^2$ and GGTP $\sim 20 \text{ \AA}^2$) and the surrounding protein residues ($\sim 25 \text{ \AA}^2$, $\sim 30 \text{ \AA}^2$ and $\sim 18 \text{ \AA}^2$, respectively) suggest that the occupancy of FPP, GGMP and GGTP in the structure is approximately 70%, 80% and 90%, respectively.

The final model of the RabGGTase_ α DLRR Δ IG:FPP complex contains 215 water molecules, one FPP molecule, one Zn^{2+} ion and one Ca^{2+} ion. The structure was refined to an R-factor of 20.4 % and R_{free} of 23.5 %. The RabGGTase_ α DLRR Δ IG:GGMP complex contains 36 water molecules, one GGMP molecule and one Zn^{2+} ion. The structure was refined to an R-factor of

21.7 % and R_{free} of 29.1 %. The RabGGTase_ $\alpha\Delta$ LRR Δ IG:GGTP complex contains 290 water molecules, one GGTP molecule, one Zn^{2+} ion and one Ca^{2+} ion. The structure was refined to an R-factor of 19.6 % and R_{free} of 23.5 %. All complexes contain one α/β heterodimer in the asymmetric unit. Of the total residues for the complex structures, 91.2 % (in FPP complex), 88.5 % (in GGMP complex) and 91.3 % (in GGTP complex) lie in the most favoured region of the Ramachandran plot (PROCHECK). Most of the residues with poorer electron density are located in the additionally allowed regions.

Comparison of the complex structures of truncated RabGGTase with its native lipid donor GGPP and the other phosphoisoprenoids by superposition of the β subunit demonstrated that in all cases the last 12 carbons of the isoprenoid moiety adopt a very similar conformation and position (Figure 4.17 ABC). Binding of these phosphoisoprenoids to RabGGTase leads to conformational changes identical to that upon binding of GGPP to the enzyme, involving rotation or displacement of side chains of the hydrophobic residues Phe293 β , Tyr241 β , Trp244 β and Tyr195 β (see Figure 4.13 B). Remarkably, the reactive carbon 1 of FPP is located 5 Å away from the position occupied by the C_1 of native GGPP (Figure 4.17 A). There, the β phosphate forms a strong hydrogen bond (2.3 Å) with Tyr241 β , which is otherwise not involved in interaction with the phosphates in the RabGGTase:GGPP structure (Figure 4.17 D and Figure 4.13 C). In addition, five water molecules form a network of hydrogen bonds to contribute to the binding of FPP to RabGGTase (Figure 4.17 D). The large difference in binding strength between FPP and GGPP can be explained by comparison of the complex structures of RabGGTase:FPP and RabGGTase:GGPP. On the one hand, the absence of one isoprene unit in the case of FPP would reduce the hydrophobic interaction of lipid tail with enzyme; on the other hand, in the complex structure with GGPP four strong hydrogen bonds are formed between diphosphate group and lipid binding site, whereas only one hydrogen bond is formed in the structure of RabGGTase complexed with FPP. This leads to >100 fold difference in the affinities of FPP and GGPP towards RabGGTase. The C_1 atom of FPP is definitely too far away from the Zn^{2+} ion to participate in catalysis. However FPP still serves as an effective lipid substrate¹²⁵. The most likely explanation for the observed reactivity of FPP is its ability to slide along the lipid binding site and coordinate with reactive cysteine and the catalytic Zn^{2+} ion.

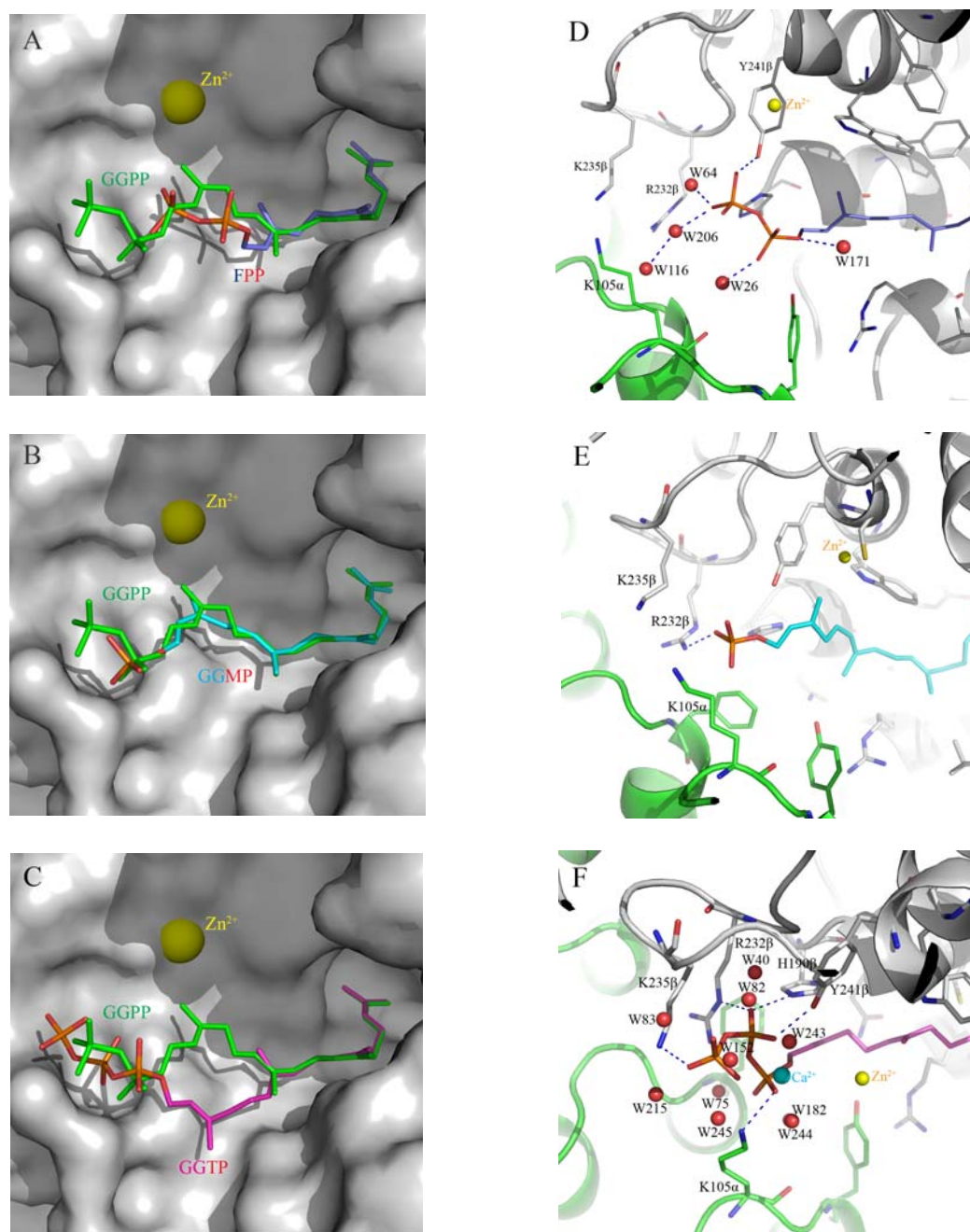


Figure 4.17: Structural analysis of the truncated RabGGTase in complex with FPP, GGMP and GGTP. (A-C) Superimposition of the RabGGTase in complex with the native lipid donor GGPP and the other phosphoisoprenoids FPP (A), GGMP (B) and GGTP (C). The active site of RabGGTase in complex with GGPP is shown in surface representation. The GGPP is shown in stick representation and coloured in green. The other phosphoisoprenoid molecules are also shown in stick representation but are displayed colour-coded for atom types. All Zn²⁺ ions are displayed as yellow spheres. (D-F) Hydrogen bonding of the phosphate groups of the phosphoisoprenoids is shown as dashed lines. The residues of the α and β subunit are coloured in green and gray. The hydrogen bonds are shown as blue dashed lines. Water molecules (red), Zn²⁺ ions (yellow) and in the case of GGTP the Ca²⁺ ion (cyan) are shown as spheres.

The structure of the RabGGTase:GGMP complex is very similar to that of the complex with GGPP (Figure 4.17 B). Due to the absence of the β -phosphate only one 2.5 Å hydrogen bond is formed by the α -phosphate of GGMP and residue Arg232 β (Figure 4.17 E), which is also involved in the binding of GGPP to RabGGTase.

The complex containing GGTP shows significant differences (Figure 4.17 C). The last 12 carbons of GGTP superimpose well with all other structures but the rest of the isoprenoid chain of GGTP adopts a conformation similar to that observed in the GGase-I:GGPP complex⁸⁹. This involves flipping of the first 8 carbons of GGTP away from Zn²⁺ on the carbon 9. As a result the reactive carbon 1 of GGTP is located 3 Å away from the position occupied by the C₁ of native GGPP (Figure 4.17 C). The flipping also leads to an inward movement of the side chain of His190 β (Figure 4.17 F). The phosphate atoms occupy similar positions in both structures of truncated RabGGTase bound either to GGPP or GGTP. However the triphosphate of GGTP forms a bend due to its interaction with a Ca²⁺ ion present in the active site. The phosphate groups of GGTP form 5 additional hydrogen bonds with the lipid binding site (Figure 4.17 F). Lys105 α forms a 2.8 Å hydrogen bond with the α -phosphate of GGTP, whereas it forms a hydrogen bond with the β -phosphate in the case of GGPP in the RabGGTase:GGPP structure. Tyr241 β forms a 2.7 Å hydrogen bond with one oxygen atom of the β phosphate of GGTP, which is otherwise not involved in interaction with phosphates in the RabGGTase:GGPP structure (Figure 4.17 F and Figure 4.13 C). The other oxygen atom of the β phosphate of GGTP forms two 2.9 Å hydrogen bonds with His190 β and Arg232 β (Figure 4.17 F). Lys235 β forms a 2.7 Å hydrogen bond with the γ -phosphate of GGTP (Figure 4.17 F). In addition 10 water molecules and a Ca²⁺ ion form a hydrogen bonding network that contributes to the binding of GGTP to RabGGTase. The structural data only provides limited clues as to why GGTP and GGMP fail to serve as lipid donors of RabGGTase.

4.9 Phosphoisoprenoid specificity of protein prenyltransferases

One of the key functional differences among the three protein prenyltransferases is their ability to selectively utilise either GGPP or FPP. The critical feature that distinguishes GGPP from FPP is the length of the lipid. The availability of the structures of the three prenyltransferases complexed with the respective isoprenoid substrate gives mechanistic insights into lipid substrate specificity of protein prenyltransferases. Superimposition of these

three protein prenyltransferases in complex with their respective phosphoisoprenoid substrate (PDB code 1FT2, 1N4P)^{89;96} provides an explanation on how the lipid's length is used to selectively bind the correct substrate (Figure 4.18).

The structures of the three protein prenyltransferases in complex with their respective isoprenoid substrate indicate that the first three isoprene units of FPP and GGPP are in a linear fashion. The fourth isoprene unit of GGPP in both GGTase-I and RabGGTase complexes is turned $\sim 90^\circ$ relative to this axis. This geometry of the bound lipid is quite different from that of the other known structures with bound isoprenoids, i.e. FTase (PDB code 1FT2⁹⁶), Rho:GDI (PDB code 1DOA²⁰⁹), phosducin-Gt $\beta\gamma$ complex (PDB code 1A0R²¹⁰), Ypt1:GDI (PDB code 2BCG⁷⁵) and Rab7:REP-1 (PDB code 1VG0¹²⁷), in which the isoprenoid chains are extended.

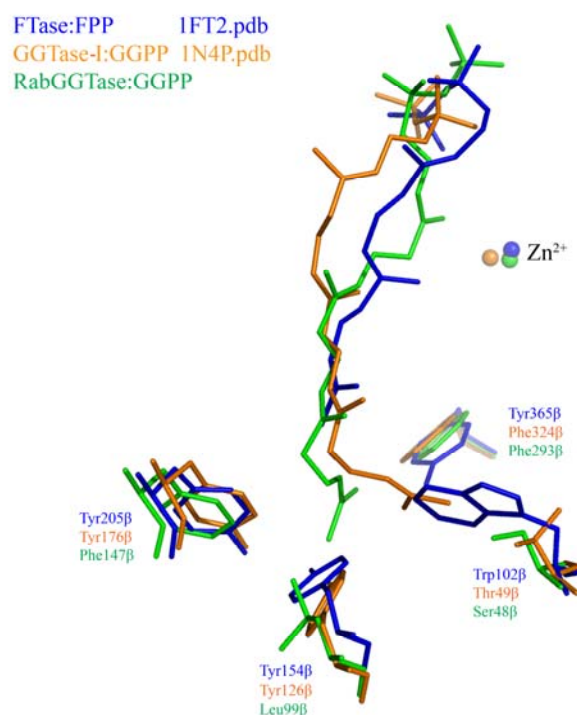


Figure 4.18: Superimposition of active sites of all three protein prenyltransferase. The three prenyltransferases in complex with their respective isoprenoid substrates were superimposed^{89;96}. Only critical residues forming the bottom of the active sites and isoprenoids are shown in stick representation, while Zn^{2+} ions are represented as spheres.

The alignment in Figure 4.18 shows that the second and third isoprene units are at similar positions in all three cases, whereas the fourth isoprene unit of the GGPP is positioned differently. Two striking differences in the arrangements of the bottom of the hydrophobic

funnel are observed, where the fourth isoprene unit of GGPP binds in GGTase-I and RabGGTase. Here, FTase has bulky tryptophan and tyrosine residues (Trp102 β and Tyr154 β). In contrast, the corresponding positions in GGTase-I are occupied by one smaller residue, threonine, and one identical tyrosine residue (Thr49 β and Tyr126 β), while in RabGGTase these positions are occupied by two smaller residues, serine and leucine (Ser48 β and Leu99 β). This suggests that residues positioned at the bottom of the hydrophobic funnel are the primary determinant of lipid specificity. In FTase, the tryptophan residue Trp102 β and the Tyrosine residue Tyr154 β fill the space where the fourth isoprene unit binds in GGTase-I and RabGGTase, respectively.

Initial studies suggested that when GGPP was bound to the active site of FTase, its pyrophosphate was located too far away from the catalytic Zn²⁺ ion for reaction to occur^{89,96}. However, comparison of the structures of FTase in complex with FPP (PDB code 1FT2) and GGPP (PDB code 1O1R)²¹¹ indicates that the diphosphate group and the last two isoprene units of GGPP and FPP adopt a very similar conformation and position. As a result, the first and second isoprene units of GGPP bulge away from the CAAX substrate binding site. As mentioned above the FPP rotates at its third isoprene unit and brings the C₁ atom of FPP closer to the activated cysteine thiolate to allow the farnesylation to take place. However, superimposition of the FTase in complex with FPP, GGPP and farnesylated CAAX peptide reveals that the bulkier isoprenoid GGPP cannot undergo this conformational change without unfavorable steric interactions with the CAAX substrate²¹¹. This explains why GGPP and FPP bind to FTase with comparable affinities but only FPP serves as an effective substrate^{16;92;99;103;106}.

The residues Phe324 β of GGTase-I and Phe293 β of RabGGTase are also positioned near the fourth isoprene unit; the hydroxyl group on the corresponding FTase Tyr365 β residue may also help to discriminate against GGPP binding in FTase. These data demonstrate that in the case of FTase steric hindrance plays the central role in choosing the correct lipid substrate.

Unlike FTase, GGTase-I and RabGGTase can (mis)transfer a farnesyl group to substrate proteins. Although in the RabGGTase:FPP structure the C₁ of FPP is too far away from the zinc ion to participate in the reaction with the Zn²⁺ activated cysteine thiolate, RabGGTase transfers GGPP and FPP at a similar rate¹²⁵. This suggests that FPP can slide in the active site to allow this reaction to take place. This must occur relatively easily to account for the prenylation reaction, and the rate of sliding must be rapid compared with the actual lipid

transfer reaction. Though *in vitro* FPP serves as an effective lipid substrate for RabGGTase, *in vivo* Rab proteins appear to only undergo geranylgeranylation mediated by RabGGTase^{107;199}. This is first explained by weaker affinities of FPP for the enzymes (330-fold to GGTase-I and 100-fold to RabGGTase)^{101;106;199}. In addition, reaction cycle progression requires the binding of fresh isoprenoid diphosphate to displace the product from the active site^{88;89}. Due to the much lower affinity of FPP towards GGTase, as compared with GGPP, the displacement is more difficult with FPP than with GGPP, which results in a reduced tendency for FPP to bind to GGTase during the reaction cycle. This leads to selection of GGPP in preference to FPP as lipid donor in GGTase-I and RabGGTase.

These conclusions were confirmed by mutagenesis studies. A mutation at the Trp102 β residue of FTase to a threonine (the corresponding residue in GGTase-I) or a mutation at the Tyr154 β residue of FTase to a threonine/leucine (the corresponding residue in RabGGTase) were tested and both single mutations result in an FTase enzyme greatly preferring GGPP over FPP as its isoprenoid substrate without significantly altering the CAAX sequence specificity^{105;212}.

The reason for the different binding of the fourth isoprene unit of GGPP in GGTase-I and RabGGTase can be explained by the presence of the bulky tyrosine residue (Tyr126 β) in GGTase-I, whereas the corresponding position in RabGGTase is replaced by a smaller residue, leucine (Figure 4.18).

4.10 Design of FTase and GGTase-I mutants capable of utilising Biotin-GPP as a lipid substrate

Expansion of the bottom of the lipid binding site in RabGGTase relative to those of FTase and GGTase-I enables it to bind phosphoisoprenoid analogues with bulky terminal groups. This idea finds support in a recent report demonstrating that of the three protein prenyltransferases, only RabGGTase can use the bulky biotingeranyl pyrophosphate (Biotin-GPP) as substrate²⁰² (Figure 4.20). Incorporation of the biotin group by RabGGTase into its cognate substrates enables rapid monitoring of the prenylation status of RabGTPases across the proteome. It enables an analysis of numerous aspects of RabGTPase biogenesis such as expression profiles in different cell types, the rates of Rab expression and prenylation, and the effect of prenylation inhibitors on Rab prenylation. Expansion of this technology to other prenyltransferases would be of great value.

Based on the obtained structural information on the RabGGTase:isoprenoid complexes, we engineered two FTase and GGTase-I mutants: FTase(W102T, Y154T) and GGTase-I(Y126T). In these mutants the bottom of the hydrophobic funnel was enlarged to resemble that of RabGGTase (Figure 4.19).

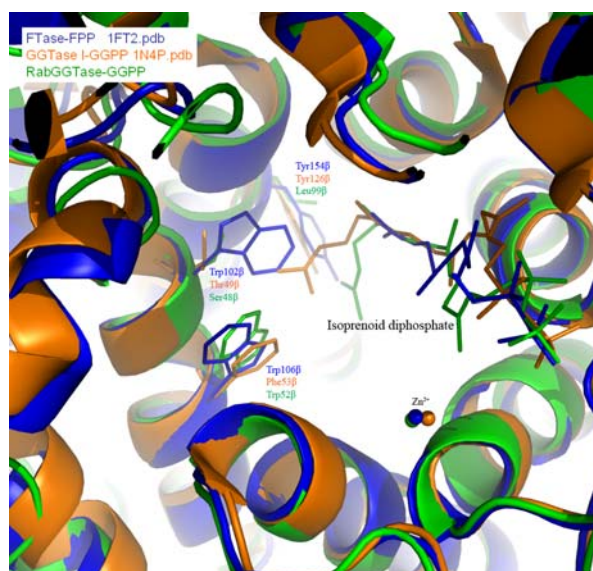


Figure 4.19: Design of FTase and GGTase-I mutants capable of using Biotin-GPP as substrate. The three prenyltransferases in complex with their respective isoprenoid substrates were superimposed and displayed as blue (FTase), orange (GGTase-I) and green (RabGGTase) cartoons. The critical residues that were selected for mutation studies and isoprenoids are shown as sticks, while Zn^{2+} ions are displayed as spheres.

Unlike the parental enzymes the obtained mutants were capable of specifically conjugating Biotin-GPP to their cognate protein substrates. However, the transfer efficiency of GGTase-I(Y126T) is much lower than that of FTase(W102T,Y154T) and RabGGTase (Figure 4.20).

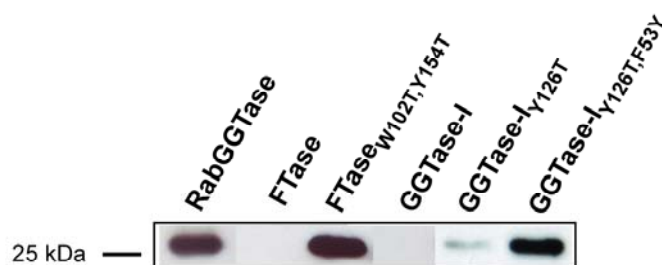


Figure 4.20: Incorporation of Biotin-geranyl into GTPases mediated by prenyltransferases *in vitro* adopted from²¹². KiRas, RhoA, and Rab7 were prenylated by FTase, GGTase-I or RabGGTase, respectively, using Biotin-GPP as a lipid donor. The reaction products were detected by Western blotting with STR-HRP. (This experiment was performed by U.T. Nguyen.)

We conjectured that the missing polar interaction of the Biotin group with the active site of GGTase-I(Y126T) may have resulted in the lower efficiency Biotin-transfer. A comparison of residues defining the active site of the three enzymes demonstrated a difference in the positioning of Phe53 β of GGTase-I by Trp106 β of FTase and Trp52 β of RabGGTase at the corresponding position (Figure 4.19). A polar interaction might be formed by the Biotin group with the indole group of tryptophan. Based on this analysis a new GGTase-I(Y126T, F53Y) mutant was generated, in which Tyr126 β and Phe53 β were mutated to threonine and tyrosine, respectively. Indeed, the new GGTase-I mutant was shown to engage Biotin-GPP as substrate with an efficiency comparable to that of RabGGTase and FTase(W102T, Y154T)²¹² (Figure 4.20). These mutants and RabGGTase can be used to rapidly identify, isolate and characterize all prenylatable proteins in mammalian cell providing a new technological venue in protein prenyltransferase research.

Section IV

Structural studies of the Rab prenylation process

4.11 Structures of the truncated RabGGTase in complex with mono- and di-prenylated Rab7 C-terminal peptides

The ability to perform two sequential geranylgeranyl transfer reactions on a single peptide substrate is a salient feature of RabGGTase. One of the longstanding questions in the field was the location of the first conjugated isoprenoid during the second transfer reaction. Comparison of the structures of GGTase-I and RabGGTase led to speculations that the first conjugated isoprenoid would be located in the cavity near the reaction center⁸⁹. The success in generating the RabGGTase:substrate complexes promoted us to attempt crystallisation of enzyme bound to the reaction intermediate and product. Three prenylated peptides, Ser-Cys-Ser-Cys(GG), Ser-Cys(GG)-Ser-Cys and Ser-Cys(GG)-Ser-Cys(GG), were generated by Dr. D. Das (Department 4, MPI Dortmund) using solid phase synthesis to mimic the mono- and di-prenylated C-terminus of Rab7. These peptides represent all three possible prenylation states of Rab7 and also give a good coverage of possible positions of geranylgeranyl group in the C-terminus of Rab7.

Determination of the affinities of the prenylated peptides towards RabGGTase was unsuccessful by ITC measurement, perhaps due to the low aqueous solubility of these peptides. Following the observation that these prenylated peptides bind to RabGGTase in a mode similar to that of native phosphoisoprenoids (described below), a competitive titration was performed to determine the affinities of these prenylated peptides towards RabGGTase. The binding of isoprenoid with prenyltransferase was monitored by the influence of the former on the interaction of the prenyltransferase with the fluorescent isoprenoid analogue (NBD-FPP)^{125;208}.

The competitive titration was carried out as described in Materials and Methods (3.4.2). 200 nM NBD-FPP was mixed with 1 μ M prenylated peptide in 50 mM HEPES pH 7.2, 50 mM NaCl, 2 mM MgCl₂, 5 mM DTE and 2% DMSO. The mixture was titrated with increasing concentrations of RabGGTase. NBD-FPP was excited at 487 nm and the fluorescence was

monitored at 550 nm. The decrease in fluorescence upon addition of the protein was measured, and at each step the values were averaged after equilibration.

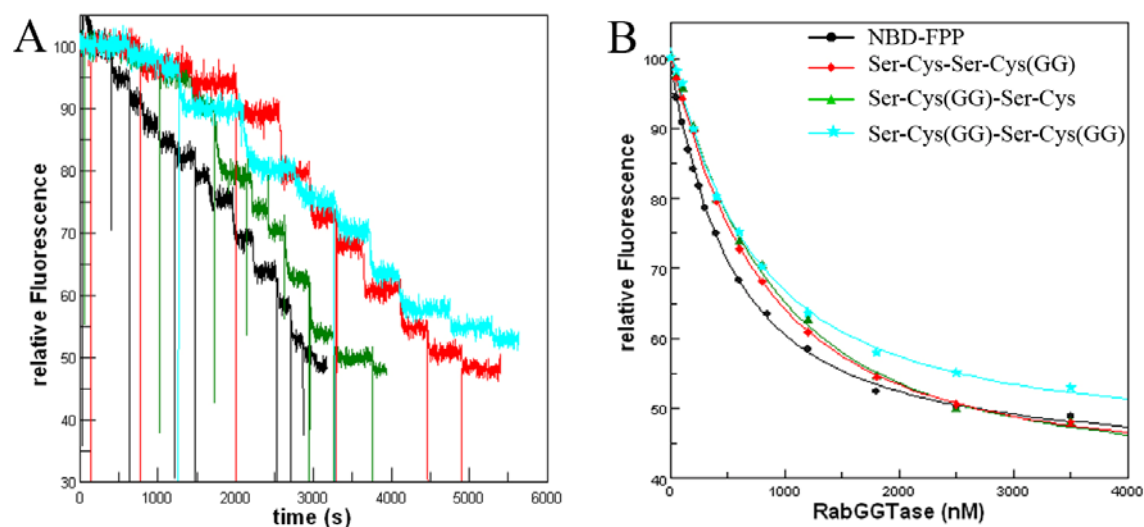


Figure 4.21: Determination of affinities of prenylated peptides towards RabGGTase by a competitive titration approach using the fluorescent isoprenoid analogue NBD-FPP. (A) Raw data of competitive titrations. The titration was carried out as described in Materials and Methods (3.4.2). NBD-FPP was excited at 487 nm and the fluorescence was monitored at 550 nm. Relative fluorescence was plotted against time. (B) Fit of the data. The relative fluorescence was plotted against concentration of RabGGTase. The curve for titration of 200 nM NBD-FPP alone was fitted resulting in a K_d of 0.4 μM , which was consistent with previous studies²⁰⁸. This K_d value was used to fit the data of the competitive titrations.

To determine the K_d value for NBD-FPP, 200 nM NBD-FPP alone was titrated with increasing concentrations of RabGGTase. The K_d -values were obtained by drawing a fit to the data using program Scientist 2.0 as described¹²⁵ (Table 4.1).

Table 4.1: Affinities of NBD-FPP and prenylated peptides towards RabGGTase.

	NBD-FPP	Ser-Cys-Ser-Cys(GG)	Ser-Cys(GG)-Ser-Cys	Ser-Cys(GG)-Ser-Cys(GG)
K_d (μM)	0.4	1.3	1.0	1.8

These data demonstrate that both mono-prenylated and di-prenylated peptides bind with comparable affinities to RabGGTase, however >1000 times more weakly than the isoprenoid substrate GGPP and ~2-5 times more weakly than NBD-FPP.

Preparation of crystals of the truncated RabGGTase complexed with the prenylated peptides, as well as the collection of diffraction data, the subsequent processing and the final structural determination were performed as described in the structural determination of the truncated

RabGGTase in complex with phosphoisoprenoids by the co-crystallisation approach (4.7). To improve the occupancy of these prenylated peptides in crystals 2.5 % DMSO was used in the reservoir solution and cyrosolution.

All crystals appeared within 2 days with a rectangular shape and a size of approximately 30*30*70 μm (Figure 4.22). The shape of the obtained crystals was different from the shape in the case of the apo enzyme, whereas it is similar to that of the enzyme:GGPP complex. All crystals belong to space group P212121 and contain one copy of the RabGGTase $_{\alpha\Delta\text{LRR}\Delta\text{IG}}$ complex in the asymmetric unit. Full data collection and refinement statistics are summarized in Table 4.2. Structure factors and coordinates will be deposited in the Protein Data Bank with entry codes xxxx (RabGGTase $\alpha\Delta\text{LRR}\Delta\text{IG}$:Ser-Cys-Ser-Cys(GG)), yyyy (RabGGTase $\alpha\Delta\text{LRR}\Delta\text{IG}$: Ser-Cys(GG)-Ser-Cys), and zzzz (RabGGTase $\alpha\Delta\text{LRR}\Delta\text{IG}$: Ser-Cys(GG)-Ser-Cys(GG)).

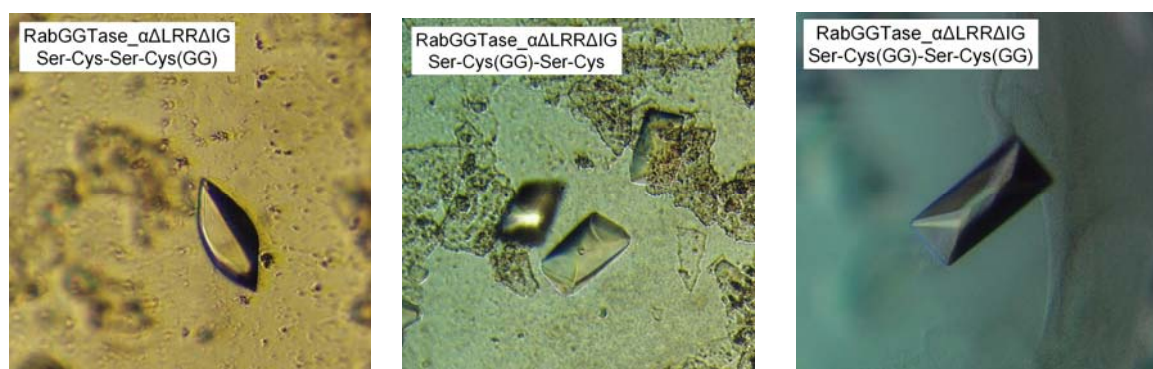


Figure 4.22: Crystals of RabGGTase $_{\alpha\Delta\text{LRR}\Delta\text{IG}}$ mutant in complex with Ser-Cys-Ser-Cys(GG) (left), Ser-Cys(GG)-Ser-Cys (middle) or Ser-Cys(GG)-Ser-Cys(GG) (right) obtained by co-crystallisation approach.

The structures of the truncated RabGGTase in complex with Ser-Cys-Ser-Cys(GG), Ser-Cys(GG)-Ser-Cys and Ser-Cys(GG)-Ser-Cys(GG) were determined at 1.9 \AA , 2.1 \AA and 2.0 \AA resolution, respectively by molecular replacement. Initial difference electron density maps (fofc-map) showed strong positive density in the hydrophobic cavity of the α - α barrel of the β subunit (Figure 4.23).

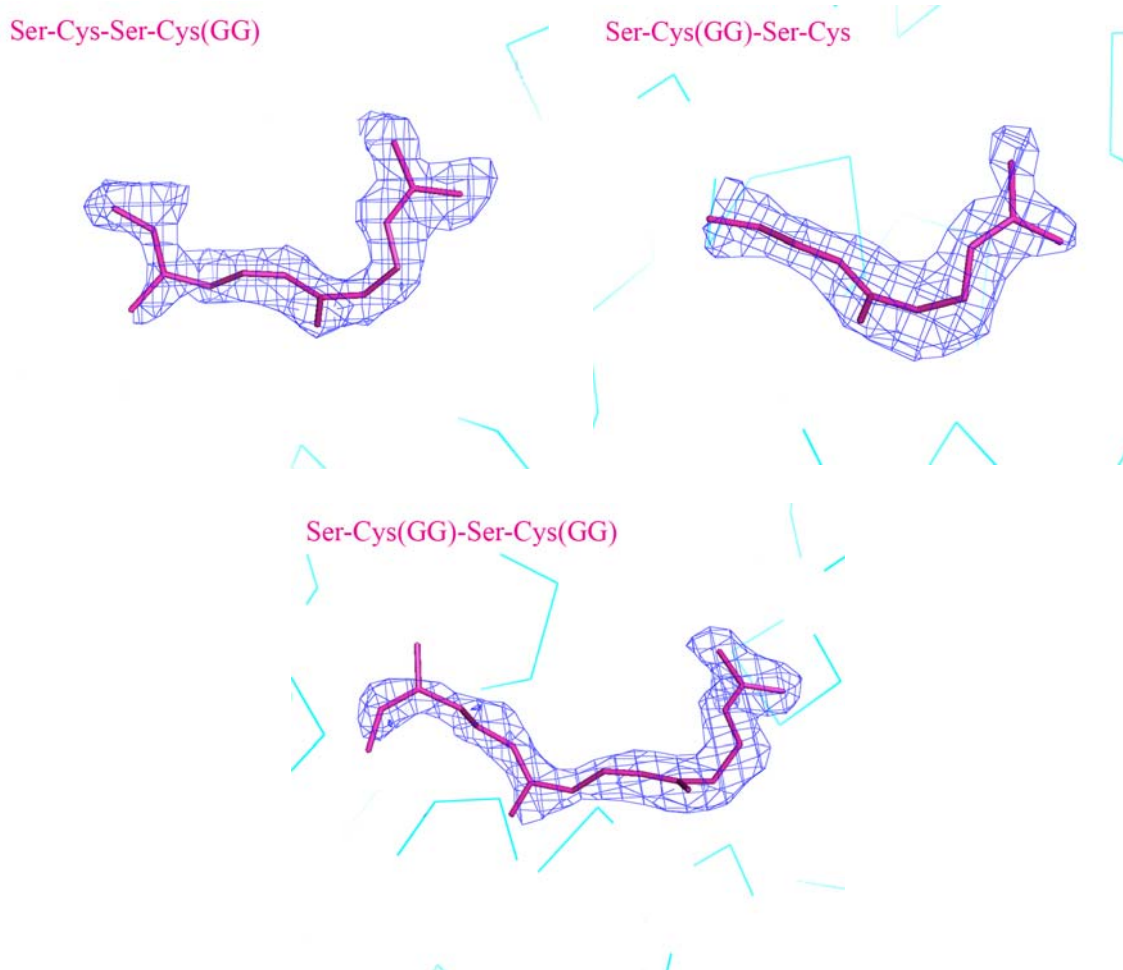


Figure 4.23: Difference electron density of Ser-Cys-Ser-Cys(GG) (upper, left), Ser-Cys(GG)-Ser-Cys (upper, right), Ser-Cys(GG)-Ser-Cys(GG) (bottom) displayed at 2.5σ . The electron density (fofc-map) was calculated before incorporation of the prenylated peptides into the model. The truncated RabGGTase and prenylated peptides are displayed in ribbon and stick representation, respectively.

One molecule of the respective prenylated peptide was modeled into the density observed and final rounds of refinement were performed using a restraints library generated with PRODRG. The quality of the final electron density map together with a comparison of the refined temperature factors of the prenylated peptides (Ser-Cys-Ser-Cys(GG) $\sim 16 \text{ \AA}^2$; Ser-Cys(GG)-Ser-Cys $\sim 25 \text{ \AA}^2$ and Ser-Cys(GG)-Ser-Cys(GG) $\sim 20 \text{ \AA}^2$) and the surrounding protein residues ($\sim 32 \text{ \AA}^2$, $\sim 50 \text{ \AA}^2$ and $\sim 40 \text{ \AA}^2$, respectively) suggests that the occupancy of these three prenylated peptides in the structure is approximately 50 %.

The final model of RabGGTase $\alpha\Delta\text{LRRAIG}$:Ser-Cys-Ser-Cys(GG) complex contains 386 water molecules, one Ser-Cys-Ser-Cys(GG) molecule, one Zn^{2+} ion and one Ca^{2+} ion. The structure is refined to an R-factor of 16.1 % and R_{free} of 22.1 %. The

RabGGTase_αΔLRRΔIG:Ser-Cys(GG)-Ser-Cys complex contains 153 water molecules, one Ser-Cys(GG)-Ser-Cys molecule, one Zn²⁺ ion and one Ca²⁺ ion. The structure is refined to an R-factor of 17.2 % and R_{free} of 23.3 %. The RabGGTase_αΔLRRΔIG:Ser-Cys(GG)-Ser-Cys(GG) complex contains 203 water molecules, one Ser-Cys(GG)-Ser-Cys(GG) molecule, one Zn²⁺ ion and one Ca²⁺ ion. The structure is refined to an R-factor of 18.1 % and R_{free} of 24.1 %. All complexes contain one α/β heterodimer in the asymmetric unit. Of the total residues for the complex structures, 91.9 % (in Ser-Cys-Ser-Cys(GG) complex), 92.7 % (in Ser-Cys(GG)-Ser-Cys complex) and 92.3 % (in Ser-Cys(GG)-Ser-Cys(GG) complex) lie in the most favoured region of the Ramachandran plot (PROCHECK). Most of the residues with poorer electron density are located in the additionally allowed regions.

In all three cases the lipid binding site was occupied by a single geranylgeranyl moiety (Figure 4.24). Binding of the geranylgeranyl moiety of the prenylated peptides to RabGGTase leads to conformational changes identical to those seen upon binding of GGPP to the enzyme, involving rotation or displacement of side chains of the hydrophobic residues Phe293β, Tyr241β, Trp244β and Tyr195β (see Figure 4.13 B).

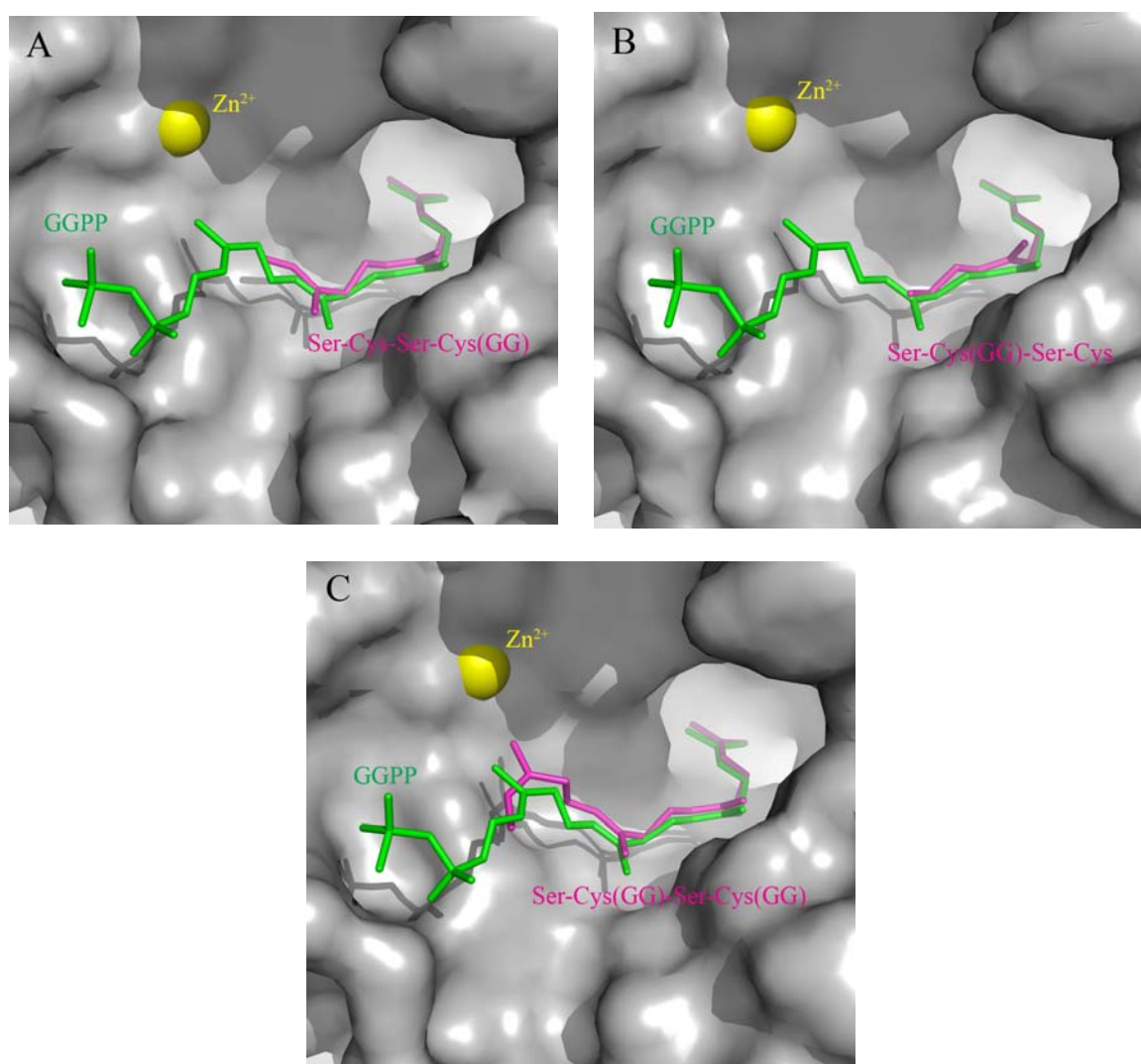


Figure 4.24: Structure analysis of the truncated RabGGTase in complex with Ser-Cys-Ser-Cys(GG), Ser-Cys(GG)-Ser-Cys and Ser-Cys(GG)-Ser-Cys(GG). (A-C) Superimposition of the RabGGTase in complex with native lipid donor GGPP and the prenylated peptides Ser-Cys-Ser-Cys(GG) (A), Ser-Cys(GG)-Ser-Cys (B) and Ser-Cys(GG)-Ser-Cys(GG) (C). The active site of RabGGTase in complex with prenylated peptides is shown in surface representation. The geranylgeranyl moiety of prenylated peptides and GGPP molecules are shown in stick representation and coloured in magenta and green, respectively. Zn^{2+} is displayed as a yellow sphere.

In the case of RabGGTase in complex with Ser-Cys(GG)-Ser-Cys the isoprenoid chain was traceable only to the last 12 carbon atoms and in the case of RabGGTase complexed with Ser-Cys-Ser-Cys(GG) to the last 15 (Figure 4.24). For the diprenylated peptide Ser-Cys(GG)-Ser-Cys(GG) bound to RabGGTase the entire isoprenoid chain was visible. Comparison of the RabGGTase:GGPP complex structure with that bound to the prenylated peptides demonstrated that in all cases the traceable carbon atoms of the prenylated peptides and the

respective carbon atoms of the GGPP adopt very similar conformations and positions (Figure 4.24). This suggests that RabGGTase has only one specific geranylgeranyl moiety binding site available for the association of substrates, reaction intermediates and product.

The invisibility of the peptide chain in the presented structures is not completely surprising. The selection of protein substrates in RabGGTase differs from the CAAX prenyltransferases. The CAAX prenyltransferases recognize the CAAX-motif of their protein substrates. However, RabGGTase must accommodate variations in the C-termini of Rab proteins. Previous studies¹²⁶ suggest that there appears to be no strict order of first isoprenoid addition. Thus, unlike the CAAX prenyltransferases, RabGGTase does not anchor the C-terminus of Rab substrates, explaining the lack of electron density in the determined structures.

The structures of FTase and GGTase-I in complex with both isoprenoid substrate and prenylated peptide product (PDB codes 1KZO and 1N4S, respectively) reveal that binding of the fresh isoprenoid diphosphate substrate dislodges the prenyl group of the prenylated peptides to an 'exit groove' (Figure 1.7), which is formed by helices 1 and 2 and the tip of the helix 12 and which is conserved in the protein prenyltransferase family⁸⁸⁻⁹⁰. The original studies of GGTase-I and FTase led to the proposal that during Rab geranylgeranylation, the first conjugated lipid chain translocates to the conserved 'exit groove' in RabGGTase by displacement of fresh isoprenoid substrate. Additionally, a tunnel located next to the lipid binding site of RabGGTase may serve to stabilize the mono-prenylated product during the processive reaction^{88,89}. Based on the structures presented here, these two scenarios appear to be unlikely since no additional electron density could be detected in this region in any of the solved structures.

The invisibility of the second lipid chain and peptide chains in the structures of RabGGTase in complex with prenylated peptide suggests that there is no specific binding site for association of the dislodged mono-prenylated C-terminus of Rab. It does not form stabilizing interactions with the active site of RabGGTase. This is consistent with the determined affinities of the prenylated peptides towards RabGGTase. The second lipid chain does not positively contribute to the affinity of interaction. The second isoprenoid conjugation is carried out when the thiol of the second C-terminal cysteine is activated by zinc ion. The first conjugated lipid probably provides sterical hindrance for the second cysteine. As a result, the rate of the second transfer step (0.039 s^{-1}) is 4 times slower than the first one (0.16 s^{-1}), despite the higher affinity of the ternary complex^{120;121;126}.

4.12 Model of Rab prenylation process

Based on the presented structures and on available biochemical results on Rab prenylation a reaction model is proposed for RabGGTase (Figure 4.26)¹²⁰⁻¹²⁶.

The Rab prenylation mechanism is different from that of the CAAX protein prenyltransferases. An additional protein factor, REP, is needed for Rab prenylation and usually Rab proteins undergo double geranylgeranylation¹¹⁸. A Rab protein, REP and RabGGTase associate together as a ternary protein complex during the Rab geranylgeranylation. Based on available biochemical data two possible mechanisms were proposed for the formation of the ternary protein complex (Figure 4.26)¹²⁰⁻¹²⁶. In ‘classical’ mechanism of Rab prenylation, the unprenylated Rab interacts with REP first, followed by association of this complex with RabGGTase. The affinity of REP for RabGGTase is increased by the binding of either Rab or GGPP. This observation has led to proposition of an ‘alternative’ mechanism for the formation of the ternary protein complex¹²³, that REP associates with RabGGTase bound to GGPP to form a binary protein complex followed by binding to Rab protein. However, the physiological significance of the presence of these two mechanisms is still unclear⁹².

REP-1 forms a complex with RabGGTase via the interactions between the α -subunit of RabGGTase and domain II of the REP⁹³. The assembly of the binary Rab:REP complex is triggered by the recognition of the GTPase domain of Rab by the Rab binding platform (RBP) of REP¹²⁷. In addition, interactions of the C-terminal interaction motif (CIM), formed by two discontinuous leucine, valine or isoleucine residues near the C-terminus of Rabs, with the C-terminal binding region (CBR) of REP-1 play an important role for the association of the C-terminus of Rabs to the active site of RabGGTase¹¹⁹. Single mutations in the CIM motif (e.g. Rab7I190H and Rab7L192S) result in a 30-70 fold reduction in Rab7:REP-1 affinity and the double mutant Rab7(I190H,L192S) showed no detectable prenylation¹⁹⁹. This suggests that CIM could be viewed as being functionally analogous to the AAX motif of the CAAX box in the case of FTase and GGTase-I, but working from a remote location. In other words both the enzyme and the substrate have “outsourced” their specificity, to the accessory factor (REP) and to a remote upstream sequence respectively. The consequence of such arrangement allows the active site to accommodate a broad variety of C-terminal sequences. However it reduces

the rate of the prenylation reaction. Compared to FTase, the rate (0.16 s^{-1}) of the first geranylgeranylation of Rab7 mediated by RabGGTase is over 100-fold slower^{88,126}.

As there is no detectable binding of the Rab C-terminus to RabGGTase, the ternary complex of RabGGTase in complex with a nonreactive isoprenoid analogue and the C-terminus of Rabs could not be characterized. Superposition of truncated RabGGTase:GGPP with GGTase-I:peptide:GGPP analogue (PDB code 1TNB)¹⁰³ could give some insight into Rab prenylation progression (Figure 4.25). This suggests that during the first Rab geranylgeranylation mediated by RabGGTase one of C-terminal cysteines of Rab is coordinated to the catalytic Zn^{2+} ion. The Zn^{2+} activated C-terminal thiolate reacts with C_1 of GGPP to form a thioether linkage.

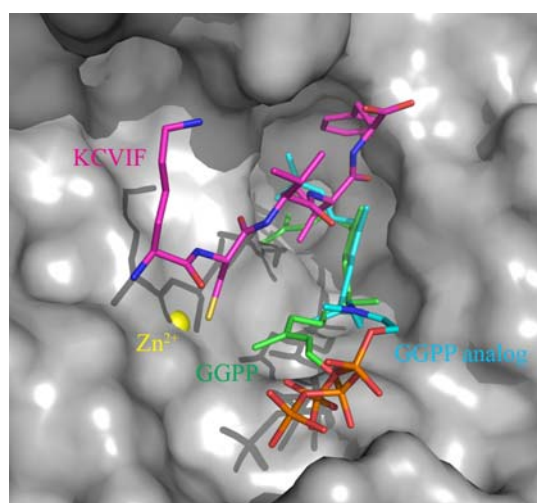


Figure 4.25: Comparison of the binding of substrates in RabGGTase and GGTase-I. The truncated RabGGTase complexed with GGPP and GGTase-I complexed with a nonreactive GGPP analog and a peptide substrate KKSCTKCVIF derived from TC21 (PDB code 1TNB)¹⁰³ were superimposed. The active site of RabGGTase is displayed in surface representation with the Zn^{2+} ion shown as yellow ball. GGPP (green), its analog (blue) and peptide (magenta) are displayed in stick representation.

Following the first geranylgeranylation, a new GGPP molecule binds to the active site and dislodges the first conjugated geranylgeranyl moiety from the hydrophobic cavity. The mono-prenylated C-terminus of Rab does not form specific interactions with the active site and adopts a flexible conformation. While the thiol of the second C-terminal cysteine is activated by Zn^{2+} ion, the second geranylgeranylation is carried out (Figure 4.26). Following the second prenylation the doubly prenylated peptide is released by competition with another GGPP molecule for the lipid binding site of RabGGTase¹²⁴. Subsequently the lipid chains of the prenylated product migrate on the surface of RabGGTase and invade the binding site on

domain II of the REP-1 molecule, resulting in dilation of the lipid-harboring hydrophobic cavity and in displacement of Phe279REP-1 and Arg290REP-1 from their binding sites on the α subunit of RabGGTase. These conformational changes lead to a decrease in the affinity of RabGGTase for the Rab:REP complex and leads to product release by the enzyme¹²⁷ (1.6.2)(Figure 4.26).

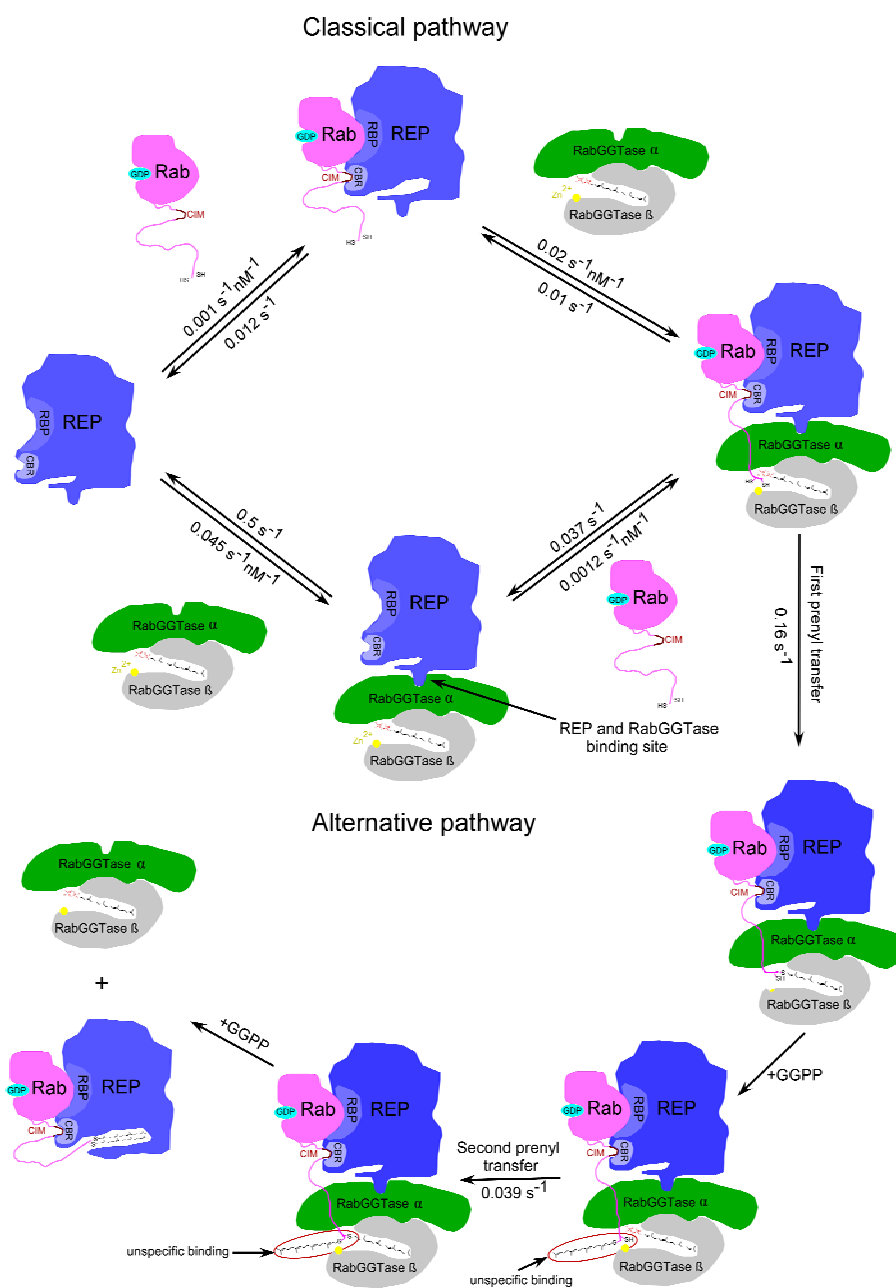


Figure 4.26: Mechanistic model of RabGGTase mediated Rab prenylation. Kinetic constants were adopted from available biochemical data¹²⁰⁻¹²⁶.

Section V

Structural studies of the engineered RabGGTase

in complex with inhibitors

Although numerous effective and specific inhibitors of FTase and GGTase-I (1.7) have been developed, so far, only one specific but weak phosphonocarboxylate inhibitor of RabGGTase has been reported¹⁷¹ in spite of the biological importance of RabGGTase and its involvement in the establishment of several diseases. More recent studies indicate that the inhibition of RabGGTase induces p53-independent apoptosis validating this enzyme as a promising target for anti-cancer therapy^{93;131}. A crystal structure of RabGGTase in complex with such inhibitors could reveal a molecular basis for their inhibitory activities, thus facilitating the development of more effective and selective inhibitors by structure-guided ligand design. The developed inhibitors could serve as candidates for anti-cancer therapy and facilitate the studies of the role of RabGGTase in skeletal disorders, cancer and the biological function of RabGTPases.

4.13 Structures of RabGGTase_αΔLRRAIG in complex with peptidomimetic inhibitors: MT650 and MT670

Compounds MT650 and MT670 were synthesized by Dr. M. Thutewohl^{213;214}. Both compounds are potent inhibitors of FTase and RabGGTase. The IC₅₀ and K_d values of MT670 towards RabGGTase are 5 μM and 1.8 μM, respectively^{208;215}. According to the kinetic results MT670 most probably associates with the peptide binding site of RabGGTase but might have a weak influence on the lipid binding site. Interaction of compound MT650 with RabGGTase showed a binding mode similar to compound MT670 albeit with somewhat lower affinity²⁰⁸. The chemical structures of MT650 and MT670 are shown in Figure 4.27.

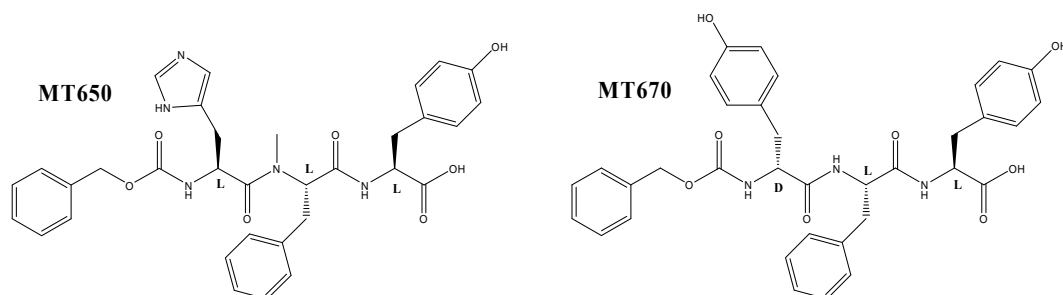


Figure 4.27: Chemical structures of MT650 and MT670.

The preparation of RabGGTase_αΔLRRΔIG in complex with MT650 or MT670 as well as the collection of diffraction data, the subsequent processing and the final structural determination were performed as described in the structural studies of the truncated RabGGTase in complex with prenylated peptides by co-crystallisation. Crystals appeared after 2 days with a rectangular shape and a size of approximately 40*40*100 μm (Figure 4.28). Both crystals belong to space group P212121 and contain one copy of the RabGGTase_αΔLRRΔIG complex in the asymmetric unit.

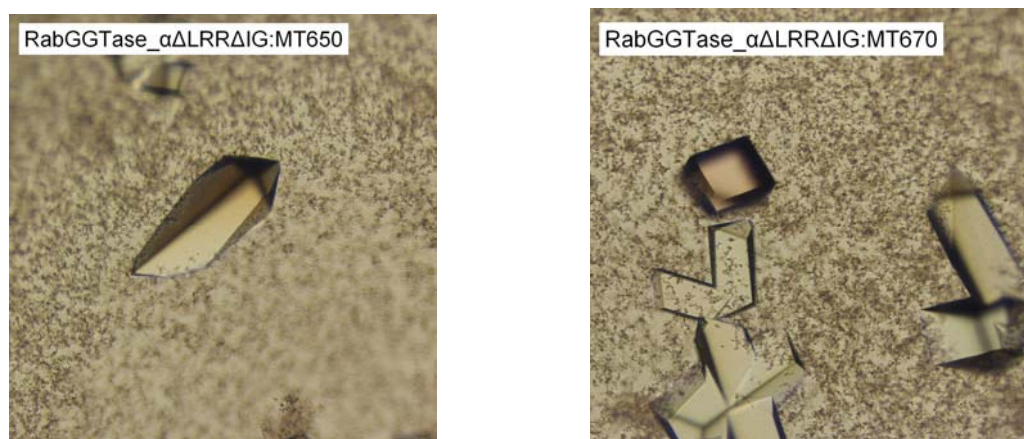


Figure 4.28: Crystals of the RabGGTase_αΔLRRΔIG mutant in complex with MT650 (left) or MT670 (right) obtained by co-crystallisation approach.

Full data collection and refinement statistics are summarized in Table 4.2. Structure factors and coordinates will be deposited in the Protein Data Bank²⁰⁶ with entry codes 3C72 (RabGGTase_αΔLRRΔIG:MT650), and zzzz (RabGGTase_αΔLRRΔIG: MT670)²¹⁵.

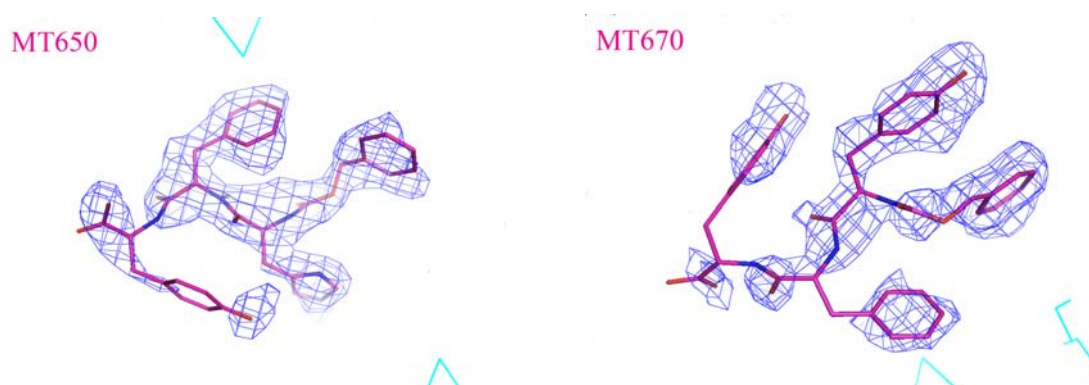


Figure 4.29: Difference electron density of compounds MT650 and MT670, displayed at 2σ . The electron density was calculated prior to incorporation of the ligands into the models.

The structures of the RabGGTase_ $\alpha\Delta$ LRR Δ IG in complex with MT650 or MT670 were determined to 2.3 Å and 2.2 Å resolution, respectively. Initial difference electron density maps (fofc-map) showed strong positive density in the hydrophobic cavity of the β subunit in both complex structures (Figure 4.29). One molecule of MT650 or MT670, respectively, was fitted into the density observed, and final rounds of refinement were performed using a restraints library generated with PRODRG (Figure 4.29).

The quality of the final electron density map together with a comparison of the refined temperature factors of MT650 or MT670 (~ 35 and ~ 30 Å², respectively) and the surrounding protein residues (~ 70 and ~ 60 Å², respectively) suggest that the occupancy of MT650 or MT670 is approximately 50%.

The final model of RabGGTase_ $\alpha\Delta$ LRR Δ IG:MT650 complex contains 191 water molecules, one MT650 molecule, one Zn²⁺ ion and two Ca²⁺ ions. The structure was refined to an R-factor of 18.9 % and R_{free} of 25.6 %. The model of RabGGTase_ $\alpha\Delta$ LRR Δ IG:MT670 complex contains 95 water molecules, one MT670 molecule and one Zn²⁺ ion. The structure was refined to an R-factor of 21.0 % and R_{free} of 28.3 %. Both structures contain one α/β heterodimer in the asymmetric unit. Of the total residues for the complex structure RabGGTase:MT650 and RabGGTase:MT670, 90.6 % and 89.4% lie in the most favoured region of the Ramachandran plot (PROCHECK), respectively. Most of the residues with poorer electron density are located in the additionally allowed regions, with no residue in the disallowed region.

The structures demonstrate that both MT650 and MT670 bind in a similar manner to RabGGTase. Compounds MT650 and MT670 bind in the hydrophobic funnel which contains

the active center in the interface of the α and β subunits of RabGGTase adopting an extended conformation with its C-terminus pointing outward (Figure 4.30 A and B). The binding of these inhibitors does not induce a change in the structure of the active site.

The interaction between RabGGTase and both inhibitors is mainly hydrophobic. In the structure of truncated RabGGTase complexed with MT650 only the carbamate group of the inhibitor forms a strong hydrogen bond (3.0 Å) to the protein, namely with the side chain of Arg144 of the β subunit. The imidazole moiety of MT650 appears to be part of a hydrogen bonding network involving several water molecules and possibly also Tyr97 (3.0 Å) of the β subunit (Figure 4.30 C). A weak hydrogen bond (3.4 Å) to Tyr241 β anchors the C-terminal carboxylate group of the inhibitor. In the structure of truncated RabGGTase in complex with MT670 the hydrogen bond (3.2 Å) between the carbamate group of the inhibitor and the side chain of Arg144 of the β -subunit is also formed. Additionally, the N-terminal tyrosyl side chain of MT670 forms another strong hydrogen bond (2.6 Å) with the side chain of Ser48 β and possibly also a weak hydrogen bond (3.5 Å) with the backbone of Leu96 β (Figure 4.30 D).

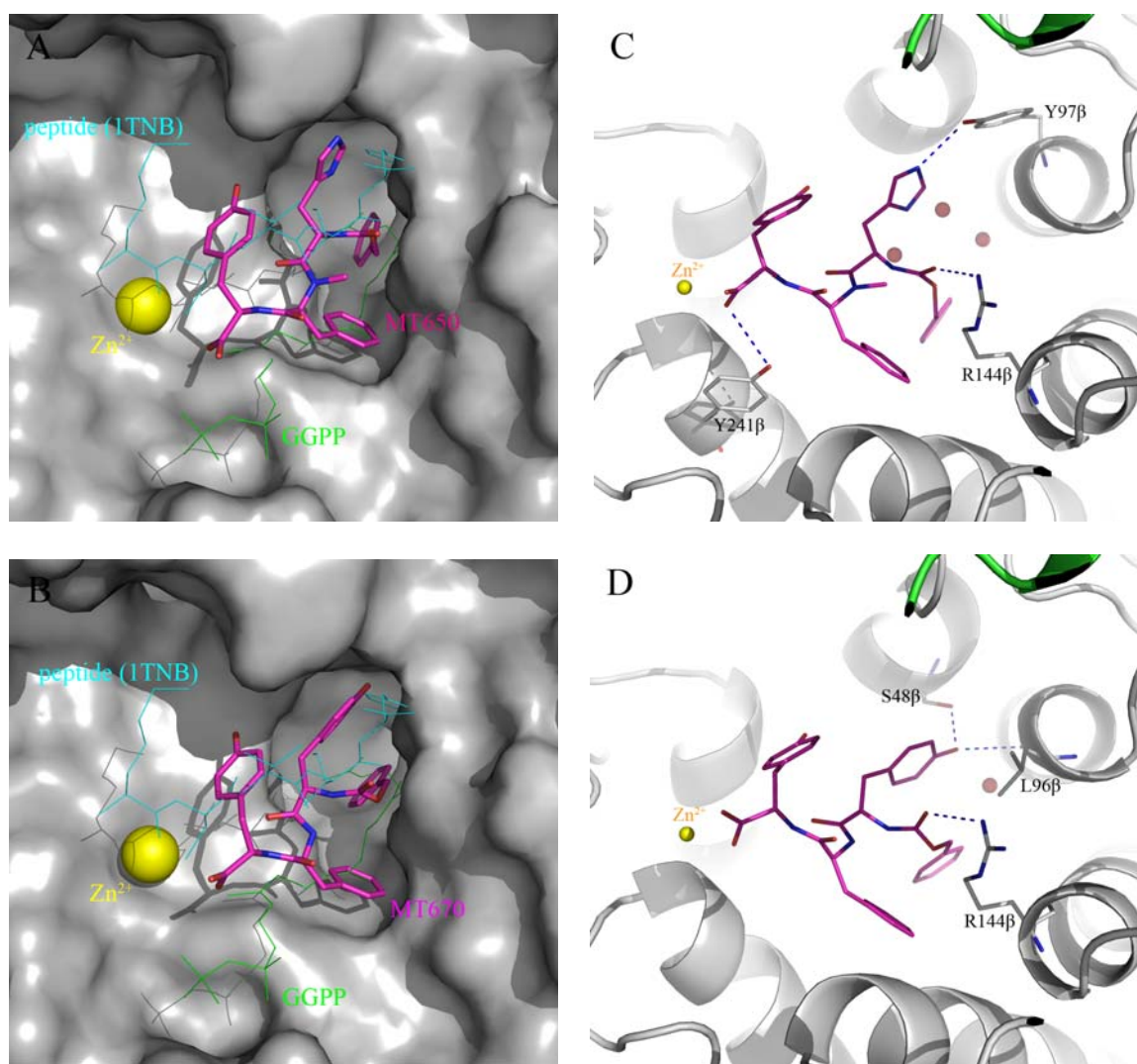


Figure 4.30: Structural analysis of truncated RabGGTase in complex with MT650 and MT670. (A-B) Superimposition of the structure of RabGGTase in complex with compound MT650 (A) or MT670 (B), the RabGGTase:GGPP structure and GGTase-I in complex with the substrate peptide KCVIF and a non-hydrolysable analogue of GGPP (PDB code 1TNB). The active site of RabGGTase in complex with inhibitors is shown in surface representation. The GGPP bound to RabGGTase and the substrate peptide KCVIF in GGTase-I complex are shown in line representation and coloured in green and cyan, respectively. Zn²⁺ ion is represented as yellow spheres, while inhibitors are displayed in stick and in atomic colours. (C-D) Interaction of compound MT650 and MT670 with the active site of RabGGTase. The α and β subunit of RabGGTase are displayed as green and gray cartoons, respectively. The inhibitors and interacting side chains of the β subunit are displayed as sticks coloured by atom type. Blue dashed lines indicate hydrogen bonds. The Zn²⁺ ion and waters participating in the interactions are shown as yellow and red spheres, respectively.

Superimposition of the enzyme:inhibitor structures, the RabGGTase:GGPP structure and the related GGTase-I in complex with a peptide substrate and an analogue of geranylgeranyl

pyrophosphate (PDB code 1TNB)¹⁰³ reveals that the backbone of both inhibitors as well as the histidyl and tyrosyl side chains of MT650 and both tyrosyl side chains of MT670 occupy the presumed protein substrate binding site (Figure 4.30 A and B). The side chain of the C-terminal tyrosine is highly flexible in both structures, indicating that it may act as a general gatekeeper to block accessibility of the protein substrate and that its exact nature may not be important. The phenylalanine of compound MT650 and MT670 protrudes into the hydrophobic isoprenoid binding pocket and therefore provides an additional potential anchoring site for the inhibitor (Figure 4.30 A and B).

Analysis of the complex structure shows more potential attachment points in the immediate vicinity of the bound inhibitor that could be employed to improve the affinity and specificity of the inhibitors. One site is formed by the Zn²⁺ ion and its coordinating His290 β , while the other site (Arg232 β and Lys235 β) is the positively charged cluster which anchors the phosphate moiety of GGPP.

The structure of truncated RabGGTase complexed with compounds MT650 or MT670 reveals the molecular basis for their inhibitory activities. Both inhibitors associate with the peptide binding site of RabGGTase but the phenylalanine side chain of these inhibitors has an influence on the lipid binding site. These observations are consistent with the kinetic results²⁰⁸.

4.14 Structures of RabGGTase α LRRAIG in complex with the first selective peptidomimetic inhibitor: KT90102

Compound KT90102 was more recently synthesized by Dr. K.T. Tan and demonstrated to be a competitive inhibitor of the isoprenoid substrate of RabGGTase²¹⁵. The compound KT90102 shows moderate to fairly good selectivity for RabGGTase compared to FTase and GGTase-I and can be regarded as the first known selective low micromolar RabGGTase inhibitor. The IC₅₀ towards RabGGTase is 10 μ M, towards FTase and GGTase-I 35 and 60 μ M, respectively. The K_d value of this compound for RabGGTase is 1 μ M²¹⁵. The chemical structure of KT90102 is shown in Figure 4.31.

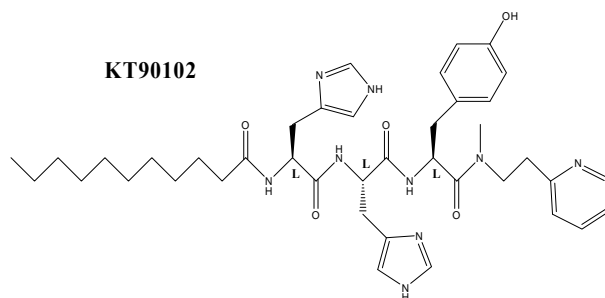


Figure 4.31: Chemical structure of KT90102.

Truncated RabGGTase in complex with KT90102 was prepared by a soaking approach (3.5.3) as follows. 2 μl of 5 mM KT90102 in methanol were applied to a glass cover slip. After evaporation of the organic solvent, 2 μl of soaking solution containing 20% (w/v) PEG3350, 0.2 M CaAc_2 , 0.1 M HEPES pH 7.2, 5mM DTE, 2.5 % DMSO were added. Then the crystals of the apo truncated RabGGTase, which were generated as described above (4.3), were transferred into the soaking solution. The drop was equilibrated at 12°C against 500 μl soaking solution for 4 days. The soaked crystals were directly flash-frozen in liquid nitrogen. Collection of diffraction data, the subsequent processing and the final structural determination were performed as described in the structural studies of the truncated RabGGTase in complex with phosphoisoprenoids. The crystals did not change their space group after soaking.

Full data collection and refinement statistics are summarized in Table 4.2. The structure of the enzyme as a complex with KT90102 was determined to 1.95 Å resolution. Initial difference density electron maps (fofc-map) showed strong positive density in the hydrophobic cavity of the α - α barrel of the β subunit of the structure (Figure 4.32).

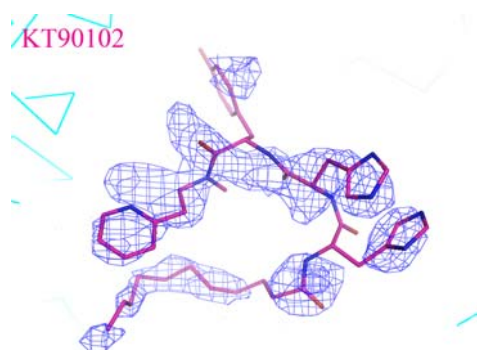


Figure 4.32: Difference electron density of compound KT90102, displayed at 2 σ . The electron density was calculated prior to incorporation of the ligand into the model.

One molecule of KT90102 was fitted into the density observed and final rounds of refinement were performed using a restraints library generated with PRODRG (Figure 4.33). The quality of the final electron density map together with a comparison of the refined temperature factors of KT90102 ($\sim 80 \text{ \AA}^2$) and the surrounding protein residues ($\sim 30 \text{ \AA}^2$) suggest that the occupancy of KT90102 is approximately 40%.

The final model of the RabGGTase_ $\alpha\Delta$ LRR Δ IG:KT90102 complex contains 183 water molecules, one KT90102 molecule, one Zn^{2+} ion and two Ca^{2+} ions. The structure was refined to an R-factor of 20.0 % and R_{free} of 24.0 %. The model of the complex contains one α/β heterodimer in the asymmetric unit. 91.3 % of the total residues for the complex structure lie in the most favoured region of the Ramachandran plot (PROCHECK). Most of the residues with poorer electron density are located in the additionally allowed regions, with no residue in the disallowed region.

The structure complex demonstrates that compound KT90102 binds in the central hydrophobic cavity in the interface of the α and β subunits of RabGGTase, adopting a bent conformation. However, the orientation of the fragment from pyridine to tyrosine of KT90102 could not be exactly determined. This fragment seems to adopt multiple conformations in the complex structure, indicating that it may form unspecific interactions with the hydrophobic tunnel and that its exact nature may not be important. The adopting of multiple conformations might be explained by no pronounced sequence specificity for the C-termini of protein substrates of RabGGTase, in general which perhaps leads to no specific anchoring of this fragment of peptidomimetic in the hydrophobic tunnel of RabGGTase.

The interaction between RabGGTase and compound KT90102 is also mainly hydrophobic. Superimposition of the RabGGTase:KT90102 structure, the RabGGTase:GGPP complex structure and the related GGTase-I in complex with a peptide substrate and an analogue of geranylgeranyl pyrophosphate (PDB code 1TNB)¹⁰³ reveals that the decane moiety of KT90102 occupies the lipid substrate binding site and that the backbone of the peptide as well as the pyridine of KT90102 occupy the presumed protein substrate binding site (Figure 4.33). Remarkably, the imidazole moiety of the histidine between the other histidine and tyrosine tightly coordinates the catalytic Zn^{2+} ion blocking the activation of the thiol of the C-terminal cysteine of protein substrate.

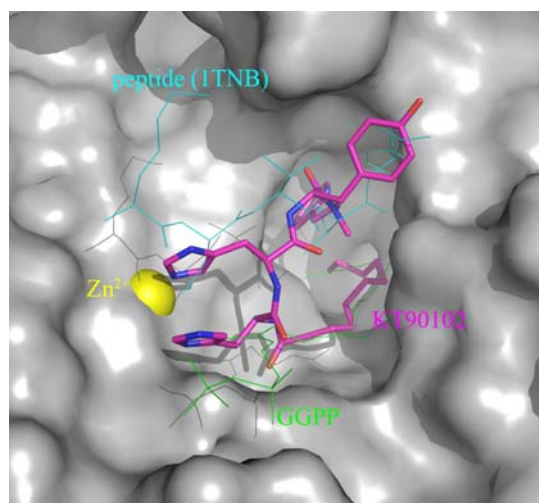


Figure 4.33: Structural analysis of truncated RabGGTase in complex with KT90102. Superimposition of the RabGGTase:KT90102 structure, the RabGGTase:GGPP structure and GGTase-I in complex with substrate peptide KCVIF and a non-hydrolysable analogue of GGPP (PDB code 1TNB). The active site of RabGGTase in complex with inhibitor is shown in surface representation. The GGPP bound to RabGGTase and the substrate peptide KCVIF in the GGTase-I complex are shown in line representation and coloured in green and cyan, respectively. Zn^{2+} ion is represented in yellow sphere, while the inhibitor is displayed in stick and in atomic colours.

The structure of truncated RabGGTase complexed with compound KT90102 reveals the molecular basis for its inhibitory activity. This observation is consistent with the kinetic results, which showed that the inhibitor associates with the lipid binding site of RabGGTase. Judging from this structure the inhibitor has a strong influence on the peptide binding site.

4.15 Structure of RabGGTase $_{\alpha}$ ΔLRRAIG in complex with a specific inhibitor: psoromic acid

Psoromic acid (PA) is a natural product from lichens and has recently been identified as a specific inhibitor of RabGGTase²¹⁶. It shows good selectivity for RabGGTase compared to FTase and GGTase-I. The IC_{50} towards RabGGTase is 1.6 μ M and, 114 and 78 μ M towards FTase and GGTase-I, respectively. The K_d value of this compound for RabGGTase was determined to be 130 nM²¹⁶. The chemical structure of psoromic acid is shown in Figure 4.34.

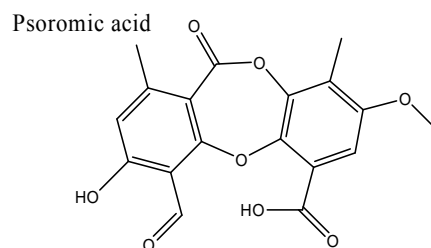


Figure 4.34: Chemical structures of Psoromic acid (PA).

After substantial experimentation, crystals of the complex of PA with a truncated version of RabGGTase were obtained and the structure was determined with a resolution of 2.5 Å.

The preparation of the truncated RabGGTase:PA complex crystals, the collection of diffraction data, the subsequent processing and the final structural determination were performed as described in the structural study of the truncated RabGGTase in complex with inhibitor KT90102. The crystals did not change their space group after soaking. Full data collection and refinement statistics are summarized in Table 4.2. Structure factors and coordinates will be deposited in the Protein Data Bank with entry codes *zzzz* (RabGGTase_αΔLRRΔIG: PA).

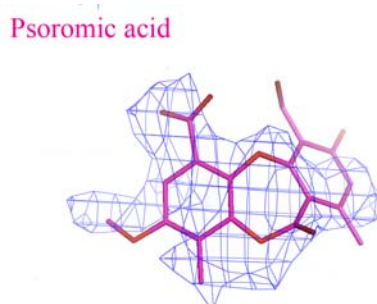


Figure 4.35: Difference electron density of PA, displayed at 2 σ . The electron density was calculated prior to the incorporation of the ligand into the model.

Initial difference electron density maps (fofc-map) showed strong positive density at the entrance of the central hydrophobic cavity of the enzyme (Figure 4.35). One psoromic acid molecule was fitted into the density observed and final rounds of refinement were performed using a restraints library generated with PRODRG. However, the exact binding mode of this compound in the structure could not be strictly determined. There were in all five possibilities for the binding of PA. This was caused by two reasons. One reason is the low aqueous solubility of PA, leading to low occupancy of the inhibitor in crystals. The other reason is the similar substituted groups at both phenyl rings of PA, which made special difficulty to

determine the binding mode because the electron densities of both substituted phenyl groups appeared similar. Though some docking studies were performed by S. Wetzel, but with limited success since the cavity was very large. Then the derivatives of PA (including active and inactive compounds), synthesized by Dr. C. Deraeve, were modeled into structure by using the five possible binding modes. Analysis the modeled structures and the inhibitory activities of these derivatives suggests that only the binding mode shown in Figure 4.36 is possible. According to the modeled structures, most of inactive derivatives of PA would clash with the enzyme by using this binding mode, but would fit well by using the other four binding modes. Finally, the binding mode of PA to RabGGTase was proposed (Figure 4.35 and Figure 4.36) by the structural determination in context with structure-activity relationship (SAR).

The quality of the final electron density map together with a comparison of the refined temperature factors of PA ($\sim 100 \text{ \AA}^2$) and the surrounding protein residues ($\sim 50 \text{ \AA}^2$) suggest that the occupancy of PA is approximately 50%.

The final model of the RabGGTase $_{\alpha\Delta\text{LRR}\Delta\text{IG}}$:PA complex contains 6 water molecules, one PA molecule and one Zn^{2+} ion. The structure was refined to an R-factor of 22.7 % and R_{free} of 29.8 %. The model of the complex contains one α/β heterodimer in the asymmetric unit. 90.6 % of the total residues for the complex structure lie in the most favoured region of the Ramachandran plot (PROCHECK). Most of the residues with poorer electron density are located in the additionally allowed regions, with no residue in the disallowed region.

The structure complex demonstrates that PA binds at the entrance of the central hydrophobic funnel (Figure 4.36). The binding of this inhibitor does not induce a significant change in the structure of the active site. Superimposition of this RabGGTase:PA structure, the RabGGTase:GGPP structure and the related GGTase-I in complex with a peptide substrate and a nonreactive GGPP analogue (PDB code 1TNB)¹⁰³ reveals that the inhibitor occupies the binding site of Rab C-terminus (Figure 4.36 A), but has a weak influence on the lipid binding site.

Besides the hydrophobic interaction between RabGGTase and PA, the lactone on the seven-membered ring of PA coordinates the Zn^{2+} ion via a water molecule. Additionally, the phenolic hydroxy group of PA forms a strong hydrogen bond (2.6 \AA) with the side chain of Tyr44 of the β subunit and a weak hydrogen bond (3.3 \AA) with Asp61 of the α subunit (Figure

4.36 B). It seems that both coordinations serve as ‘anchors’ for the binding of PA at the entrance of the cavity. Superimposition of this structure, the GGTase-I structure (PDB code 1N4P)⁸⁹ and the FTase structure (PDB code 1FT1)⁹¹ illustrates the molecular basis for its high specificity for RabGGTase compared to GGTase-I and FTase (Figure 4.36 C). As described above one ‘anchor’ is formed by residues Tyr44 β and Asp61 α in RabGGTase, whereas the corresponding positions in GGTase-I are occupied by Thr45 β and Ala129 α , in FTase by Ala98 β and Ala129 α . The lack of this ‘anchor’ in GGTase-I and FTase is probably responsible for the much higher IC₅₀-values towards both enzymes.

Analysis of the complex structure reveals several attachment points in the immediate vicinity of the bound inhibitor that could serve to improve the affinity and specificity of the inhibitors. One site formed by Arg232 β and Lys235 β is a positively charged cluster, which coordinates the phosphate moiety of GGPP. The other sites are composed of residue His190 β positioned to the methyl ether moiety of PA and of residue Arg144 β positioned to the carboxylic acid group of PA.

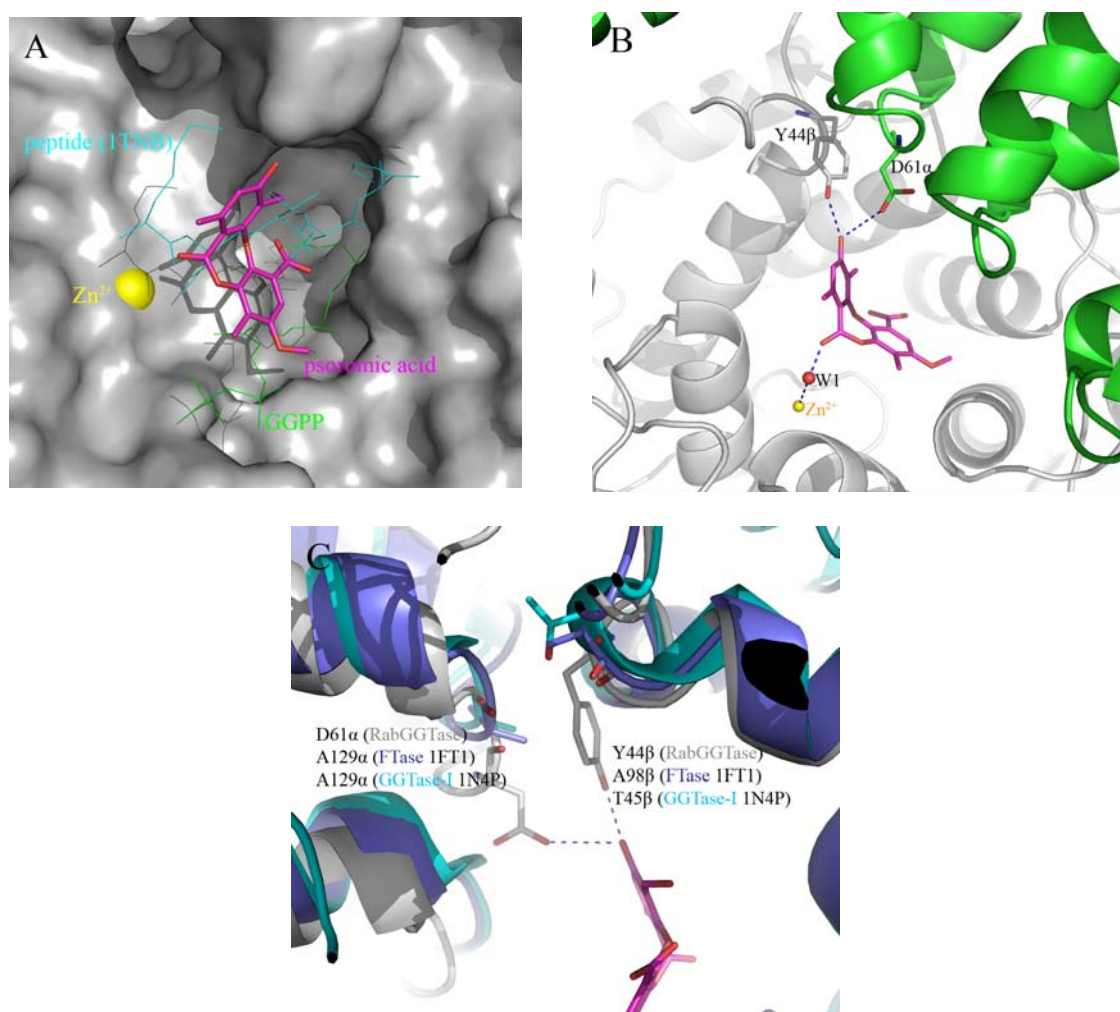


Figure 4.36: Structural analysis of truncated RabGGTase in complex with psoromic acid. (A) Superimposition of the of RabGGTase:PA structures, the RabGGTase:GGPP structure and the GGTase-I in complex with substrate peptide KCVIF and a non-hydrolysable analogue of GGPP (PDB code 1TNB). The active site of RabGGTase in complex with inhibitors is shown in surface representation. The GGPP bound to RabGGTase and the substrate peptide KCVIF in the GGTase-I complex are shown in line representation and coloured in green and cyan, respectively. The Zn^{2+} ion is represented in yellow sphere, while the inhibitors are displayed in stick and in atomic colours. **(B)** Interactions of compound PA with the active site of RabGGTase. The α and β subunit of RabGGTase are displayed as green and gray cartoons, respectively. The inhibitors and interacting side chains of RabGGTase are displayed as sticks coloured by atom type. Blue dashes indicate hydrogen bonds, the Zn^{2+} ion and water molecule participating in the interaction are shown as yellow and red spheres, respectively. **(C)** Superimposition of this complex structure and the structure of GGTase-I (PDB code 1N4P) and FTase (PDB code 1FT1) reveals the molecular basis for its high specificity for RabGGTase compared to GGTase-I and FTase. RabGGTase, GGTase-I and FTase are displayed as gray, cyan and blue cartoon, respectively, while the Zn^{2+} ion is shown as yellow sphere. The residues Y44 β and D61 α in RabGGTase and the corresponding residues in GGTase-I Thr45 β and Ala129 α , in FTase Ala98 β and Ala129 α , are displayed as stick.

Table 4.2 Data collection statistics for the truncated FTase, RabGGTase and its complexes.

Data collection	RabGGTase	FTase	RabGGTase:GGPP
Wavelength (Å)/Beamline	0.9800/ SLS-PXII	0.9825 / SLS-PXII	1.0007/ SLS-PXII
Resolution (Highest Shell, Å)	29.4 – 1.8 (1.9 – 1.8)	30.0 – 2.8 (2.85 – 2.8)	29.4 – 1.85 (1.9 – 1.85)
Space group	P2 ₁ 2 ₁ 2 ₁	P6 ₁	P2 ₁ 2 ₁ 2 ₁
Cell constants (Å; °)	a=66.7, b=90.6, c=114.1; $\alpha=\beta=\gamma=90$	a=172.9, b=172.9, c=70.5; $\alpha=\beta=90, \gamma=120$	a=67.3, b=90.6, c=114.5; $\alpha=\beta=\gamma=90$
V _M	2.5	2.5	2.5
Total measurements	294558	181484	278888
Unique reflections	64333	29762	60104
Average redundancy	4.6 (3.4)	6.1 (6.3)	4.6 (4.5)
I/ σ	16.4 (4.7)	12.3 (3.9)	20.5 (3.9)
Completeness (%)	99.3 (99.7)	99.6 (99.9)	99.5 (99.5)
R _{sym} ^a	6.3 (27.5)	33.9 (68.0)	4.2 (44.6)
Wilson B-factor (Å ²)	30	54.55	48.4
Refinement			
Resolution (Highest Shell, Å)	1.8 (1.85 – 1.8)	2.8 (2.87 – 2.8)	1.85 (1.9 – 1.85)
R ^b	18.52	17.69	21.32
R _{free} ^c	21.77	23.22	24.99
rmsd bonds (Å)/angles (°)	0.008/1.267	0.019/1.786	0.011/1.392
B-factor deviation bonds/angles (Å ²)			
main chain	0.943/1.657	1.595/2.725	1.183/2.002
side chain	2.111/3.069	3.123/4.977	2.367/3.327
Residues in Ramachandran Core (%) ^d	90.8	86.5	91.0
Protein atoms	5016	5749	4869
Solvent atoms	394	54	127
Ligand atoms	3	1	32
Average B-factor (Å ²)	24.18	53.01	45.71
PDB accession code			

Table 4.2: Data collection statistics for the truncated FTase, RabGGTase and its complexes (continuous).

Data collection	RabGGTase:FPP	RabGGTase:GGMP	RabGGTase:GGTP
Wavelength (Å)/Beamline	0.9998/ SLS-PXII	0.9794/ SLS-PXII	1.0002 / SLS-PXII
Resolution (Highest Shell, Å)	29.4 – 1.85 (1.9 – 1.85)	29.7 – 2.55 (2.6 – 2.55)	29.4 – 2.0 (2.1 – 2.0)
Space group	P2 ₁ 2 ₁ 2 ₁	P2 ₁ 2 ₁ 2 ₁	P2 ₁ 2 ₁ 2 ₁
Cell constants (Å; °)	a=66.9, b=90.9, c=114.2; $\alpha=\beta=\gamma=90$	a=67.5, b=92.2, c=114.5; $\alpha=\beta=\gamma=90$	a=66.2, b=91.2, c=115.4; $\alpha=\beta=\gamma=90$
V _M	2.5	2.5	2.5
Total measurements	339708	94709	236439
Unique reflections	59021	23795	47955
Average redundancy	5.8 (5.8)	4.0 (4.1)	4.9 (5.0)
I/ σ	21.0 (3.4)	13.3 (3.1)	21.2 (4.9)
Completeness (%)	98.2 (98.0)	99.3 (99.9)	99.8 (99.9)
R _{sym} ^a	4.9 (56.5)	6.5 (40.0)	5.3 (32.7)
Wilson B-factor (Å ²)	34.7	56.4	31.79
Refinement			
Resolution (Highest Shell, Å)	1.85 (1.9 – 1.85)	2.55 (2.62 – 2.55)	2.0 (2.05 – 2.0)
R ^b	20.41	21.67	19.58
R _{free} ^c	23.53	29.06	23.49
rmsd bonds (Å)/angles (°)	0.010/1.349	0.015/1.635	0.008/1.240
B-factor deviation bonds/angles (Å ²)			
main chain	0.982/1.775	1.356/2.393	0.816/1.448
side chain	1.871/2.880	2.429/3.754	1.506/2.228
Residues in Ramachandran Core (%) ^d	91.2	88.5	91.3
Protein atoms	5137	4922	4897
Solvent atoms	215	36	290
Ligand atoms	26	26	35
Average B-factor (Å ²)	31.33	52.69	27.62
PDB accession code			

Table 4.2: Data collection statistics for the truncated FTase, RabGGTase and its complexes (continuous).

Data collection	RabGGTase Ser-Cys-Ser-Cys(GG)	RabGGTase Ser-Cys(GG)-Ser-Cys	RabGGTase Ser-Cys(GG)-Ser-Cys(GG)
Wavelength (Å)/Beamline	0.9999/ SLS-PXII	0.9825/ SLS-PXII	0.9841 / SLS-PXII
Resolution (Highest Shell, Å)	29.4 – 1.9 (1.95 – 1.9)	29.4 – 2.1 (2.15 – 2.1)	29.4 – 2.0 (2.05 – 2.0)
Space group	P2 ₁ 2 ₁ 2 ₁	P2 ₁ 2 ₁ 2 ₁	P2 ₁ 2 ₁ 2 ₁
Cell constants (Å; °)	a=67.0, b=90.6, c=114.4; $\alpha=\beta=\gamma=90$	a=67.1, b=90.9, c=114.3; $\alpha=\beta=\gamma=90$	a=67.4, b=91.2, c=114.6; $\alpha=\beta=\gamma=90$
V _M	2.5	2.5	2.5
Total measurements	996311	165055	350190
Unique reflections	55522	41204	48343
Average redundancy	17.9 (16.3)	4.0 (4.1)	7.2 (7.4)
I/σ	24.6 (4.6)	14.4 (4.2)	20.7 (4.3)
Completeness (%)	99.8 (99.4)	99.2 (100)	99.8 (99.9)
R _{sym} ^a	10.3 (91.0)	7.5 (47.6)	6.5 (66.6)
Wilson B-factor (Å ²)	29.1	38.8	37.9
Refinement			
Resolution (Highest Shell, Å)	1.9 (1.95 – 1.9)	2.1 (2.1 – 2.15)	2.0 (2.05 – 2.0)
R ^b	16.05	17.22	18.12
R _{free} ^c	22.07	23.27	24.05
rmsd bonds (Å)/angles (°)	0.021/1.833	0.020/1.787	0.019/1.730
B-factor deviation bonds/angles (Å ²)			
main chain	1.899/2.833	1.703/2.680	1.812/2.741
side chain	4.441/6.039	4.076/5.666	4.140/5.617
Residues in Ramachandran Core (%) ^d	91.9	92.7	92.3
Protein atoms	4926	4962	4959
Solvent atoms	386	153	203
Ligand atoms	17	14	22
Average B-factor (Å ²)	25.21	36.17	33.57
PDB accession code			

Table 4.2: Data collection statistics for the truncated FTase, RabGGTase and its complexes (continuous).

Data collection	RabGGTase:MT650	RabGGTase:MT670	RabGGTase:KT90102
Wavelength (Å)/Beamline	0.9797 / SLS-PXII	0.9816 / SLS-PXII	0.9794 / SLS-PXII
Resolution (Highest Shell, Å)	20.0 – 2.3 (2.4 – 2.3)	29.4 – 2.2 (2.25 – 2.2)	29.4 – 1.95 (2.0 – 1.95)
Space group	P2 ₁ 2 ₁ 2 ₁	P2 ₁ 2 ₁ 2 ₁	P2 ₁ 2 ₁ 2 ₁
Cell constants (Å; °)	a=66.2, b=91.7, c=115.4; $\alpha=\beta=\gamma=90$	a=66.5, b=90.6, c=115.2; $\alpha=\beta=\gamma=90$	a=66.4, b=90.6, c=114.9; $\alpha=\beta=\gamma=90$
V _M	2.5	2.5	2.5
Total measurements	181449	168703	415495
Unique reflections	31830	35201	50656
Average redundancy	5.7 (5.8)	4.8 (4.7)	8.2 (8.2)
I/ σ	20.0 (4.7)	17.1 (3.8)	20.4 (4.1)
Completeness (%)	99.7 (100.0)	97.6 (99.0)	98.9 (100.0)
R _{sym} ^a	5.2 (40.7)	5.5 (41.7)	9.0 (102.6)
Wilson B-factor (Å ²)	50.3	43.1	37.44
Refinement			
Resolution (Highest Shell, Å)	2.3 (2.36 – 2.3)	2.2 (2.26 – 2.2)	1.95 (2.0 – 1.95)
R ^b	18.92	21.03	20.00
R _{free} ^c	25.63	28.33	24.00
rmsd bonds (Å)/angles (°)	0.019/1.622	0.018/1.761	0.010/1.258
B-factor deviation bonds/angles (Å ²)			
main chain	0.878/1.451	1.392/2.274	1.114/1.885
side chain	2.100/2.958	3.191/4.536	3.054/4.967
Residues in Ramachandran Core (%) ^d	90.6	89.4	91.3
Protein atoms	5017	4891	4881
Solvent atoms	191	95	183
Ligand atoms	47	47	57
Average B-factor (Å ²)	31.26	44.34	33.73
PDB accession code	3C72		

Table 4.2: Data collection statistics for the truncated FTase, RabGGTase and its complexes (continuous).

Data collection	RabGGTase:PA
Wavelength (Å)/Beamline	1.0007 / SLS-PXII
Resolution (Highest Shell, Å)	20.2 – 2.5 (2.6 – 2.5)
Space group	P2 ₁ 2 ₁ 2 ₁
Cell constants (Å; °)	a=65.6, b=92.0, c=116.0; α=β=γ=90
V _M	2.5
Total measurements	109349
Unique reflections	24579
Average redundancy	4.4 (4.5)
I/σ	21.4 (3.7)
Completeness (%)	98.5 (99.3)
R _{sym} ^a	4.0 (46.9)
Wilson B-factor (Å ²)	67.3
Refinement	
Resolution (Highest Shell, Å)	2.5 (2.56 – 2.5)
R ^b	22.69
R _{free} ^c	29.82
rmsd bonds (Å)/angles (°)	0.016/1.602
B-factor deviation bonds/angles (Å ²)	
main chain	1.446/2.409
side chain	2.883/4.192
Residues in Ramachandran Core (%) ^d	90.6
Protein atoms	4689
Solvent atoms	6
Ligand atoms	27
Average B-factor (Å ²)	64.40
PDB accession code	

^aR_{sym} = $\frac{\sum \sum I(h)_j - \langle I(h) \rangle}{\sum \sum I(h)_j}$ where I(h)_j is the measured diffraction intensity and the summation includes all observations.

^bR is the R-factor = $(\sum |F_O| - \sum |F_C|) / \sum |F_O|$.

^cR_{free} is the R-factor calculated using 5 % of the data that were excluded from the refinement.

^dRamachandran core refers to the most favoured regions in the φ/ψ-Ramachandran plot as defined by Laskowski *et al.* (Laskowski *et al.*, 1993).

5 Summary and Conclusion

5.1 Summary and Conclusion (English)

The structural analysis of RabGGTase was previously hampered by difficulties in obtaining well diffracting crystals in a reliable and reproducible manner. In this project, an engineered rat RabGGTase without the LRR and IG domains was designed and produced in recombinant from *E. coli*. This RabGGTase mutant was able to prenylate Rab7 with an efficiency comparable to that of wild type enzyme. This confirms an earlier proposal that the LRR and IG domains of mammalian RabGGTase are not involved in the prenylation reaction and play another, as yet unidentified function. Unlike wild type enzyme the RabGGTase $_{\alpha\Delta\text{LRR}\Delta\text{IG}}$ mutant could be easily crystallized and yielded high-quality crystals which produced diffraction data allowing structure determination to a resolution of 1.8 Å. As expected, the overall structure of the engineered enzyme changed very little compared to the wild type enzyme and was similar to that of FTase and GGTase-I.

The availability of an easily crystallisable variant of RabGGTase enabled solution of its structure in complex with the isoprenoid substrate, GGPP, to 1.85 Å resolution. This structure has completed the picture of enzyme:substrate complexes for the protein prenyltransferase family and provided mechanistic insights into the lipid substrate specificity of protein prenyltransferases. Analysis of the structure of the complex revealed several critical amino acids at the bottom of hydrophobic lipid binding site that play an essential role in selecting the respective isoprenoid substrate. Compared to FTase and GGTase-I, RabGGTase has an expanded lipid binding pocket which enables it to accept bulky substrates such as biotinyleranyl pyrophosphate (Biotin-GPP)²⁰². By comparing all three prenyltransferases in complex with lipid substrates we were able to design the mutants of FTase and GGTase-I capable of conjugating Biotin-GPP to their cognate protein substrates. These mutants can be used to rapidly identify, isolate and characterize prenylatable proteins in mammalian cell. This provides a new technological venue in protein prenyltransferase research.

The structural and biochemical data obtained in this work suggested that FPP can serve as a lipid substrate of RabGGTase. Interestingly, we showed that GGMP and GGTP can not serve as lipid donors in Rab prenylation. The structures of the truncated RabGGTase complexed

with FPP, GGMP and GGTP have been determined at 1.85 Å, 2.55 Å and 2.0 Å resolution, respectively. These structures provide insight into the mode of isoprenoid binding to RabGGTase. The RabGGTase:GGMP complex is very similar to the complex with GGPP, while the complex with GGTP shows significant differences. Remarkably, comparison of the structures of GGPP and FPP bound to the RabGGTase mutant reveals the molecular basis of the large difference in their binding affinities. FPP has significantly fewer hydrogen bonds between the diphosphate group and the active site, and this in combination with the reduction of hydrophobic interactions by the lack of one isoprene unit in FPP leads to >100 times reduction in the affinity of FPP relative to GGPP for RabGGTase.

To complete the structural picture of the RabGGTase cycle, we attempted co-crystallization of RabGGTase with prenylated peptides mimicking reaction intermediates and the final products of Rab7 prenylation. The structures of the truncated RabGGTase in complex with Ser-Cys-Ser-Cys(GG), Ser-Cys(GG)-Ser-Cys and Ser-Cys(GG)-Ser-Cys(GG) mimicking mono- and di-prenylated Rab7, were determined at 1.9 Å, 2.1 Å and 2.0 Å resolution, respectively. These prenylated peptides bind to RabGGTase with comparable affinities (K_d ca. 1-2 μ M). The lack of electron density for the peptide chain in these structures is caused by the fact that RabGGTase cannot and indeed does not need to anchor the C-terminus of the Rab substrates. The invisibility of the second lipid chain in the case of di-prenylated peptide indicates that, unlike the CAAX-prenyltransferases, an 'exit groove' is not available for stabilizing of the dislodged prenyl group. Based on these structures and on available biochemical data on Rab prenylation, a reaction cycle is proposed for RabGGTase.

The structures of the truncated RabGGTase in complex with inhibitors MT650, MT670, KT90102 and psoromic acid have been determined at 2.3 Å, 2.2 Å, 1.95 Å and 2.5 Å resolution, respectively. Analysis of these complex structures reveals the molecular basis for their inhibitory activities, which relies predominantly on blocking the putative peptide binding site of RabGGTase. These observations are consistent with the available kinetic results. From the analysis of RabGGTase:inhibitor structures it transpires that several modifications of the chemical structures of these inhibitors could be preformed to improve the affinity and specificity of the inhibitors by structure-guided ligand design. Inhibitors with increased potency and specificity for RabGGTase are candidates for anti-cancer therapy and anti-osteoporosis therapy.

5.2 Summary and Conclusion (Deutsch)

Schwierigkeiten in der verlässlichen und reproduzierbaren Herstellung gut streuender Kristalle erschwerte bislang die strukturelle Analyse von RabGGTase.

In diesem Projekt wurde daher eine veränderte RabGGTase aus Ratte ohne die LRR- und IG-Domäne generiert und rekombinant in *E. coli* hergestellt. Diese RabGGTase-Mutante war in der Lage, Rab7 mit einer dem Wildtyp vergleichbaren Effizienz zu prenylieren. Dieser Umstand bestätigt eine frühere Vermutung, dass die LRR- und IG-Domänen von Säuger-RabGGTase nicht an der Prenylierungs-Reaktion beteiligt sind und eine andere, bislang unbekannt Funktion haben.

Im Gegensatz zum Wildtyp-Enzym konnte aus der $\alpha\Delta\text{LRR}\Delta\text{IG}$ -Mutante von RabGGTase einfach hochwertige Kristalle erhalten werden. Die erhaltenen Diffraktionsdaten erlaubte eine Strukturaufklärung mit einer Auflösung von 1,8 Å. Wie erwartet, zeigte die Gesamtstruktur des modifizierten Enzyms nur sehr geringe Unterschiede zum Wildtypenzym und war den Strukturen von FTase und GGTase-I ähnlich.

Die Verfügbarkeit einer einfach kristallisierbaren Variante von RabGGTase ermöglichte die Strukturlösung des Enzyms im Komplex mit dem Isoprenoid-Substrats GGPP mit einer Auflösung von 1,85 Å. Die Struktur vervollständigte das Bild der Enzym-Substrat-Komplexe der Prenyltransferase-Familie und ermöglichte Einblicke in den Mechanismus der Lipid-Substratspezifität der Prenyltransferasen. Die Analyse der Komplex-Struktur zeigte am Boden der hydrophoben Lipid-Bindungsstelle mehrere essentielle Aminosäuren, die eine entscheidende Rolle in der Selektion der betreffenden Isoprenoid-Substrate haben. Im Gegensatz zu FTase und GGTase-I besitzt die RabGGTase eine ausgedehnte Lipid-Bindetasche, die es erlaubt große Substrate, wie Biotingeranyl-Pyrophosphat (Biotin-GPP)²⁰² zu binden. Ein Vergleich aller drei Prenyltransferasen im Komplex mit den Lipid-Substraten ermöglichte das Design von FTase- und GGTase-I-Mutanten, die in der Lage waren Biotin-GPP an ihre entsprechenden Protein-Substrate zu konjugieren.

Die in dieser Arbeit erhaltenen strukturellen und biochemischen Daten lassen vermuten, daß FPP als Lipid-Substrat für RabGGTase fungieren kann. Interessanterweise konnten wir zeigen, daß GGMP bzw. GGTP nicht als Lipid-Donoren der Rab-Prenylation fungieren können. Die Strukturen der verkürzten RabGGTase im Komplex mit FPP, GGMP oder GGTP wurden mit 1,85 Å, 2,55 Å bzw. 2,0 Å Auflösung bestimmt. Diese Strukturen ermöglichten

Einblicke in den Bindungsmodus des Isoprenoids an die RabGGTase. Der RabGGTase:GGMP-Komplex ist sehr ähnlich zum GGPP-Komplex, wohingegen der GGTP-Komplex signifikante Unterschiede zeigt. Der Vergleich der Strukturen von RabGGTase gebundenem GGPP und FPP läßt die molekulare Grundlage für die großen Unterschiede in den Bindungsaffinitäten erkennen. FPP weist signifikant weniger Wasserstoffbrücken zwischen der Diphosphat-Gruppe und dem aktiven Zentrum auf. Dies und die geringere Anzahl an hydrophoben Interaktionen durch das Fehlen einer Isopren-Einheit in FPP führt zu einer mehr als 100-fach erniedrigten Affinität von FPP zu RabGGTase im Vergleich zu GGPP.

Um das strukturelle Bild des RabGGTase- Zyklus zu vervollständigen, wurden Cokristallisation von RabGGTase mit prenylierten Peptiden durchgeführt, welche als Analoga für Reaktionsintermediate bzw. Endprodukte der Rab7-Prenylierung dienten. Die Strukturen der verkürzten RabGGTase im Komplex mit Ser-Cys-Ser-Cys(GG), Ser-Cys(GG)-Ser-Cys bzw. Ser-Cys(GG)-Ser-Cys(GG) als Analoga für mono- und diprenyliertes Rab7 wurden mit 1,9 Å, 2,1 Å bzw. 2,0 Å Auflösung bestimmt. Diese prenylierten Peptide binden mit vergleichbaren Affinitäten (K_d ca. 1-2 μ M) an RabGGTase. Das Fehlen einer Elektronendichte für die Peptidkette in den Strukturen ist darin begründet, daß RabGGTase nicht in der Lage ist und nicht in der Lage sein muss, den C-Terminus des Rab-Substrates zu verankern. Die Nichtsichtbarkeit der zweiten Lipid-Kette im Falle des diprenylierten Peptids zeigt, dass, im Gegensatz zu den CAAX-Prenyltransferasen, keine „Ausgangsfurche“ zur Stabilisierung der entfernteren Prenylgruppe vorhanden ist. Auf Grundlage der erhaltenen Strukturen und verfügbaren biochemischen Daten zur Rab-Prenylierung konnte ein Reaktionszyklus für RabGGTase aufgestellt werden.

Die Strukturen von verkürzter RabGGTase im Komplex mit den Inhibitoren MT650, MT670, KT90102 und psoromic acid wurden mit einer Auflösung von 2,3 Å, 2,2 Å, 1,95 Å bzw. 2,5 Å bestimmt. Die Analyse dieser Komplex-Strukturen zeigte die molekulare Grundlage ihrer inhibitorischen Aktivitäten, die in erster Linie in der Blockierung der vermuteten Peptid-Bindungsstelle von RabGGTase besteht. Diese Beobachtungen stehen in Übereinstimmung mit verfügbaren kinetischen Ergebnissen. Auf Grundlage der RabGGTase:Inhibitor-Strukturen konnten verschiedene chemische Modifikationen an den Inhibitorstrukturen ausgeführt werden, um die Affinität und Spezifität der Inhibitoren durch Struktur-gesteuertes

Ligand-Design zu verbessern. Inhibitoren mit gesteigerter Wirksamkeit und Spezifität für RabGGTasen sind Kandidaten für Anti-Krebs- und Anti-Osteoporose-Therapien.

6 Acknowledgements

I would like to take this opportunity to convey my heartfelt thanks to the following people.

First and foremost, I sincerely thank my supervisors, Prof. Dr. Roger S. Goody and Dr. Kirill Alexandrov for giving me the opportunity to work in this institute and to work on such an exciting topic. Both of them have given me tremendous encouragement, creative ideas and wonderful discussion in my work.

I sincerely thank Dr. Wulf Blankenfeldt for his invaluable help, discussion and wonderful supervision in protein crystallography.

I am very grateful to Prof. Dr. Henning Mootz for agreeing to be the co-referent for my thesis and for wonderful discussions.

I am grateful to Prof. Dr. Herbert Waldmann for his support in the providing of RabGGTase inhibitors and prenylated peptides. I thank Dr. Luc Brunsveld for his support in providing of prenylated peptides.

I would like to thank the following colleagues for their support to my work. Shen introduced me into crystallography. The identification of RabGGTase inhibitors and the biochemical studies of RabGGTase and Rab prenylation mechanism were performed by Yao-Wen Wu. The cellular activity of the inhibitors was determined by Dr. Christine Delon. The conjugating of Biotin-GPP mediated by wild-type and engineered protein prenyltransferase was evaluated by Uyen T. Nguyen. The prenylated peptides were synthesized by Dr. Debapratim Das. The inhibitors, MT650 and MT670, were synthesized by Dr. Michael Thutewohl, KT90102 by Dr. Kui-Thong Tan, the derivatives of psoromic acid by Dr. Celine Deraeve and BMS3 by Dr. Robin Bon. The docking experiments were performed by Stefan Wetzel.

I thank our skilful technicians, particularly Nataliya Lupilova, Melina Terbeck, Sandra Thuns and Tina Rogowsky, for the cloning and protein purification. I am also thankful to Nathalie Bleimling, Petra Geue, Aymelt Itzen, TimBergbrede and Susanna Kushnir for the help in the lab.

I would like to thank the X-ray community at the Max Planck for a wonderful atmosphere at work and data collection, particularly Dr. Ingrid Vetter, Georg Holtermann and Lothar Gremer for useful tips and tricks in crystallography.

I am very grateful to Dr. Waltraud Hofmann-Goody, Dr. Christine Delon, Dr. Tim Bergbrede and Uyen T. Nguyen for the critical reading of this manuscript and wonderful suggestions.

I also thank all other members of the department physical biochemistry for the nice working atmosphere.

Reference List

- (1) Bourne, H. R. *Nature* **1993**, *366*, 628-629.
- (2) Pfeffer, S. R. *Trends Cell Biol.* **2001**, *11*, 487-491.
- (3) Ulku, A. S.; Der, C. J. *Cancer Treat.Res.* **2003**, *115*, 189-208.
- (4) Hinshaw, J. E. *Annu.Rev.Cell Dev.Biol.* **2000**, *16*, 483-519.
- (5) Rodnina, M. V.; Wintermeyer, W. *Annu.Rev.Biochem.* **2001**, *70*, 415-435.
- (6) Koch, H. G.; Moser, M.; Muller, M. *Rev.Physiol Biochem.Pharmacol.* **2003**, *146*, 55-94.
- (7) Vetter, I. R.; Wittinghofer, A. *Science* **2001**, *294*, 1299-1304.
- (8) Bourne, H. R.; Sanders, D. A.; McCormick, F. *Nature* **1991**, *349*, 117-127.
- (9) Ahmadian, M. R.; Stege, P.; Scheffzek, K.; Wittinghofer, A. *Nat.Struct.Biol.* **1997**, *4*, 686-689.
- (10) Wu, S. K.; Zeng, K.; Wilson, I. A.; Balch, W. E. *Trends Biochem.Sci.* **1996**, *21*, 472-476.
- (11) Geyer, M.; Wittinghofer, A. *Curr.Opin.Struct.Biol.* **1997**, *7*, 786-792.
- (12) Mackay, D. J.; Hall, A. *J.Biol.Chem.* **1998**, *273*, 20685-20688.
- (13) Sander, E. E.; Collard, J. G. *Eur.J.Cancer* **1999**, *35*, 1905-1911.
- (14) Schimmoller, F.; Simon, I.; Pfeffer, S. R. *J.Biol.Chem.* **1998**, *273*, 22161-22164.
- (15) Somsel, R. J.; Wandinger-Ness, A. *J.Cell Sci.* **2000**, *113 Pt 2*, 183-192.
- (16) Moss, J.; Vaughan, M. *J.Biol.Chem.* **1998**, *273*, 21431-21434.
- (17) Jackson, C. L.; Casanova, J. E. *Trends Cell Biol.* **2000**, *10*, 60-67.
- (18) Colicelli, J. *Sci.STKE.* **2004**, *2004*, RE13.
- (19) Arnaud, C.; Burger, F.; Steffens, S.; Veillard, N. R.; Nguyen, T. H.; Trono, D.; Mach, F. *Arterioscler.Thromb.Vasc.Biol.* **2005**, *25*, 1231-1236.
- (20) Wennerberg, K.; Rossman, K. L.; Der, C. J. *J.Cell Sci.* **2005**, *118*, 843-846.
- (21) Valencia, A.; Chardin, P.; Wittinghofer, A.; Sander, C. *Biochemistry* **1991**, *30*, 4637-4648.

-
- (22) Casey, P. J.; Seabra, M. C. *J.Biol.Chem.* **1996**, *271*, 5289-5292.
- (23) Zhang, F. L.; Casey, P. J. *Annu.Rev.Biochem.* **1996**, *65*, 241-269.
- (24) Moss, J.; Vaughan, M. *J.Biol.Chem.* **1995**, *270*, 12327-12330.
- (25) Zerial, M.; McBride, H. *Nat.Rev.Mol.Cell Biol.* **2001**, *2*, 107-117.
- (26) Novick, P.; Zerial, M. *Curr.Opin.Cell Biol.* **1997**, *9*, 496-504.
- (27) An, Y.; Shao, Y.; Alory, C.; Matteson, J.; Sakisaka, T.; Chen, W.; Gibbs, R. A.; Wilson, I. A.; Balch, W. E. *Structure.* **2003**, *11*, 347-357.
- (28) Dirac-Svejstrup, A. B.; Sumizawa, T.; Pfeffer, S. R. *EMBO J.* **1997**, *16*, 465-472.
- (29) Sakisaka, T.; Meerlo, T.; Matteson, J.; Plutner, H.; Balch, W. E. *EMBO J.* **2002**, *21*, 6125-6135.
- (30) Machner, M. P.; Isberg, R. R. *Science* **2007**, *318*, 974-977.
- (31) Murray, J. T.; Panaretou, C.; Stenmark, H.; Miaczynska, M.; Backer, J. M. *Traffic.* **2002**, *3*, 416-427.
- (32) Lindsay, A. J.; Hendrick, A. G.; Cantalupo, G.; Senic-Matuglia, F.; Goud, B.; Bucci, C.; McCaffrey, M. W. *J.Biol.Chem.* **2002**, *277*, 12190-12199.
- (33) Mattera, R.; Arighi, C. N.; Lodge, R.; Zerial, M.; Bonifacino, J. S. *EMBO J.* **2003**, *22*, 78-88.
- (34) Cai, H.; Reinisch, K.; Ferro-Novick, S. *Dev.Cell* **2007**, *12*, 671-682.
- (35) Bonifacino, J. S.; Glick, B. S. *Cell* **2004**, *116*, 153-166.
- (36) Grosshans, B. L.; Ortiz, D.; Novick, P. *Proc.Natl.Acad.Sci.U.S.A* **2006**, *103*, 11821-11827.
- (37) Carroll, K. S.; Hanna, J.; Simon, I.; Krise, J.; Barbero, P.; Pfeffer, S. R. *Science* **2001**, *292*, 1373-1376.
- (38) McLauchlan, H.; Newell, J.; Morrice, N.; Osborne, A.; West, M.; Smythe, E. *Curr.Biol.* **1998**, *8*, 34-45.
- (39) Mammoto, A.; Sasaki, T.; Kim, Y.; Takai, Y. *J.Biol.Chem.* **2000**, *275*, 13167-13170.
- (40) Pagano, A.; Crottet, P.; Prescianotto-Baschong, C.; Spiess, M. *Mol.Biol.Cell* **2004**, *15*, 4990-5000.
- (41) Hanna, J.; Carroll, K.; Pfeffer, S. R. *Proc.Natl.Acad.Sci.U.S.A* **2002**, *99*, 7450-7454.
- (42) Bloom, G. S.; Goldstein, L. S. *J.Cell Biol.* **1998**, *140*, 1277-1280.
- (43) Jordens, I.; Marsman, M.; Kuijl, C.; Neefjes, J. *Traffic.* **2005**, *6*, 1070-1077.

-
- (44) Young, J.; Stauber, T.; del Nery, E.; Vernos, I.; Pepperkok, R.; Nilsson, T. *Mol.Biol.Cell* **2005**, *16*, 162-177.
- (45) Jordens, I.; Westbroek, W.; Marsman, M.; Rocha, N.; Mommaas, M.; Huizing, M.; Lambert, J.; Naeyaert, J. M.; Neefjes, J. *Pigment Cell Res.* **2006**, *19*, 412-423.
- (46) Jordens, I.; Fernandez-Borja, M.; Marsman, M.; Dusseljee, S.; Janssen, L.; Calafat, J.; Janssen, H.; Wubbolts, R.; Neefjes, J. *Curr.Biol.* **2001**, *11*, 1680-1685.
- (47) Fukuda, M.; Kuroda, T. S.; Mikoshiba, K. *J.Biol.Chem.* **2002**, *277*, 12432-12436.
- (48) Westbroek, W.; Lambert, J.; Bahadoran, P.; Busca, R.; Herteleer, M. C.; Smit, N.; Mommaas, M.; Ballotti, R.; Naeyaert, J. M. *J.Invest Dermatol.* **2003**, *120*, 465-475.
- (49) Strom, M.; Hume, A. N.; Tarafder, A. K.; Barkagianni, E.; Seabra, M. C. *J.Biol.Chem.* **2002**, *277*, 25423-25430.
- (50) Johansson, M.; Rocha, N.; Zwart, W.; Jordens, I.; Janssen, L.; Kuijl, C.; Olkkonen, V. M.; Neefjes, J. *J.Cell Biol.* **2007**, *176*, 459-471.
- (51) Whyte, J. R.; Munro, S. *J.Cell Sci.* **2002**, *115*, 2627-2637.
- (52) Allan, B. B.; Moyer, B. D.; Balch, W. E. *Science* **2000**, *289*, 444-448.
- (53) Jahn, R.; Scheller, R. H. *Nat.Rev.Mol.Cell Biol.* **2006**, *7*, 631-643.
- (54) Zwilling, D.; Cypionka, A.; Pohl, W. H.; Fasshauer, D.; Walla, P. J.; Wahl, M. C.; Jahn, R. *EMBO J.* **2007**, *26*, 9-18.
- (55) Pobbati, A. V.; Razeto, A.; Boddener, M.; Becker, S.; Fasshauer, D. *J.Biol.Chem.* **2004**, *279*, 47192-47200.
- (56) Ossig, R.; Schmitt, H. D.; de Groot, B.; Riedel, D.; Keranen, S.; Ronne, H.; Grubmuller, H.; Jahn, R. *EMBO J.* **2000**, *19*, 6000-6010.
- (57) Mayer, A.; Wickner, W.; Haas, A. *Cell* **1996**, *85*, 83-94.
- (58) McNew, J. A.; Weber, T.; Parlati, F.; Johnston, R. J.; Melia, T. J.; Sollner, T. H.; Rothman, J. E. *J.Cell Biol.* **2000**, *150*, 105-117.
- (59) Starai, V. J.; Jun, Y.; Wickner, W. *Proc.Natl.Acad.Sci.U.S.A* **2007**, *104*, 13551-13558.
- (60) McBride, H. M.; Rybin, V.; Murphy, C.; Giner, A.; Teasdale, R.; Zerial, M. *Cell* **1999**, *98*, 377-386.
- (61) Lupashin, V.; Sztul, E. *Biochim.Biophys.Acta* **2005**, *1744*, 325-339.
- (62) Maurer-Stroh, S.; Washietl, S.; Eisenhaber, F. *Genome Biol.* **2003**, *4*, 212.
- (63) Sinensky, M. *Biochim.Biophys.Acta* **2000**, *1484*, 93-106.
- (64) Pechlivanis, M.; Kuhlmann, J. *Biochim.Biophys.Acta* **2006**, *1764*, 1914-1931.

-
- (65) Maurer-Stroh, S.; Eisenhaber, B.; Eisenhaber, F. *J.Mol.Biol.* **2002**, *317*, 541-557.
- (66) Maurer-Stroh, S.; Eisenhaber, B.; Eisenhaber, F. *J.Mol.Biol.* **2002**, *317*, 523-540.
- (67) Resh, M. D. *Biochim.Biophys.Acta* **1999**, *1451*, 1-16.
- (68) Resh, M. D. *Sci.STKE.* **2006**, *2006*, re14.
- (69) Sinensky, M. *Biochim.Biophys.Acta* **2000**, *1529*, 203-209.
- (70) Gelb, M. H. *Science* **1997**, *275*, 1750-1751.
- (71) Gelb, M. H.; Scholten, J. D.; Sebolt-Leopold, J. S. *Curr.Opin.Chem.Biol.* **1998**, *2*, 40-48.
- (72) Glomset, J. A.; Farnsworth, C. C. *Annu.Rev.Cell Biol.* **1994**, *10*, 181-205.
- (73) Omer, C. A.; Gibbs, J. B. *Mol.Microbiol.* **1994**, *11*, 219-225.
- (74) Caldwell, G. A.; Naider, F.; Becker, J. M. *Microbiol.Rev.* **1995**, *59*, 406-422.
- (75) Pylypenko, O.; Rak, A.; Durek, T.; Kushnir, S.; Dursina, B. E.; Thomae, N. H.; Constantinescu, A. T.; Brunsveld, L.; Watzke, A.; Waldmann, H.; Goody, R. S.; Alexandrov, K. *EMBO J.* **2006**, *25*, 13-23.
- (76) Rak, A.; Pylypenko, O.; Durek, T.; Watzke, A.; Kushnir, S.; Brunsveld, L.; Waldmann, H.; Goody, R. S.; Alexandrov, K. *Science* **2003**, *302*, 646-650.
- (77) Moores, S. L.; Schaber, M. D.; Mosser, S. D.; Rands, E.; O'Hara, M. B.; Garsky, V. M.; Marshall, M. S.; Pompliano, D. L.; Gibbs, J. B. *J.Biol.Chem.* **1991**, *266*, 14603-14610.
- (78) Moomaw, J. F.; Casey, P. J. *J.Biol.Chem.* **1992**, *267*, 17438-17443.
- (79) Yokoyama, K.; Gelb, M. H. *J.Biol.Chem.* **1993**, *268*, 4055-4060.
- (80) Trueblood, C. E.; Boyartchuk, V. L.; Picologlou, E. A.; Rozema, D.; Poulter, C. D.; Rine, J. *Mol.Cell Biol.* **2000**, *20*, 4381-4392.
- (81) Bergo, M. O.; Leung, G. K.; Ambroziak, P.; Otto, J. C.; Casey, P. J.; Gomes, A. Q.; Seabra, M. C.; Young, S. G. *J.Biol.Chem.* **2001**, *276*, 5841-5845.
- (82) Pei, J.; Grishin, N. V. *Trends Biochem.Sci.* **2001**, *26*, 275-277.
- (83) Winter-Vann, A. M.; Casey, P. J. *Nat.Rev.Cancer* **2005**, *5*, 405-412.
- (84) Hancock, J. F.; Magee, A. I.; Childs, J. E.; Marshall, C. J. *Cell* **1989**, *57*, 1167-1177.
- (85) Alexandrov, K.; Simon, I.; Yurchenko, V.; Iakovenko, A.; Rostkova, E.; Scheidig, A. J.; Goody, R. S. *Eur.J.Biochem.* **1999**, *265*, 160-170.
- (86) Seabra, M. C.; Mules, E. H.; Hume, A. N. *Trends Mol.Med.* **2002**, *8*, 23-30.

-
- (87) Saderholm, M. J.; Hightower, K. E.; Fierke, C. A. *Biochemistry* **2000**, *39*, 12398-12405.
- (88) Long, S. B.; Casey, P. J.; Beese, L. S. *Nature* **2002**, *419*, 645-650.
- (89) Taylor, J. S.; Reid, T. S.; Terry, K. L.; Casey, P. J.; Beese, L. S. *EMBO J.* **2003**, *22*, 5963-5974.
- (90) Zhang, H.; Seabra, M. C.; Deisenhofer, J. *Structure*. **2000**, *8*, 241-251.
- (91) Park, H. W.; Boduluri, S. R.; Moomaw, J. F.; Casey, P. J.; Beese, L. S. *Science* **1997**, *275*, 1800-1804.
- (92) Dursina, B.; Thoma, N. H.; Sidorovitch, V.; Niculae, A.; Iakovenko, A.; Rak, A.; Albert, S.; Ceacareanu, A. C.; Kolling, R.; Herrmann, C.; Goody, R. S.; Alexandrov, K. *Biochemistry* **2002**, *41*, 6805-6816.
- (93) Pylypenko, O.; Rak, A.; Reents, R.; Niculae, A.; Sidorovitch, V.; Cioaca, M. D.; Bessolitsyna, E.; Thoma, N. H.; Waldmann, H.; Schlichting, I.; Goody, R. S.; Alexandrov, K. *Mol. Cell* **2003**, *11*, 483-494.
- (94) Reiss, Y.; Brown, M. S.; Goldstein, J. L. *J. Biol. Chem.* **1992**, *267*, 6403-6408.
- (95) Chen, W. J.; Moomaw, J. F.; Overton, L.; Kost, T. A.; Casey, P. J. *J. Biol. Chem.* **1993**, *268*, 9675-9680.
- (96) Long, S. B.; Casey, P. J.; Beese, L. S. *Biochemistry* **1998**, *37*, 9612-9618.
- (97) Reiss, Y.; Stradley, S. J.; Gierasch, L. M.; Brown, M. S.; Goldstein, J. L. *Proc. Natl. Acad. Sci. U.S.A* **1991**, *88*, 732-736.
- (98) Furfine, E. S.; Leban, J. J.; Landavazo, A.; Moomaw, J. F.; Casey, P. J. *Biochemistry* **1995**, *34*, 6857-6862.
- (99) Yokoyama, K.; Zimmerman, K.; Scholten, J.; Gelb, M. H. *J. Biol. Chem.* **1997**, *272*, 3944-3952.
- (100) Armstrong, S. A.; Hannah, V. C.; Goldstein, J. L.; Brown, M. S. *J. Biol. Chem.* **1995**, *270*, 7864-7868.
- (101) Strickland, C. L.; Windsor, W. T.; Syto, R.; Wang, L.; Bond, R.; Wu, Z.; Schwartz, J.; Le, H. V.; Beese, L. S.; Weber, P. C. *Biochemistry* **1998**, *37*, 16601-16611.
- (102) Long, S. B.; Casey, P. J.; Beese, L. S. *Structure*. **2000**, *8*, 209-222.
- (103) Reid, T. S.; Terry, K. L.; Casey, P. J.; Beese, L. S. *J. Mol. Biol.* **2004**, *343*, 417-433.
- (104) Dolence, J. M.; Steward, L. E.; Dolence, E. K.; Wong, D. H.; Poulter, C. D. *Biochemistry* **2000**, *39*, 4096-4104.
- (105) Pompilano, D. L.; Schaber, M. D.; Mosser, S. D.; Omer, C. A.; Shafer, J. A.; Gibbs, J. B. *Biochemistry* **1993**, *32*, 8341-8347.

-
- (106) Hightower, K. E.; Huang, C. C.; Casey, P. J.; Fierke, C. A. *Biochemistry* **1998**, *37*, 15555-15562.
- (107) Yokoyama, K.; McGeady, P.; Gelb, M. H. *Biochemistry* **1995**, *34*, 1344-1354.
- (108) Stirtan, W. G.; Poulter, C. D. *Biochemistry* **1997**, *36*, 4552-4557.
- (109) Reiss, Y.; Goldstein, J. L.; Seabra, M. C.; Casey, P. J.; Brown, M. S. *Cell* **1990**, *62*, 81-88.
- (110) Huang, C. C.; Casey, P. J.; Fierke, C. A. *J.Biol.Chem.* **1997**, *272*, 20-23.
- (111) Huang, C.; Hightower, K. E.; Fierke, C. A. *Biochemistry* **2000**, *39*, 2593-2602.
- (112) Hightower, K. E.; Fierke, C. A. *Curr.Opin.Chem.Biol.* **1999**, *3*, 176-181.
- (113) Pickett, J. S.; Bowers, K. E.; Fierke, C. A. *J.Biol.Chem.* **2003**, *278*, 51243-51250.
- (114) Hartman, H. L.; Bowers, K. E.; Fierke, C. A. *J.Biol.Chem.* **2004**, *279*, 30546-30553.
- (115) Pompilano, D. L.; Rands, E.; Schaber, M. D.; Mosser, S. D.; Anthony, N. J.; Gibbs, J. B. *Biochemistry* **1992**, *31*, 3800-3807.
- (116) Tschantz, W. R.; Furfine, E. S.; Casey, P. J. *J.Biol.Chem.* **1997**, *272*, 9989-9993.
- (117) Mathis, J. R.; Poulter, C. D. *Biochemistry* **1997**, *36*, 6367-6376.
- (118) Andres, D. A.; Seabra, M. C.; Brown, M. S.; Armstrong, S. A.; Smeland, T. E.; Cremers, F. P.; Goldstein, J. L. *Cell* **1993**, *73*, 1091-1099.
- (119) Goody, R. S.; Rak, A.; Alexandrov, K. *Cell Mol.Life Sci.* **2005**, *62*, 1657-1670.
- (120) Shen, F.; Seabra, M. C. *J.Biol.Chem.* **1996**, *271*, 3692-3698.
- (121) Anant, J. S.; Desnoyers, L.; Machius, M.; Demeler, B.; Hansen, J. C.; Westover, K. D.; Deisenhofer, J.; Seabra, M. C. *Biochemistry* **1998**, *37*, 12559-12568.
- (122) Alory, C.; Balch, W. E. *J.Cell Biol.* **2000**, *150*, 89-103.
- (123) Thoma, N. H.; Iakovenko, A.; Goody, R. S.; Alexandrov, K. *J.Biol.Chem.* **2001**, *276*, 48637-48643.
- (124) Thoma, N. H.; Iakovenko, A.; Kalinin, A.; Waldmann, H.; Goody, R. S.; Alexandrov, K. *Biochemistry* **2001**, *40*, 268-274.
- (125) Thoma, N. H.; Iakovenko, A.; Owen, D.; Scheidig, A. S.; Waldmann, H.; Goody, R. S.; Alexandrov, K. *Biochemistry* **2000**, *39*, 12043-12052.
- (126) Thoma, N. H.; Niculae, A.; Goody, R. S.; Alexandrov, K. *J.Biol.Chem.* **2001**, *276*, 48631-48636.
- (127) Rak, A.; Pylypenko, O.; Niculae, A.; Pyatkov, K.; Goody, R. S.; Alexandrov, K. *Cell* **2004**, *117*, 749-760.

- (128) Alory, C.; Balch, W. E. *Mol.Biol.Cell* **2003**, *14*, 3857-3867.
- (129) Andres, D. A.; Goldstein, J. L.; Ho, Y. K.; Brown, M. S. *J.Biol.Chem.* **1993**, *268*, 1383-1390.
- (130) Rowinsky, E. K.; Windle, J. J.; Von Hoff, D. D. *J.Clin.Oncol.* **1999**, *17*, 3631-3652.
- (131) Lackner, M. R.; Kindt, R. M.; Carroll, P. M.; Brown, K.; Cancilla, M. R.; Chen, C.; de Silva, H.; Franke, Y.; Guan, B.; Heuer, T.; Hung, T.; Keegan, K.; Lee, J. M.; Manne, V.; O'Brien, C.; Parry, D.; Perez-Villar, J. J.; Reddy, R. K.; Xiao, H.; Zhan, H.; Cockett, M.; Plowman, G.; Fitzgerald, K.; Costa, M.; Ross-Macdonald, P. *Cancer Cell* **2005**, *7*, 325-336.
- (132) Philips, M. R.; Cox, A. D. *J.Clin.Invest* **2007**, *117*, 1223-1225.
- (133) Schubbert, S.; Shannon, K.; Bollag, G. *Nat.Rev.Cancer* **2007**, *7*, 295-308.
- (134) Bos, J. L. *Cancer Res.* **1989**, *49*, 4682-4689.
- (135) Shaw, R. J.; Cantley, L. C. *Nature* **2006**, *441*, 424-430.
- (136) Konstantinopoulos, P. A.; Karamouzis, M. V.; Papavassiliou, A. G. *Nat.Rev.Drug Discov.* **2007**, *6*, 541-555.
- (137) Sahai, E.; Marshall, C. J. *Nat.Rev.Cancer* **2002**, *2*, 133-142.
- (138) Kamai, T.; Tsujii, T.; Arai, K.; Takagi, K.; Asami, H.; Ito, Y.; Oshima, H. *Clin.Cancer Res.* **2003**, *9*, 2632-2641.
- (139) Ridley, A. J. *Trends Cell Biol.* **2006**, *16*, 522-529.
- (140) Ellenbroek, S. I.; Collard, J. G. *Clin.Exp.Metastasis* **2007**, *24*, 657-672.
- (141) Preudhomme, C.; Roumier, C.; Hildebrand, M. P.; Dallery-Prudhomme, E.; Lantoine, D.; Lai, J. L.; Daudignon, A.; Adenis, C.; Bauters, F.; Fenaux, P.; Kerckaert, J. P.; Galiegue-Zouitina, S. *Oncogene* **2000**, *19*, 2023-2032.
- (142) Pasqualucci, L.; Neumeister, P.; Goossens, T.; Nanjangud, G.; Chaganti, R. S.; Kuppers, R.; Dalla-Favera, R. *Nature* **2001**, *412*, 341-346.
- (143) Malliri, A.; Rygiel, T. P.; van der Kammen, R. A.; Song, J. Y.; Engers, R.; Hurlstone, A. F.; Clevers, H.; Collard, J. G. *J.Biol.Chem.* **2006**, *281*, 543-548.
- (144) Minard, M. E.; Kim, L. S.; Price, J. E.; Gallick, G. E. *Breast Cancer Res.Treat.* **2004**, *84*, 21-32.
- (145) Yuan, B. Z.; Zhou, X.; Durkin, M. E.; Zimonjic, D. B.; Gumundsdottir, K.; Eyfjord, J. E.; Thorgerisson, S. S.; Popescu, N. C. *Oncogene* **2003**, *22*, 445-450.
- (146) Johnstone, C. N.; Castellvi-Bel, S.; Chang, L. M.; Bessa, X.; Nakagawa, H.; Harada, H.; Sung, R. K.; Pique, J. M.; Castells, A.; Rustgi, A. K. *Gene* **2004**, *336*, 59-71.

- (147) Jones, M. B.; Krutzsch, H.; Shu, H.; Zhao, Y.; Liotta, L. A.; Kohn, E. C.; Petricoin, E. F., III *Proteomics*. **2002**, *2*, 76-84.
- (148) Theodorescu, D.; Sapinoso, L. M.; Conaway, M. R.; Oxford, G.; Hampton, G. M.; Frierson, H. F., Jr. *Clin.Cancer Res.* **2004**, *10*, 3800-3806.
- (149) Cheng, K. W.; Lahad, J. P.; Gray, J. W.; Mills, G. B. *Cancer Res.* **2005**, *65*, 2516-2519.
- (150) Cheng, K. W.; Lahad, J. P.; Kuo, W. L.; Lapuk, A.; Yamada, K.; Auersperg, N.; Liu, J.; Smith-McCune, K.; Lu, K. H.; Fishman, D.; Gray, J. W.; Mills, G. B. *Nat.Med.* **2004**, *10*, 1251-1256.
- (151) Croizet-Berger, K.; Daumerie, C.; Couvreur, M.; Courtoy, P. J.; van den Hove, M. F. *Proc.Natl.Acad.Sci.U.S.A* **2002**, *99*, 8277-8282.
- (152) He, H.; Dai, F.; Yu, L.; She, X.; Zhao, Y.; Jiang, J.; Chen, X.; Zhao, S. *Gene Expr.* **2002**, *10*, 231-242.
- (153) Tamanoi, F.; Gau, C. L.; Jiang, C.; Edamatsu, H.; Kato-Stankiewicz, J. *Cell Mol.Life Sci.* **2001**, *58*, 1636-1649.
- (154) Reid, T. S.; Long, S. B.; Beese, L. S. *Biochemistry* **2004**, *43*, 9000-9008.
- (155) Reid, T. S.; Beese, L. S. *Biochemistry* **2004**, *43*, 6877-6884.
- (156) Basso, A. D.; Kirschmeier, P.; Bishop, W. R. *J.Lipid Res.* **2006**, *47*, 15-31.
- (157) Kohl, N. E.; Conner, M. W.; Gibbs, J. B.; Graham, S. L.; Hartman, G. D.; Oliff, A. *J.Cell Biochem.Suppl* **1995**, *22*, 145-150.
- (158) Caponigro, F.; Casale, M.; Bryce, J. *Expert.Opin.Investig.Drugs* **2003**, *12*, 943-954.
- (159) Morgan, M. A.; Ganser, A.; Reuter, C. W. *Leukemia* **2003**, *17*, 1482-1498.
- (160) Dinsmore, C. J.; Bell, I. M. *Curr.Top.Med.Chem.* **2003**, *3*, 1075-1093.
- (161) Kelland, L. R. *Expert.Opin.Investig.Drugs* **2003**, *12*, 413-421.
- (162) Field, H.; Blench, I.; Croft, S.; Field, M. C. *Mol.Biochem.Parasitol.* **1996**, *82*, 67-80.
- (163) Yokoyama, K.; Trobridge, P.; Buckner, F. S.; Van Voorhis, W. C.; Stuart, K. D.; Gelb, M. H. *J.Biol.Chem.* **1998**, *273*, 26497-26505.
- (164) Ohkanda, J.; Lockman, J. W.; Yokoyama, K.; Gelb, M. H.; Croft, S. L.; Kendrick, H.; Harrell, M. I.; Feagin, J. E.; Blaskovich, M. A.; Sebti, S. M.; Hamilton, A. D. *Bioorg.Med.Chem.Lett.* **2001**, *11*, 761-764.
- (165) Nishimura, S.; Matsunaga, S.; Shibasaki, M.; Suzuki, K.; Furihata, K.; van Soest, R. W.; Fusetani, N. *Org.Lett.* **2003**, *5*, 2255-2257.

- (166) Murthi, K. K.; Smith, S. E.; Kluge, A. F.; Bergnes, G.; Bureau, P.; Berlin, V. *Bioorg.Med.Chem.Lett.* **2003**, *13*, 1935-1937.
- (167) Einav, S.; Glenn, J. S. *J.Antimicrob.Chemother.* **2003**, *52*, 883-886.
- (168) Bordier, B. B.; Ohkanda, J.; Liu, P.; Lee, S. Y.; Salazar, F. H.; Marion, P. L.; Ohashi, K.; Meuse, L.; Kay, M. A.; Casey, J. L.; Sebti, S. M.; Hamilton, A. D.; Glenn, J. S. *J.Clin.Invest* **2003**, *112*, 407-414.
- (169) El Oualid, F.; Cohen, L. H.; van der Marel, G. A.; Overhand, M. *Curr.Med.Chem.* **2006**, *13*, 2385-2427.
- (170) Peterson, Y. K.; Kelly, P.; Weinbaum, C. A.; Casey, P. J. *J.Biol.Chem.* **2006**, *281*, 12445-12450.
- (171) Coxon, F. P.; Helfrich, M. H.; Larijani, B.; Muzylak, M.; Dunford, J. E.; Marshall, D.; McKinnon, A. D.; Nesbitt, S. A.; Horton, M. A.; Seabra, M. C.; Ebetino, F. H.; Rogers, M. J. *J.Biol.Chem.* **2001**, *276*, 48213-48222.
- (172) Strickland, C. L.; Weber, P. C.; Windsor, W. T.; Wu, Z.; Le, H. V.; Albanese, M. M.; Alvarez, C. S.; Cesarz, D.; del Rosario, J.; Deskus, J.; Mallams, A. K.; Njoroge, F. G.; Piwinski, J. J.; Remiszewski, S.; Rossman, R. R.; Taveras, A. G.; Vibulbhan, B.; Doll, R. J.; Girijavallabhan, V. M.; Ganguly, A. K. *J.Med.Chem.* **1999**, *42*, 2125-2135.
- (173) Rose, W. C.; Lee, F. Y.; Fairchild, C. R.; Lynch, M.; Monticello, T.; Kramer, R. A.; Manne, V. *Cancer Res.* **2001**, *61*, 7507-7517.
- (174) Gartner, A.; Milstein, S.; Ahmed, S.; Hodgkin, J.; Hengartner, M. O. *Mol.Cell* **2000**, *5*, 435-443.
- (175) Stergiou, L.; Hengartner, M. O. *Cell Death.Differ.* **2004**, *11*, 21-28.
- (176) Roelofs, A. J.; Hulley, P. A.; Meijer, A.; Ebetino, F. H.; Russell, R. G.; Shipman, C. M. *Int.J.Cancer* **2006**, *119*, 1254-1261.
- (177) Sambrook J.; Fritsch E.F.; Maniatis t. *Cold Spring Harbor Laboratory Press* **1989**.
- (178) Mullis, K.; Faloona, F.; Scharf, S.; Saiki, R.; Horn, G.; Erlich, H. *Biotechnology* **1992**, *24*, 17-27.
- (179) Tung, W. L.; Chow, K. C. *Trends Genet.* **1995**, *11*, 128-129.
- (180) Sanger, F.; Nicklen, S.; Coulson, A. R. *Biotechnology* **1992**, *24*, 104-108.
- (181) Kalinin, A.; Thoma, N. H.; Iakovenko, A.; Heinemann, I.; Rostkova, E.; Constantinescu, A. T.; Alexandrov, K. *Protein Expr.Purif.* **2001**, *22*, 84-91.
- (182) Bradford, M. M. *Anal.Biochem.* **1976**, *72*, 248-254.
- (183) Wu, Y. W.; Waldmann, H.; Reents, R.; Ebetino, F. H.; Goody, R. S.; Alexandrov, K. *Chembiochem.* **2006**, *7*, 1859-1861.

- (184) Hampel, A.; Labanauskas, M.; Connors, P. G.; Kirkegard, L.; RajBhandary, U. L.; Sigler, P. B.; Bock, R. M. *Science* **1968**, *162*, 1384-1387.
- (185) Danley, D. E. *Acta Crystallogr.D.Biol.Crystallogr.* **2006**, *62*, 569-575.
- (186) Vilenchik L.Z.; Griffith J.P.; Navia M.A.; Margolin A.L. *J.Am.Chem.Soc.* **1998**.
- (187) Petsko, G. A. *J.Mol.Biol.* **1975**, *96*, 381-392.
- (188) Kabsch w. *journal of applied crystallography* **1993**, *26*, 795-800.
- (189) Matthews, B. W. *J.Mol.Biol.* **1968**, *33*, 491-497.
- (190) Taylor G. *Acta Crystallogr.D.Biol.Crystallogr.* **2003**, *59*, 1881-1890.
- (191) Rossmann M.; Blow D.M. *Acta Crystallographica* **1962**, *15*, 14-31.
- (192) Drenth J. *Springer Verlag* **1999**.
- (193) Rhodes G. *Academic Press* **2000**.
- (194) Brunger A.T. *Methods and Applications.Acta Cryst.* **1993**, *1349*, 24-36.
- (195) Murshudov, G. N.; Vagin, A. A.; Dodson, E. J. *Acta Crystallogr.D.Biol.Crystallogr.* **1997**, *53*, 240-255.
- (196) Emsley, P.; Cowtan, K. *Acta Crystallogr.D.Biol.Crystallogr.* **2004**, *60*, 2126-2132.
- (197) Laskowski R.A.; MacArthur M.W.; Moss D.S.; Thornton J.M. *journal of applied crystallography* **1993**, *26*, 283-291.
- (198) Lane, K. T.; Beese, L. S. *J.Lipid Res.* **2006**, *47*, 681-699.
- (199) WU Y.W. Identification of RabGGTase inhibitors and mechanistic studies of RabGTPase prenylation and recycling using fluorescent sensors. 2008.
- Ref Type: Thesis/Dissertation
- (200) Bishop, W. R.; Bond, R.; Petrin, J.; Wang, L.; Patton, R.; Doll, R.; Njoroge, G.; Catino, J.; Schwartz, J.; Windsor, W.; . *J.Biol.Chem.* **1995**, *270*, 30611-30618.
- (201) Wu, Z.; Demma, M.; Strickland, C. L.; Syto, R.; Le, H. V.; Windsor, W. T.; Weber, P. C. *Protein Eng* **1999**, *12*, 341-348.
- (202) Nguyen, U. T.; Cramer, J.; Gomis, J.; Reents, R.; Gutierrez-Rodriguez, M.; Goody, R. S.; Alexandrov, K.; Waldmann, H. *Chembiochem.* **2007**, *8*, 408-423.
- (203) Dursina, B. E.; Reents, R.; Niculae, A.; Veligodsky, A.; Breitling, R.; Pyatkov, K.; Waldmann, H.; Goody, R. S.; Alexandrov, K. *Protein Expr.Purif.* **2005**, *39*, 71-81.
- (204) McCoy, A. J.; Grosse-Kunstleve, R. W.; Storoni, L. C.; Read, R. J. *Acta Crystallogr.D.Biol.Crystallogr.* **2005**, *61*, 458-464.

- (205) SERC Daresbury Lab. *Acta Crystallogr.D.Biol.Crystallogr.* **1994**, *D50*, 760-763.
- (206) Berman, H. M.; Battistuz, T.; Bhat, T. N.; Bluhm, W. F.; Bourne, P. E.; Burkhardt, K.; Feng, Z.; Gilliland, G. L.; Iype, L.; Jain, S.; Fagan, P.; Marvin, J.; Padilla, D.; Ravichandran, V.; Schneider, B.; Thanki, N.; Weissig, H.; Westbrook, J. D.; Zardecki, C. *Acta Crystallogr.D.Biol.Crystallogr.* **2002**, *58*, 899-907.
- (207) Schuttelkopf, A. W.; Van Aalten, D. M. *Acta Crystallogr.D.Biol.Crystallogr.* **2004**, *60*, 1355-1363.
- (208) Dursina, B.; Reents, R.; Delon, C.; Wu, Y.; Kulharia, M.; Thutewohl, M.; Veligodsky, A.; Kalinin, A.; Evstifeev, V.; Ciobanu, D.; Szedlacsek, S. E.; Waldmann, H.; Goody, R. S.; Alexandrov, K. *J.Am.Chem.Soc.* **2006**, *128*, 2822-2835.
- (209) Hoffman, G. R.; Nassar, N.; Cerione, R. A. *Cell* **2000**, *100*, 345-356.
- (210) Loew, A.; Ho, Y. K.; Blundell, T.; Bax, B. *Structure.* **1998**, *6*, 1007-1019.
- (211) Turek-Etienne, T. C.; Strickland, C. L.; Distefano, M. D. *Biochemistry* **2003**, *42*, 3716-3724.
- (212) Nguyen U.T., Goody R.S., and Alexandre, K. 2008.
Ref Type: Unpublished Work
- (213) Thutewohl, M.; Waldmann, H. *Bioorg.Med.Chem.* **2003**, *11*, 2591-2615.
- (214) Thutewohl, M.; Kissau, L.; Popkirova, B.; Karaguni, I. M.; Nowak, T.; Bate, M.; Kuhlmann, J.; Muller, O.; Waldmann, H. *Angew.Chem.Int.Ed Engl.* **2002**, *41*, 3616-3620.
- (215) Guo Z., WU Y.W., Tan K.T., Bon R.S., Guiu-Rozas E., Delon C., Nguyen U.T., Wetzel S., Arndt S., Goody R.S., Blankenfeldt W., Alexandre, K., and Waldmann, H. Development of selective RabGGTase inhibitors and the first crystal structure of a RabGGTase-Inhibitor complex. *Angew.Chem.Int.Ed Engl.* 2008.
Ref Type: In Press
- (216) Zhou W.Y. Characterization of novel inhibotirs of protein prenytransferases. 2007.
Ref Type: Thesis/Dissertation
- (217) Hunt, J. T.; Ding, C. Z.; Batorsky, R.; Bednarz, M.; Bhide, R.; Cho, Y.; Chong, S.; Chao, S.; Gullo-Brown, J.; Guo, P.; Kim, S. H.; Lee, F. Y.; Leftheris, K.; Miller, A.; Mitt, T.; Patel, M.; Penhallow, B. A.; Ricca, C.; Rose, W. C.; Schmidt, R.; Slusarchyk, W. A.; Vite, G.; Manne, V. *J.Med.Chem.* **2000**, *43*, 3587-3595.
- (218) Cortes, J.; Faderl, S.; Estey, E.; Kurzrock, R.; Thomas, D.; Beran, M.; Garcia-Manero, G.; Ferrajoli, A.; Giles, F.; Koller, C.; O'Brien, S.; Wright, J.; Bai, S. A.; Kantarjian, H. *J.Clin.Oncol.* **2005**, *23*, 2805-2812.